STUDY OF MOLECULAR PROPERTIES AND RESONANCE WITHIN THE COUPLED CLUSTER FRAMEWORK

Thesis submitted to the
Savitribai Phule Pune University
for the Degree of

Doctor of Philosophy
in
Chemistry

By

Aryya Ghosh

Dr. Sourav Pal
(Research Guide)

Dr. Nayana Vaval
(Research Co-Guide)

Physical Chemistry Division
CSIR-National Chemical Laboratory
Pune 411008

September 2014

CERTIFICATE

CERTIFIED THAT the work done in the thesis entitled,

Study of molecular properties and resonance within the coupled cluster framework

submitted by **Aryya Ghosh** was carried out by the candidate under my supervision in the Physical Chemsitry Division, National Chemical Laboratory, Pune 411008, India. Any material that has been obtained from other sources has been duly acknowledged in the thesis.

Date:
Place:

Dr. Sourav Pal
(Research Superviser)
Physical Chemistry Division
National Chemical Laboratory
Pune 411008, India

CERTIFICATE

CERTIFIED THAT the work done in the thesis entitled,

Study of molecular properties and resonance within the coupled cluster framework

submitted by **Aryya Ghosh** was carried out by the candidate under my supervision in the Physical Chemsitry Division, National Chemical Laboratory, Pune 411008, India. Any material that has been obtained from other sources has been duly acknowledged in the thesis.

Date:
Place:

Dr. Nayana Vaval
(Research co-superviser)
Physical Chemistry Division
National Chemical Laboratory
Pune 411008, India

DECLARATION

I hereby declare that the work incorporated in the thesis entiled

Study of molecular properties and resonance within the coupled cluster framework

submitted by me to the **Savitribai Phule Pune University** for the degree of Doctor of Philosophy is original and has not been submitted to this or other University or Institution for the award of Degree or Diploma. Such material, as has been obtained from other sources has been duly acknowledged.

Aryya Ghosh

To my parents

Acknowledgements

I take immense pleasure in thanking my supervisor Dr. Sourav Pal for accepting me to work under his valuable guidance. I am truly inspired by his nature and freedom to learn attitude. The motivation I got from his teaching made me to pursue in the field of many-body approach.

There is no words to acknowledge Dr. Nayana Vaval my co-supervisor for her constant support and continuous encouragement during the completion of this thesis. She helped me in each and every moment of my stay in lab. I am grateful for her guidance and patience. I appreciate all the suggestions given by her at each level.

I thank my all lab seniors Dr. Arijit Bag, Dr. Subrata Banik, Dr. Lalitha Ravichandan, Dr. Himadri Dey, Dr. Sapna Shedge and Dr. Sumantra Bhattachray, Depti Mishra for making my life comfortable in my initial days. I thank all my labmates Himadri, Susanta, Achintya, Sudip, Turbasu, Deepak, Manzoor, Debaratidi, Sayali, Kamalika, Anagha, Jitendra, Mudit, Vidika, Madhulika, Saba for giving me a nice working environment in lab. I have always enjoyed my lab in my working time.

I thank all my computer room friends Monoj, Prathit, Amrita, Yuvraj, Yugal, Shantanu, Tamal, Nisha, Jaya, Mritunjoy.

I thank all my hostel friends Arpan, Kanak, Pravat, Anjan, Abhik, Prithvi, Sujit, Saikat da, Debasis da, Tamos da, Chandan da, Partha da, Animesh da, Jayasis da, Krishanu da, Shyam da, Subha di, Munmun, Doss, Tanaya, Sujit da, Subhadip da, Jhumur, Sajal da, Raju, Jitu, Wahid, Saleem, Manoj.

I thank all my hostel juniors Anup, Soumen, Saibal, Mrinmoy, Santigopal, Atanu, Santanu, Suman, Arunava, Hridesh, Prasenjit, Jagadish, Ramkrishna, Bikash

I want to express my gratitude towards my university teachers Dr. Pranab Sarkar, Dr. Bidhan Chandra Bag for motivating me towards this fascinating world of research.

I have no words to thank my parents and my brother for their love and affection. The

support and encouragement they showed at every state of my life is enormous and moved me ahead. I like to thank them in my all actions.

At last I like to express my gratitude to God almighty for his grace.

Aryya

Contents

List of Tables

Abstract

In this thesis, an explicitly complex absorbing potential (CAP) based equation-of-motion coupled cluster with singles and doubles (EOM-CCSD) formalism is developed. The method is termed as CAP/EOM-CCSD method. The method is designed to compute the position and lifetime of the shape resonance. [1] It has also been applied to explore the different spectroscopic phenomena such as Interatomic or Intermolecular coulombic decay (ICD),[2–11] Auger decay,[12, 13] etc. The decay rate of ICD and Auger decay is computed using the CAP/EOM-CCSD method. The calculated decay rate is found to be very fast for the ICD as well as auger decay.

Resonance states are quasi bound or metastable states with finite lifetime. Generally, resonance states appear in electron molecule scattering and it provides deep insight about the physical system. Resonances play a significant role in various energy exchange process like, vibrational excitations of the molecules, dissociative attachment, etc. It also play an important role in high precession single molecular engineering and quantum dot fabrication. However, resonance phenomena becomes one of the most amazing phenomena in chemical physics after it has been proved that resonance states are responsible for the radiation damage[14, 15] in biological system.Thus, the resonance phenomena can be used as powerful tool to measure the genotoxic effects in living tissues.

Structural and spectroscopic properties of resonance states are quite similar to the bound state. The accurate calculation of position and lifetime of the resonance states are required to describe the several non-radiative decay processes in chemical physics such as Auger decay, ICD, [16] decay of double core hole states.[17] However, main difficulty in the calculation of resonance state is the treatment of the non square integrable resonance wavefunction. Thus, the usual bound state methods are not applicable. Resonance state can also be described as compound state between bound and continuum state. Thus, the calculation of resonance state requires simultaneous treatment of correlation and continuum effects.

Analytic continuation of the Hamiltonian in the complex energy plane is used to describe the resonance states. Two approaches are well known in literature through which analytic continuation of the Hamiltonian can be achieved, one is complex scaling approach [18] and another is complex absorbing potential (CAP) approach.[19–24] The complex scaling approach is suitable for the atomic systems. However, it is difficult to implement for the molecular systems. The main advantage of the CAP approach is that it is easy to implement with any $ab\ initio$ electronic structure methods.

For the accurate description of auto ionizing resonance states electron correlation and relaxation plays significant role. The EOM-CC method[25–33] treats relaxation effect and electron correlation in an effective manner. The EOM-CC method includes dynamic correlation through coupled cluster T operator and it includes non-dynamic correlation through R operator. The main advantage of method is that it gives direct intensive energy difference. This makes the EOM-CC method suitable for the accurate description of auto-ionizing resonance state.

The thesis is organized as follows:

CHAPTER I : This chapter deals with the brief overview of resonance phenomena. Eventually, in this chapter evaluation of position and lifetime of the resonance state using various L^2 approaches such as complex scaling, complex absorbing potential (CAP), complex basis function method are presented in detail. We discuss the various $ab\ initio$ methods used in the literature for resonance energy evaluation such as Fock-space multi-reference coupled cluster (FSMRCC) method, Multi-reference configuration interaction (MRCI), Algebraic diagrammatic construction approach (ADC) and EOM-CC approach. In this chapter, We also include brief discussion about the Interatomic or Intermolecular coulombic decay (ICD) and Auger decay.

CHAPTER II : In this chapter, the equation-of-motion coupled-cluster method (EOM-CC) is applied for the first time to calculate the energy and width of a shape resonance in an electron-molecule scattering. The procedure is based on inclusion of complex absorbing potential with EOM-CC theory. We have applied this method to investigate the

shape resonance in $e - N_2$, $e - CO$, and $e - C_2H_2$. We have also applied this method to study the potential energy curve (PEC) of $^2\Pi_g$ $e - N_2$ and $^2\Pi$ $e - CO$ resonance states.

CHAPTER III :In this chapter, the equation-of-motion coupled cluster (EOM-CC) method employing the complex absorbing potential (CAP) has been used to investigate the low energy electron scattering by CO_2. We have studied the potential energy curve (PEC) for the $^2\Pi_u$ resonance states of CO_2^- upon bending as well as symmetric and asymmetric stretching of the molecule. Specifically, we have stretched the $C - O$ bond length from 1.1 $\mathring{A}$ to 1.6 $\mathring{A}$ and the bending angles are changed between 180° to 132°. Upon bending, the low energy $^2\Pi_u$ resonance state is split into two components, i.e. $^2A_1$, $^2B_1$ due to the Renner-Teller effect (RT), which behave differently as the molecule is bent.

CHAPTER IV : In this chapter, we have explored about the Interatomic or Intermolecular coulombic decay (ICD) process. ICD is an efficient and ultrafast radiation less decay mechanism which can be initiated by removal of an electron from the inner-valence shell of an atom or molecule. Generally, the ICD mechanism is prevailed in weakly bound clusters. A very promising approach, known as CAP/EOM-CC, consists of the combination of complex absorbing potential (CAP) with the equation-of-motion coupled-cluster (EOM-CC) method, is applied for the first time to study the nature of the ICD mechanism. We have applied this technique to determine the lifetime of an auto-ionized, inner-valence excited state of the $Ne(H_2O)$, $Ne(H_2O)_2$ and $Ne(H_2O)_3$ systems. The lifetime is found to be very short and decreases significantly with the number of neighboring water molecules.

We have also applied this method to study the interatomic coulombic decay (ICD) mechanism in small hydrogen bonded clusters. The lifetime of F 2s inner-valence ionized state of $(\mathrm{HF})_\mathrm{n}$, (n=2-3) clusters were calculated using this method. The lifetime is found to be very short and decreases substantially with increasing the number of HF monomer.

CHAPTER V :In this chapter, we have explored about the Auger decay. The recent development of Linac coherent light source high intense x-ray laser makes it possible

to create double core ionization in the molecule. The generation of double core hole state and its decay is identified by Auger spectroscopy. The decay of this double core hole (DCH) states can be used as a powerful spectroscopic tool in chemical analysis. In this present work, we have implemented a promising approach, known as CAP/EOM-CC method, for the first time to calculate the decay rate of double core hole (kk) state. We have applied this method to calculate the lifetime of auto-ionized double core hole excited state in various systems. The calculated lifetime is found to be very short and the decay rate is faster compare to the single core hole (k) Auger decay.

CHAPTER VI :In this chapter, we have applied the CAP/EOM-CCSD method to compute how the interatomic or intermolecular coulombic decay (ICD) rate of molecule changes with changing the internuclear distance of the molecule. The calculation of ICD decay rate in different internuclear distances is a step towards understanding the dynamics in challenging systems involving inner valence excited states. In this chapter, the summary of the thesis is presented. We have also discuss the future perspective in this field.

References

[1] T. Sommerfeld, U. V. Riss, H. D. Meyer, L. S. Cederbaum, B. Engels, and H. U. Suter, *J. Phys. B* **31**, 4107 (1998);

[2] L. S. Cederbaum, J. Zobeley, and F. Tarantelli, *Phys. Rev. Lett.* **79**, 4778 (1997); N. Moiseyev, R. Santra, J. Zobeley, and L. S. Cederbaum, *J. Chem. Phys.* **114**, 7351 (2001).

[3] R. Santra, J. Zobeley, L. S. Cederbaum and N. Moiseyev, *Phys. Rev. Lett.* **85**, 4490 (2000)

[4] J. Zobeley, L. S. Cederbaum, and F. Tarantelli, *J. Phys. Chem. A* **103**, 11145 (1999).

[5] G. Öhrwall, M. Tchaplyguine, M. Lundwall, R. Feifel, H. Bergersen, T. Rander, A. Lindblad, J. Schulz, S. Peredkov, S. Barth, S. Marburger, U. Hergenhahn, S. Svensson, and O. Björneholm, *Phys. Rev. Lett.* **93**, 173401 (2004)

[6] S. Scheit, V. Averbukh, H. D. Meyer, N. Moiseyev, R. Santra, T. Sommerfeld, J. Zobeley, and L. S. Cederbaum, *J. Chem. Phys.* **121**, 8393 (2004).

[7] S. Scheit, V. Averbukh, H. D. Meyer, J. Zobeley, and L. S. Cederbaum, *J. Chem. Phys.* **124**, 154305 (2004).

[8] S. Barth, S. Joshi, S. Marburger, V. Ulrich, A. Lindblas, G. Öhrwall, O. Björneholm, and U. Hergenhahn, *J. Chem. Phys.* **122**, 241102 (2005).

[9] T. Jahnke, H. Sann, T. Havermeier, K. Kreidi, C. Stuck, M. Meckel, M. Schffler, N. Neumann, R. Wallauer, S. Voss, A. Czasch, O. Jagutzki, A. Malakzadeh, F. Afaneh, Th. Weber, H. Schmidt-Böcking, and R. Dörner, *Nature Phys.*, **6**, 139 (2010);

[10] M. Mucke, M. Braune, S. Barth, M. Förstel, T. Lischke, V. Ulrich, T. Arion, U. Becker, A. Bradshaw, and U. Hergenhahn, *Nature Phys.* **6**, 143 (2010); T. Jahnke, A. Czasch, M. S. Schöffler, S. Schössler, A. Knapp, M. Käsz, J. Titze, C. Wimmer, K.

Kreidi, R. E. Grisenti, A. Staudte, O. Jagutzki, U. Hergenhahn, H. Schmidt-Böcking, and R. Dörner, *Phys. Rev. Lett.* **93**, 163401 (2004).

[11] N. Sisourat, N. V. Kryzhevoi, P. Kolorenč, S. Scheit, T. Jahnke, and L. S. Cederbaum, *Nature Phys.* **6**, 508 (2010).

[12] P. Auger, *J. Phys. Radium* **6**, 205 (1925).

[13] L. S. Cederbaum, Y. C. Chiang, P. V. Demekhin, and N. Moiseyev, *Phys. Rev. Lett* **106**, 123001 (2011).

[14] J. Simons, *Acc. Chem. Res.* **39** 772 (2006).

[15] B. Boudïffa, P. Cloutier, D. Hunting, M. A. Huels, and L. Sanche, *Science* **287**, 1658 (2000)

[16] N. Vaval and L. S. Cederbaum, *J. Chem. Phys.* **126**, 164110 (2007).

[17] L. Inhester, G. Groenhof, and H. Grubmüller, *J. Chem. Phys.* **138**, 164304 (2013).

[18] N. Rom, N. Lipkin, and N. Moiseyev, *Chem. Phys.* **151**, 199 (1991).

[19] G. Jolicard and E. J. Austin, *Chem. Phys. Lett.* **121**, 106 (1985).

[20] W. P. Reinhardt, *Annu. Rev. Phys. Chem.* **33**, 223 (1982).

[21] N. Moiseyev, *Phys. Rep.* **302**, 211 (1998).

[22] U. V. Riss and H. D. Meyer, *J. Phys. B* **26**, 4503 (1993).

[23] N. Moiseyev, *J. Phys. B* **31**, 1431 (1998).

[24] U. V. Riss and H. D. Meyer, *J. Phys. B* **31**, 2279 (1998).

[25] M. Nooijen and R. J. Bartlett, *J. Chem. Phys.* **102**, 3629 (1995).

[26] M. Nooijen and R. J. Bartlett, *J. Chem. Phys.* **102**, 6735 (1995).

[27] J. F. Stanton and J. Gauss, *J. Chem. Phys.* **101**, 8938 (1994).

[28] J. F. Stanton and R. J. Bartlett, *J. Chem. Phys.* **98**, 7029 (1993).

[29] D. C. Comeau and R. J. Bartlett, *Chem. Phys. Lett.* **207**, 414 (1993).

[30] J. Geertsen, M. Rittby, and R. J. Bartlett, *Chem. Phys. Lett.* **164**, 57 (1989).

[31] L. Meissner and R. J. Bartlett, *J. Chem. Phys.* **102**, 7490 (1995).

[32] M. Nooijen and R. J. Bartlett, *J. Chem. Phys.* **107**, 6812 (1997).

[33] M. Musial and R. J. Bartlett, *J. Chem. Phys.* **134**, 034106 (2011).

List of Publications

1. Aryya Ghosh, Jitendra Gupta, Sourav Pal, and Nayana Vaval, 'Constrained variational approach for energy derivatives in Intermediate Hamiltonian Fock-space coupled-cluster theory' Chem. Phys. 401, 45 (2012).

2. Aryya Ghosh, Nayana Vaval, Sourav Pal, 'Equation-of-motion coupled-cluster method for the study of shape resonance' J. Chem. Phys. 136, 234110 (2012).

3. Aryya Ghosh, Sourav Pal, and Nayana Vaval, 'Study of interatomic Coulombic decay of $Ne(H_2O)_n$ (n = 1,3) clusters using equation-of-motion coupled-cluster method' J. Chem. phys. 139, 064112 (2013).

4. Aryya Ghosh, Anagha Karne, Sourav Pal, and Nayana Vaval, 'CAP/EOM-CCSD method for the study of potential curves of resonant states' Phys. Chem. Chem. Phys. 15, 17915 (2013).

5. Aryya Ghosh, Sourav Pal, and Nayana Vaval, 'Interatomic Coulombic decay in $(HF)_n$ (n = 23) clusters using CAP/EOM-CCSD method' Mol. Phys. 112, 669 (2014).

6. Jitendra Gupta, P. U. Manohar, Aryya Ghosh, Nayana Vaval, Sourav Pal, 'Extended coupled cluster through nth perturbation order for molecular response properties: A comparative study' Chem. Phys. 417, 45 (2013).

7. Himadri Pathak, Aryya Ghosh, B. K. Sahoo, B. P. Das, Nayana Vaval, and Sourav Pal, 'Relativistic equation-of-motion coupled-cluster method for the double-ionization potentials of closed-shell atoms' Phys. Rev. A 90, 010501(R) (2014).

8. Y Sajeev, Aryya Ghosh, Nayana Vaval, and Sourav Pal, 'Coupled cluster methods for autoionisation resonances' Int. Rev. Phys. Chem. 33, 397 (2014).

9. Aryya Ghosh, Nayana Vaval, Rodney J. Bartlett, and Sourav Pal, 'CAP/EOM-CCSD method for the potential energy curve of CO_2^- anion' J. Chem. Phys. (2014) (under revision).

10. Aryya Ghosh and Nayana Vaval, 'The potential curve for the lifetime of Interatomic coulombic decay(ICD) mechanism using equation-of-moton coupled cluster (EOMCC) method' J. Chem. Phys. (2014). (Under review).

11. Aryya Ghosh, Sourav Pal, and Nayana vaval, 'Equation-of-motion coupled cluster method for the core hole and double core hole Auger decay' J. Phys. Chem. Lett. (2014) (Submitted).

12. Aryya Ghosh, Sourav Pal and Nayana Vaval 'Equation-of-motion coupled cluster for the calculation of lifetime of core hole and double core hole satellite states' J. Chem. Phys. (to be submit).

13. Aryya Ghosh, Sourav Pal and Nayana Vaval 'Equation-of-motion coupled cluster for the Interatomic coulombic decay(ICD) of double ionized states' (manuscript under preparation).

Chapter 1

A brief Overview: shape resonance, Interatomic or Intermolecular coulombic decay (ICD), Auger decay and various ab initio methods

1.1 Introduction

Resonance phenomena,[1–14] which occur in electron molecule collision, are considered as the most useful phenomena in atomic or molecular physics due to its role in various energy exchange processes like vibrational excitation, dissociative attachment, etc. It provides deep insight about the molecular system. One of the most amazing feature of resonance phenomena is that it plays a significant role in long lasting DNA damage [15–17] of the biomolecular system. Thus the resonance phenomena can be used as a powerful tool in the measurement of genotoxic effects in biological system.

Resonance phenomena are associated with quasi bound states or metastable states which has sufficient energy and finite lifetime and finally it breaks into two fragments. Resonance state can also described as discrete state which is strongly interconnected with the continuum state. Generally, resonance phenomena are sub-dvided into two classes, one is shape resonance and another is Feshbach resonance. Shape resonances are those where electron capture occurs through the shape of the potential barrier. The shape resonances can also be characterized by intermediate negetive anionic complexes, which have very short lifetime and finally, it decay into the neutral target molecule and and a scattered electron. Generally, it occurs in femto-second(fs) (10^{-13}- 10^{-15}) time domain.

The metastable resonance states are described by complex eigenvalues, which are known as Siegert energies,[18, 19]

$$E_{res} = E_R - i\Gamma/2. \tag{1.1}$$

where E_R represents the resonance position and Γ is the decay width. The decay width Γ is inversely related with the lifetime $\tau = \hbar/\Gamma$.

From the structural and spectroscopic point of view resonance states have strong similarities with the bound states. The accurate description of resonance states is extremely important to explore the various spectroscopic phenomena. It also plays a crucial role in describing various non-radiative decay processes like Auger decay,[20–22] Interatomic or Intermolecular decay (ICD),[23–38] double core hole Auger decay, etc. However, the main difficulty in the calculation of resonance states is that the Siegert wave function is not square integrable in nature. Thus, the usual bound state methods are not applicable. The electron correlation and relaxation effects also play an important role in the calculation of resonance state. Thus, the calculation of resonance state required simultaneous treatment of both electron correlation and relaxation effects.

The complex resonance energy can be calculated directly within the hilbert space using the analytic continuation of the Hamiltonian technique. [39, 40] The main advantage

of this technique is that it can be applicable to the all existing $ab\ initio$ quantum chemistry methods and resonance energies come out simple as eigenvalues. Two approaches are very much well known in literature through which analytic continuation of Hamiltonian can be achieved, one is complex absorbing potential approach (CAP) and another is complex scaling approach. The other approach is complex basis function method. The complex scaling approach has been implemented successfully for the atomic systems. However, it is difficult to implement for the molecular systems. The CAP approach is very easy to implement in any $ab\ initio$ electronic structure methods.

The aim of the present chapter is to give a brief over-view of resonance phenomena and various $ab\ initio$ methods which have been used to calculate the position and lifetime of the resonance state. In particular, the literature towards complex absorbing potential (CAP), complex scaling approaches are discussed. A brief discussion on Interatomic or Intermolecular coulombic decay (ICD) and Auger decay are also presented.

1.2 Resonances in Scattering

The resonaces appear through two kinds of collision channels, one is elastic collision channels and another is inelastic channels. The formalism of resonances through elstic channels is much simpler compared to the inelastic channel. In this thesis, we have discussed briefly about the resonances through elastic collision channels.

Consider the elastic scattering of an incident particle in the z direction by a central field potential V(r). The incident particle behaves as a free particle in a large negetive values of time t. For a large negetive values of t the incident particle is not influenced by the potential V(r). Its state can be represented by a plane wave e^{ikz}. However, the incident particle behaves differently in the field of V(r). it is now split into two wave packets, one is transmitted wave packet which continues to propagate in the positive z direction and another is scattered wave. The eigenstates satisfying these conditions is called stationary scattering state $\gamma_k^{diff}(r)$ and is obtained by the superposition of a plane

wave and a scatterd wave. The asymptotic behavior of the stationary scattering state is of the form:

$$\gamma_k^{diff}(r) \sim e^{ikz} + f_k(\theta\phi)e^{ikz}/r \tag{1.2}$$

where $f_k(\theta, \phi)$ is called the scattering amplitudes.

The scattering wave function is defined by the asymtotic form of the wave function,

$$\Psi(r,t) \sim \int_0^\infty g(k)e^{ikz}e^(-iE_kt/\hbar)dk + \int_0^\infty g(k)f_k(\theta,\phi)e^{ikr}/re^(-iE_kt/\hbar)dk, \tag{1.3}$$

which is a sum of plane wave packet and scattered wave packet.

In a particular value of V(r), the orbital angular momentum is constant in motion. Thus, there exist stationary state with well defined angular momentum. We can call these states as partial waves. For the large r value corresponding wave function behaves like a free spherical wave function. The expression for the partial wave and spherical wave can be determined from the superposition of incoming wave and outgoing wave. However, there is a phase shift in presence of V(r) in the partial waves. Generally, phase shift changes slowly with the energy change. The resonance occurs when the phase shift changes rapidly over a small energy change. The phase shift can be split into back ground phase shift and the resonance phase shift. Neglecting the background phase shift Breit-Winger formulla can describe an isolated scattering resonance. The mathamatical form of the Breit-Winger formulla is

$$\sigma_l = 4\pi/k^2(2l+1)(\Gamma/2)^2/(E_0 - E)^2 + (\Gamma/2)^2 \tag{1.4}$$

The negative ion resonances in electron-molecule collision appear as sharp changes in scattering cross section at low incident electron energies. At some incident energies, the electron wavefunction has large amplitude within the target. This happens only when the incident energy falls in one of the discrete bands, where the incident electron finds

a comfortable quasistationary orbit in the field of target molecule. The quasi stationary nature of the compound state is usually follw two mechanism. The first possibility and the most common situation that causes the appearance of resonance is an effective potential made up of attractive potential [attractive polarization force at small distances] combined with a repulsive potential [repulsive centrifugal force at long distances] produces a barrier in the potential. For energies below the maximum in the barrier, there would be bound states inside the attractive part of the potential if tunneling could be ignored. However, the quantum mechanical tunneling permits particle trapped inside the attractive part of the potential to escape to infinity, and the tunneling rate depends on the height and thickness of the barrier. Conversely, particles incident on the potential at energy close to the virtual states are able to penetrate inside the attractive barrier. This behavior explains why resonance generally becomes narrower as l increases. Larger l values causes bigger centrifugal barriers, thus suppressing tunneling. Once the electron has entered the region inside the barrier, it will take some time before the electron leaks out to the outer region again by a tunnel effect. This type of resonance is called shape resonance or potential resonance since the resonance state is produced by an appropriate shape of the effective interaction potential between the electron and the molecule.

The second possibility arises when the inelastic channels are introduced. By exciting the target molecule, the electron loses its energy. Suppose that the incident electron energy is not large that after the excitation the electron energy becomes negative, and furthermore, its value coincides with one of the bound-state energies allowed in the field produced by the excited target molecule. Then it will take some time before the electron gets its energy back from the target and escape to outside. Thus one has a new type of resonance process which is called core-excited type I resonance or the resonance of Feshbach resonance. There exists also shape resonances associated with the effective potential in the inelastic channel. They are called core-excited type II resonance or core excited shape resonances.

1.3 complex scaling

Complex scaling approach has capability to solve the resonance eigenvalue problems directly. This approach is based on the fundamental work of Balslev, Combes and Simon. [41–43] This method is based with a unbound similarity transformation.[44–46] The resonanace state can be identified by square integrable functions associated with the eigenfunctions of a transformed Hamiltonian UHU^{-1}, which is obtained from the original Hamiltonian H by an unbound similarity transformation. That is,

$$(UHU^{-1})(U\Psi_R) = (E_{res} - i\Gamma/2)(U\Psi_R) \tag{1.5}$$

such that

$U\Psi_R \to 0$ and r $\to \infty$

and $U\Psi_R$ is in Hilbert space although Ψ_R are not.

The complex scaling operator can be defined as

$$U = e^{i\theta r\partial/\partial r} \tag{1.6}$$

such that

$$Uf(r) = f(re^{i\theta}) \tag{1.7}$$

for any analytical function f(r).

By scaling the reaction coordinate, the resonance wave function becomes square integrable and, consequently, the number of particles in the coordinate space is conserved. Therefore, complex scaling [47–52] has the advantage of associating the resonance phenomenon with the discrete part of the spectrum of the complex scaled Hamiltonian. Moreover, the resonance state is associated with a single square integrable function, rather than with a collection of continuum eigenstates of the unscaled Hermitian Hamiltonian. Complex scaling may be viewed as a procedure which compresses the information about the evolution of a resonance state at infinity into a small well defined part of the space.

1.4 Complex absorbing potential

Complex absorbing potential approach is very promising in the description of the energy position and lifetime of atomic, molecular and nuclear collision processes. [53–58] The molecular Hamiltonian is perturbed by an appropriate complex potential, which creates an absorbing boundary condition. This complex potential absorbs the outgoing particle and consequently convert the resonance wave function into a bound state one.

In the CAP approach [59, 60] CAP potential -$i\eta W$ is added to the Hamiltonian H to describe the electronic resonance state,

$$H(\eta) = H - i\eta W \tag{1.8}$$

where η is a real positive number representing the CAP strength and W is a local positive-semidenite one-particle operator. The new Hamiltonian $H(\eta)$ satises the Schródinger equation

$$H(\eta)\Psi(\eta) = E(\eta)\Psi(\eta). \tag{1.9}$$

The presence of CAP makes the Hamiltonian operator non-Hermitian. If one chooses the appropriate CAP form, the addition of complex potential causes an asymptotic damping of the Siegert eigenfunction which makes the wave function square integrable. The spectrum becomes discrete. However, the artificial introduction of the CAP potential perturbs the Hamiltonian, one can obtain the exact resonance eigenvalues in the limit $\eta \to 0$ for a complete basis set. In practical computation, one cannot solve the Siegert energy spectrum exactly since incomplete basis sets are used and one is forced to use finite η values. The resonance energies are obtained through the diagonalization of $H(\eta)$ for a number of η values. The combination of resulting eigenvalues give an η trajectory. The η trajectory is examined by using the logarithmic velocity $\upsilon(\eta)$. The resonance energy is explored through the minimization of logarithmic velocity

$$\upsilon(\eta) = \eta\partial E/\partial\eta. \tag{1.10}$$

The existence of a distinct minimum,

$$|\upsilon(\eta_{opt})| = min, \tag{1.11}$$

gives the optimal η value.

Historically, CAP has been used for the first time to calculate the resonance parameters by Jolicard and Austin. [61, 62] They have illustrated the stability of the resonance eigenvalue could be achieved by varying the strength or the location of the absorbing potential. Riss and Meyer addressed the question under what condition the resonances obtained by the CAP are the poles of the scattering matrix.[59] Nimrod Moiseyev has developed a universal energy independent complex absorbing potential (CAP) [53] on the basis of the Moiseyev -Hirschfelder generalization of complex coordinate method. This CAP consists of flux and diffusion type operator. When a smooth exterior scaling is used, the CAP gets non zero values in the region where the interaction potential vanishes. Riss and Meyer also developed another method called transformative CAP (TCAP). [63] There is a connection between the smooth exterior scaling [SES] with the transformative CAP [TCAP]. The TCAP and SES in fact become identical for cut-off potentials. For the TCAP method, Riss and Meyer started from the Hamiltonian perturbed by a CAP and ended up with a complex-scaled operator. Instead, For the SES method, Moiseyev started with the complex coordinate method and ended up with a non-scaled Hamiltonian perturbed by a perfectly absorbing [universal] potential which is energy and problem independent. Moiseyev and co-workers [64] have also developed a continuum remover complex absorbing potential (CR-CAP) [65] where a real-valued potential is added to the conventionally used negative imaginary potential in the peripheral of the molecule. This new approach has excellent capability to separate out the non-physical resonance states form the physical states.

1.5 Analytic continuation of various $ab\ initio$ methods

The analytically continued $ab\ initio$ methods are well known in the calculation of direct resonance energy. [66] The various analytically continued $ab\ initio$ methods are available in literature. The self consistent field (SCF) is the starting point of any $ab\ initio$ correlated method. McCurdy et al. [67] have developed complex scaled SCF method for the calculation of resonance energies. In their approach, a real Hamiltonian is used together with the complex wave functions. However, another complex SCF method has been developed by Öhrn and co-workers. [68, 69] In their approach, complex Hamiltonian is used. Recently, Yeager and co-workers have proposed the quadratically convergent complex-scaled multi-configurational self-consistent field method (CMCSCF), [70] the complex-scaled multi-configurational time-dependent Hartree-Fock method (CMCTDHF) [71] and complex-scaled multi-reference configuration interaction method (CMRCI). [72] Buenker and co-workers [73, 74] have used self-consistent field and multireference single- and double-excitation configuration interaction (MR-CISD) calculations employing the complex basis function approach for the calculation of anionic resonances. The complex basis function method has also been developed by Moiseyev and McCurdy. [49]

The CAP [75–80] is an one-electron potential and its use in *ab initio* methods is rather easy compared to the complex scaling. The CAP approach has already been successfully implemented in various $ab\ initio$ methods. The first implementation of CAP method within the configuration interaction (CI) approach has been done by Sommerfeld et al. [78]for metastable anions. Santra et al. [76] have also implemented CAP within the CI framework for metastable cations. Later on, Santra et al. have applied CAP to the the propagator theories and used CAP/ADC approach [79] to describe the resonanaces of metastable anions. Mishra and coworkers [81] have introduces bivariational self consistent field (SCF) based second order propagator method to describe the Auger and shape resonances. Ehara et al. have introduced CAP within the SAC/CI framework. [82]

The CAP [83] has also been implemented within the Rayleigh-Schrödinger perturbation theory.[84]

Recently, Sajeev et al. [85] have introduced CAP within the Fock-space multireference coupled cluster (FSMRCC) framework to study the resonances of anions. Very recently, CAP has also been implemented successfully within the density functional theory (DFT).[86].

1.6 Coupled cluster

The coupled cluster (CC) methods form another popular approach to the problem of constructing correlated wave functions. The CC theory has been employed for decades in the physics community, particularly in the area of nuclear physics by Cöester and Kümmel [87] to deal with double magic atomic nuclei. It was originally introduced into the quantum chemistry community by $\check{C}\acute{i}\check{z}$ek and Paldus [88, 89] in the late 1960's. These early formulations used Feynman-like diagrams and the notation of second quantization to aid in the derivation of programmable CC equations. Both Feynman diagrams and second quantization concepts were alien to quantum chemists, it was Hurley [90] to present derivation of CC theory in terms accessible to chemists. Despite Huley's derivation, the use of second quantization and diagrammatic theory is still beneficial in the efficient derivation of CC equations. The use of these efficient derivation tools is so important to CC theory[91, 92] because, unlike CI theory in which the core problem is the diagonalization of the Hamiltonian matrix with elements given by Slater's rules and in which individual methods only differ in the basis functions used to construct this matrix, standard CC theory requires the iterative solution of algebraic equations which must be re-derived with each change in method.

The CC method employs an excitation operator $\hat{T}$,

$$\hat{T} = \hat{T}_1 + \hat{T}_2 + ... = \sum_{n}^{N} \hat{T}_n. \tag{1.12}$$

with

$$\hat{T}_n = (\frac{1}{n!})^2 \sum_{ij...ab...}^{n} t_{ij...}^{ab...} a_a^\dagger a_b^\dagger ... a_j a_i \tag{1.13}$$

The $\hat{T}$ operator of CC theory acts exponentially:

$$\Psi_{CC} = e^{\hat{T}} |\Phi_0\rangle. \tag{1.14}$$

The $t_{ij...}^{ab...}$ coefficients in the $\hat{T}_n$ operators are known as cluster amplitudes. An truncated CC method may be constructed by including only the desired excitation operators within $\hat{T}$. For example, the popular CCSD method is realized when only the $\hat{T}_1$ and $\hat{T}_2$ operators are included within $\hat{T}$. The interesting thing is that the exponential approach produces a method which is both size consistent and size extensive, provided the reference function possesses these qualities, even when $\hat{T}$ is truncated at a chosen excitation level.

Beginning from the universal starting point, the Schrödinger equation, one substitutes in the form of the CC wave function given by eq 1.14 and finds

$$\hat{H} e^{\hat{T}} |\Phi_0\rangle = E e^{\hat{T}} |\Phi_0\rangle. \tag{1.15}$$

Projecting through on the left by the reference, $|\Phi_0\rangle$, one can obtain an expression for the energy

$$\langle \Phi_0 | \hat{H} e^{\hat{T}} |\Phi_0\rangle = E \langle \Phi_0 | e^{\hat{T}} |\Phi_0\rangle = E, \tag{1.16}$$

provided one employs the technique of intermediate normalization and sets the overlap between the reference and the CC wave function i.e., $\langle \Phi_0 | \Psi_{CC} \rangle$ equal to unity. Obtaining an energy expression is only the first step, however one must also determine all of the cluster amplitudes which define the wave function with this energy. In order to accomplish this, one must left-project eq 1.16 by the excited determinants produced by the action of the $\hat{T}$ operator:

$$\langle \Phi_{ij...}^{ab...} | \hat{H} e^{\hat{T}} |\phi_0\rangle = E \langle \Phi_{ij...}^{ab...} | e^{\hat{T}} |\Phi_0\rangle. \tag{1.17}$$

For example, one can produce an equation for the specific amplitude t_{ij}^{ab} by left-projecting by the $|\Phi_{ij}^{ab}\rangle$ excited determinant. The resulting equation is non-liner and depends upon other cluster amplitudes. However, these equations are exact, and if one were able to solve them with the full $\hat{T}$ operator, one would indeed obtain the full CI energy and wave function.

The CC method depends upon the action of the exponential excitation operator $e^{\hat{T}}$ on the reference. The excitation operator is expanded as the power series

$$e^{\hat{T}} = 1 + \hat{T} + \frac{\hat{T}^2}{2!} + \frac{\hat{T}^3}{3!} + \cdots . \tag{1.18}$$

As a matter of fact, the equivalence of $e^{\hat{T}}$ and this power series is commonly used in the various arguments employed to justify the exponential ansatz. From eq.1.16 one get

$$E = \langle\Phi_0|\hat{H}|\Phi_0\rangle + \langle\Phi_0|\hat{H}T|\Phi_0\rangle + \langle\Phi_0|\hat{H}\frac{\hat{T}^2}{2!}|\Phi_0\rangle + \langle\Phi_0|\hat{H}\frac{\hat{T}^3}{3!}|\Phi_0\rangle + \cdots \tag{1.19}$$

from which one can find another benefit of the exponential formalism. The Hamiltonian operator only includes one- and two- particle operators, and thus, according to Slater's rules, matrix elements of the Hamiltonian between determinants which differ by more than two spin orbitals must vanish. Therefore, the fourth and subsequent terms in the above expansion, in which the $\hat{T}$ operator is raised to the third or higher power and can thus produce only triply or higher excited determinants when operated upon the reference, must also vanish and the energy expression is truncated to

$$E = \langle\Phi_0|\hat{H}|\Phi_0\rangle + \langle\Phi_0|\hat{H}T|\Phi_0\rangle + \langle\Phi_0|\hat{H}\frac{\hat{T}^2}{2!}|\Phi_0\rangle. \tag{1.20}$$

This is a natural truncation of the CC equations due to the nature of the Hamiltonian and also applies to the amplitude equations, although the exact range of allowed powers of $\hat{T}$ will vary from that seen for the energy expression. Therefore, in practical CC derivations, theorists exploit a bit of mathematical experience and multiply eq 1.16 through on the left by $e^{-\hat{T}}$. Subsequent left-projection by the reference and excited determinants produces the following new set of energy and amplitude equations:

$$E = \langle\Phi_0|e^{-\hat{T}}\hat{H}e^{\hat{T}}|\Phi_0\rangle \tag{1.21}$$

$$\langle \Phi_{ij\cdots}^{ab\cdots} | e^{-\hat{T}} \hat{H} e^{\hat{T}} | \Phi_0 \rangle = E \langle \Phi_{ij\cdots}^{ab\cdots} | e^{-\hat{T}} e^{\hat{T}} | \Phi_0 \rangle = E \langle \Phi_{ij\cdots}^{ab\cdots} | \Phi_0 \rangle = 0 \tag{1.22}$$

respectively. Notice that the introduction of the $e^{-\hat{T}}$ operator cancels out its $e^{\hat{T}}$ counterpart in the amplitude equations and guarantees that the right hand side vanishes, taking any dependence of the amplitudes on the energy with it. The similarity transformed Hamiltonian, $e^{-\hat{T}} \hat{H} e^{\hat{T}}$, employed in the above energy and amplitude equations is not a Hermitian operator; therefore, the energy equation does not satisfy any variational conditions where the energy is derived from the Average Value Theorem. Despite this disadvantage, which is considered to be small by a number of theorists, the use of this similarity transformed Hamiltonian has as a second benefit which makes this formulation of the CC equations both practical and desirable. The $e^{-\hat{T}} \hat{H} e^{\hat{T}}$ operator may be expanded as a linear combination of nested commutators

$$e^{-\hat{T}} \hat{H} e^{\hat{T}} = \hat{H} + [\hat{H}, \hat{T}] + \frac{1}{2!}[[\hat{H}, \hat{T}], \hat{T}] + \frac{1}{3!}[[[\hat{H}, \hat{T}], \hat{T}], \hat{T}] + \frac{1}{4!}[[[[\hat{H}, \hat{T}], \hat{T}], \hat{T}], \hat{T}] + \cdots \tag{1.23}$$

according to the Campbell-Baker-Hausdorff formula.

While the expansion of the similarity transformed Hamiltonian given above in equation 1.23 may not, at first glance, appear to be simple but the sequence of nested commutators naturally truncates due to the structure of the electronic Hamiltionian. The second quantized form of the Hamiltonian includes strings containing at most a total of four general-index creation and annihilation operators. When one evaluates the commutator between the Hamiltonian and the $\hat{T}$ operator, one replaces one of these operators by a Kronecker delta function. This reduces the number of available general-index operators in the Hamiltonian by one. Thus, the sequence of nested commutators in eq.1.23 must truncate after the five terms explicitly written. Using this truncated Hausdorff expansion, it is possible to obtain analytic expressions for the commutators which may be inserted into both the energy and amplitude equations. Finally, these equations may then be reduced into expressions that depend only on the amplitudes and the known one- and two-electron integrals.

1.7 Equation-of-motion coupled cluster

The starting point for the EOM-CC method [93–97] is a coupled cluster (CC) ground state wave function. In CC method, the ground state wave function can be defined as

$$|\psi_0\rangle = e^T|\phi_0\rangle, \tag{1.24}$$

where ϕ_0 is the N-electron close shell reference determinant .e.g., the restricted Hartree-Fock determinant (RHF) and T is the cluster operator. In the coupled cluster singles and doubles (CCSD) approximation, T operator can be defined as follows

$$T = \sum_{ia} t_i^a a_a^+ a_i + 1/4 \sum_{ab} \sum_{ij} t_{ij}^{ab} a_a^+ a_b^+ a_i a_j + ..., . \tag{1.25}$$

where the standard convention for the indices is used, i.e., indices a,b,..., refer to the virtual spin orbitals and indices i,j,.., refer to the occupied spin orbitals.

Within the EOM-CCSD formalism [98–106], the wave function for the ionized, electron attached, double ionized states, ψ_μ, can be expressed as

$$|\psi_\mu\rangle = R(\mu)|\psi_0\rangle, \tag{1.26}$$

where $R(\mu)$ is ionization, electron attachment, double ionization, etc, operator

$$R(\mu) = r_0(\mu) + R_1(\mu) + R_2(\mu) + R_3(\mu) + ... \tag{1.27}$$

The $R(\mu)$ can be defined via creation -annihilation operator depending on the considered process as follows

$$R(\mu)^{IP} = \sum_i r_i(\mu) a_i + 1/2 \sum_a \sum_{ij} r_{ij}^a(\mu) a_a^+ a_j a_i + ... \tag{1.28}$$

$$R(\mu)^{EA} = \sum_a r^a(\mu) a_a^+ + 1/2 \sum_{ab} \sum_i r_i^{ab}(\mu) a_a^+ a_b^+ a_i + ... \tag{1.29}$$

$$R(\mu)^{DIP} = 1/2 \sum_{ij} r_{ij}(\mu) a_i a_j + 1/6 \sum_a \sum_{ijk} r_{ijk}^a(\mu) a_a^+ a_k a_j a_i + ... \tag{1.30}$$

The $R_1(\mu)$ operator does not contribute to the expansion of $R(\mu)^{DIP}$ operator. The r_0 operator is zero for IP, EA, DIP, etc.

The Schrödinger equation for IP, EA, DIP states can be expressed as

$$H_N R(\mu)|\psi_0\rangle = \Delta E_\mu R(\mu)|\psi_0\rangle \tag{1.31}$$

where $\mathrm{H_N}$ is the normal ordered Hamiltonian and it can be expressed as

$$H_N = H - \langle\phi_0|H|\phi_0\rangle \tag{1.32}$$

The final form of EOM-CC equation is

$$\bar{H_N} R(\mu)|\phi_0\rangle = w_\mu R(\mu)|\phi_0\rangle \tag{1.33}$$

where w_μ is the energy change connected with the considered process. The $\bar{H_N}$ is the similarity transformed Hamiltonian, in terms of connected diagrams and it can be defined as

$$\bar{H_N} = e^{-T} H e^{T} - \langle\phi_0|e^{-T} H e^{T}|\phi_0\rangle \tag{1.34}$$

In a matrix form eq 6.10 is

$$\bar{H_N} R(\mu) = w_\mu R(\mu) \tag{1.35}$$

The $\bar{H_N}$ matrix is diagonalized in the sub space of 1h and 2h1p space to get the required ionization potential (IP) values and EA values are obtained through the diagonalization of $\bar{H_N}$ matrix in the sub space of 1p and 2p1h space.

The double ionization potential (DIP) values are obtained through non-symmetric diagonalization of $\bar{H_N}$ matrix in the subspace of 2h and 3h1p space.

1.8 CAP/EOMCC

In the CAP/EOM-CCSD method, CAP is applied to the EOM-CCSD method to calculate the resonance energy and lifetime of the resonance state. Here, CAP has been applied to

the CC method to generate the complex $T(\eta)$ amplitudes, which has been used latter to generate the $\bar{H_N}$ matrix. After addition of CAP to the CC method, the modified ground state wave function of CC method can be written as

$$|\psi_0(\eta)\rangle = e^{T(\eta)}|\phi_0\rangle \tag{1.36}$$

Then, the CAP is added to the one-body particle-particle part ($\bar{f_pp}$) of the $\bar{H_N}$ matrix. The new form of the modified $\bar{H_N}$ modified matrix is

$$\bar{H_N}(\eta) = e^{-T(\eta)}H_N(\eta)e^{T(\eta)} - \langle\phi_0|e^{-T(\eta)}H_N(\eta)e^{T(\eta)}|\phi_0\rangle \tag{1.37}$$

$$\bar{H_N}(\eta)R_\eta(\mu) = w_\mu R_\eta(\mu) \tag{1.38}$$

Finally, the $\bar{H_N}$ matrix is diagonalized for different η values . Diagonalization of $\bar{H_N}$ matrix gives the complex eigenvalues. However, the resonance energy is obtained by using the following equation since the ground state energies are supposed to be CAP free.

$$E_{res}(\eta) = w_\mu(\eta) + E_{srcc}(\eta) - E_{srcc}(\eta = 0). \tag{1.39}$$

However, in this procedure the entire steps need to be done for few 100 times for different η values starting from $\eta = 0$. The calculation of SRCC for each η value is computationally expensive since it scales as N^6. we also loose the advantage of direct energy difference. To overcome all these difficulties a new approximation has been introduced for the inclusion of CAP at the EOM-CC level by keeping the ground state ψ_0 CAP free. Thus the ground state wave function can be defined as

$$\psi_\mu(\eta)\rangle = R_\mu(\eta)|\psi_0\rangle. \tag{1.40}$$

The SRCC has been solved first without any CAP potential. The cluster amplitudes $T(\eta = 0)$ are scaled with the CAP potential by using the following equations

$$D_1 = f_{aa} - f_{ii} \tag{1.41}$$

$$t_i^a = [t_i^a(\eta = 0) * D_1]/[D_1 + W_{aa}(\eta)] \tag{1.42}$$

$$D_2 = f_{aa} + f_{bb} - f_{ii} - f_{jj} \tag{1.43}$$

$$t_{ij}^{ab}(\eta) = [t_{ij}^{ab}(\eta = 0) * D_2]/[D_2 + W_{aa}(\eta) + W_{bb}(\eta)] \tag{1.44}$$

With these new amplitudes $\bar{H_N}$ matrix is constructed. Then, the CAP is added to the one-body particle particle ($\bar{f_{pp}}$) of the $\bar{H_N}$ matrix. So, the modified $\bar{H_N}(\eta)$ can be defined as

$$\bar{H_N}(\eta) = e^{-T(\eta)} H_N(\eta) e^{T(\eta)} - \langle \phi_0 | e^{-T} H_N e^{T} | \phi_0 \rangle \tag{1.45}$$

$$\bar{H_N}(\eta) R_\mu(\eta) = w_\mu(\eta) R_\mu(\eta). \tag{1.46}$$

Thus the SRCC part is independent of CAP perturbation. The advantage of this approximation is that it enormously reduces the computational time since in this approximation the SRCC calculation needs to be done only once to generate the η trajectory. The resonance energy comes out to be the direct energy difference obtained as eigenvalues of $\bar{H_N}(\eta)$ matrix for different η values.

The Davidson Algorithm is used to diagonalize the $\bar{H_N}$ matrix. In the EOM-CCSD method, the matrix dimension becomes sufficiently large. The dimension becomes more than 10,000 even if the small molecules and moderate size basis sets are used. A full diagonalization of such matrices are not possible. The Davidson Algorithm [107, 108] helps to use the EOM-CC method for the study of resonance problem of the moderate size systems. The main idea of Davidson Algorithm is that the eigenvalues are obtained through an iterative technique which avoids the computational storage of complete matrix and stops when certain convergence criteria is fulfilled. In the Davidson Algorithm, the dimension of the matrix is equal to the number of iterations.

The complex eigenvalues $w_\mu(\eta)$ are obtained after solving the eq. 1.38 and eq. 1.46 for the different η values. By plotting the complex solutions in the complex energy plane with the real part and imaginary part of the energy axes. We get the η trajectory. A resonance energy is identified with the appearance of stabilization cusps

$$\upsilon_\mu(\eta) = \eta \partial w_\mu(\eta)/\partial \eta. \tag{1.47}$$

1.9 Interatomic or Intermolecular coulombic decay (ICD)

When an atom or molecule is electronically excited, it can relax via radiative decay or non-radiative decay . If the atom or molecule is excited by creating a vacancy in the outer valence level then the atom or molecule preferably follow the radiative decay pathway like photon emission for relaxation. If the excitation occurs by creating a vacancy in the core level then the electronically excited atom or molecule decay via non-radiative electron emission. However, another alternative ultrafast non-radiative decay mode is operative, called Interatomic or Intermolecular coulombic decay (ICD), if the excited atom or molecule is embedded into the chemical environment. The ICD [23–28] occurs only in the presence of neighbors. It is highly sensitive to the chemical environment. Thus, the ICD can be used as a powerful spectroscopic tool to probe the chmical environment.

The ICD [29–31] can be initiated by emitting an electron from the inner valence level of an atom or molecule. In ICD, after creating a vacancy in the inner valence level of a particular monomer, an outer valence electron from the same monomer comes out to fill up the vacancy in the inner valence level and the released energy is transferred to the neighboring monomer from which a secondary electron is ejected. The ejected secondary electron is called ICD electron. The ICD electron contains very low energy of the order of few electron volts. In ICD, the initial state is an inner valence hole and final state is identified by two outer valence hole which are placed on two different monomers. Thus, the two positive charged ions are formed in the ICD process. Being presence of two positive charges, they repel each other and their occurs a coulomb explosion in the system. After coulomb explosion the two positively charged ions fly apart from each other and finally, the system breaks down into two separate fragments. Thus, the ICD process produces free radicals. Being highly reactive, these free radicals can give additional damage to the biological system when these free radicals interact with the biomolecular system. The ICD process also produces low energy electrons from the molecular neighbor of initially excited molecular ion of the order of 3-5 electron volts

(eV). Recently, it has been proved that the low energy electron can efficiently break up the DNA stand break.[16, 17] Thus, the ICD process can act as a source of electrons which can produce radiation damage to the biomolecular system.

The ICD is a very fast relaxation process in environment. Generally, it occurs in femto second (fs) time domain. No other process such as photon emission, the process involving nuclear dynamics can not compete with the ICD process. These are very very slow process compare to the ICD. They occus in nano second (ns) time domain.[109] Another non-radiative relaxation process which can compete with ICD is called Auger decay. It also occurs in femto second time domain or even atto-second time domain.

In principle, ICD can be suppressed by Intramolecular Auger decay if it is energetically favorable. However, if the intramolecular auto-ionization is energetically favorable for the inner valence ionized atom or molecule and the molecule has neighbors then the molecule prefers to follow the ICD pathway for relaxation. The ICD relaxation process is very much general in nature. It prevails in weakly bound clusters. The weakly bound hydrogen bonded clusters, [110] Van der Waals clusters [111–113] are the suitable systems for ICD.

The spatial separation of two positively charged holes on two different monomers makes the ICD process energetically viable because the presence of two positive holes on two different monomers reduces the coulomb repulsion between them which lowers the double ionization potential (DIP) value.[111–113] Finally, the DIP value becomes lower than the one inner valence IP value. This makes the system energetically favorable [114] because when it goes from one inner valence ionized state to two outer valence double ionized state the system gains energy.

The ICD has been studied quite throughly for both theoretically and experimentally. The ICD is a phenomena which has been predicted theoretically first and later on it has been proved experimentally. The existence of ICD phenomena has been predicted theoretically for the first time by Cederbaum et al. in 1997.[23] In their work, they have shown the existence of ICD for the first time on hydrogen bonded $(HF)_3$ $(H_2O)_3$

clusters. The study of ICD of hydrogen fluoride and water clusters [115] is extended later using various theoretical approaches. Santra et al. [76] have implemented the CAP/CI approach for the first time to study the ICD decay rate of an inner valence excited state of small hydrogen bonded cluster. In their work, they have applied the CAP/CI method to study the lifetime of 2s inner valence excited state of F atom om in HF_2. The results obtained in this method suggested that the ICD decay rate is very fast in nature and it occurs in femto second time scale in HF clusters. The existence of ICD has also been proved in mixed hydrogen bonded $\mathrm{HF}(\mathrm{H_2O})_2$ cluster.[116]

The existence of ICD has also been proved for the noble gas clusters. Among the noble gas clusters, the neon dimer $\mathrm{Ne_2}$ is the system which has been investigated in a more elaborate manner. The various theoretical approaches have been applied to calculate the lifetime of 2s inner valence excited state of $\mathrm{Ne_2}$. Santra et al. have applied the CAP/CI method to calculate the ICD decay rate of 2s inner valence excited state of Ne_2. In their work, they have found that in equilibrium bond distance ($3.2\mathring{A}$) the lifetime of 2s inner valence excited state of $\mathrm{Ne_2}$ is 64 fs. [77] Cederbaum and co-workers have developed the CAP/ADC approach [38] and successfully implemented this approach to calculate the lifetime of inner valence excited state of $\mathrm{Ne_n}$ clusters. Another alternative approach which has been applied successfully to investigate the ICD decay width is Wigner- Weisskopf theory. [27] It has been used to investigate how the ICD decay width changes in increasing the cluster size. It has been observed that the lifetime for the ICD decay rate decrases rapidly from 100 fs in $\mathrm{Ne_2}$ to less than 10 fs in $\mathrm{Ne_{13}}$. Santra et al. [24] have also investigated how the lifetime of the ICD decay rate depends on the internuclear distance between two atoms in a diatomic molecule. The ICD decay width of $^2\Sigma_g^+$ and $^2\Sigma_u^+$ states of Ne_2 are computed as a function of internuclear distance. It has been observed that ICD decay rate is strongly depends on internuclear distance. The dynamics behind the ICD has also been investigated using the wave packet propagation technique. The existence of ICD in mixed van der Waals clusters such as NeAr,[113] NeHe [117] is also established.

Recently, Cederbaum and co-workers [36] have investigated the ICD in weakly bound He_2. In their work, they have investigated how far two helium atom can exchange energy in He_2. It is reported that the two helium atoms in He_2 can exchange energy by ICD over distance of more than 45 times of their atomic radious. It has also been established thet ICD spectroscopy can be used for imaging vibrational wave function of the ionized excited helium dimers. Generally, electronically excited molecule relaxes via ICD through virtual photon exchange mechanism. However, He_2 does not have any inner valence inner valence electron. Thus, it goes through a new kind of ICD mechanism. The ICD mechanism in He_2 can be expressed as follows : After simultaneous ionization and excitation of one helium atom within the dimer, the energy stored by this excited ion suffices to ionize the neighboring neutral helium atom.

The ICD has also been observed in endohedral fullerene complexes. The ICD mechanism is possible after ionization of an atom X in an endohedral fullerene complexes $X@C_{60}$. Cederbaum and co-workers have calculated the decay rates of ICD in $Ne@C_{60}$ complex. [118] It is shown that the ICD mechanism is forbidden in the isolated X atom. The correlation between the endohedral atom electrons and fullerene electrons is responsible for ICD mechanism. It is also shown that the ICD rate in endohedral fullerene complexes is ultrafast in nature. It is reported that the ICD lifetime in $Ne@C_{60}$ is 2 fs. Moreover, it is suggested that interatomic decay in an endohedral fullerene does not necessarily lead to the destruction of the complex.

The ICD has also been observed in hydrated ions. [119] It is also established that a new Coster-kronig (CK) type of core level ICD process operating in the microsolvated ions which involves dipole allowed transition in the atomic ions. Therefore this process is much more efficient compares to the normal core hole ICD process.

The ICD process has been observed experimentally for the first time in clusters. However, Jahnke et al. [26] have performed a remarkable experiment on Ne_2. Very recently, the lifetime of ICD in is investigated via an extreme ultraviolet pump-probe experiment at the free electron laser. The lifetime is found to be of the order of (150$\pm$50) fs.[32]

The experimental measurement of ICD in is performed by Jahnke et al. [35] In their experiment, the ultrafast energy transfer between two water molecules is observed directly. In a similar kind of experiment, Mucke et al. [120] have observed the production of low energy electrons in amorphous medium size water clusters. The ICD has also been confirmed exprimentally for the mixed NeAr clusters.

The ICD has also been investigated theoretically for small hydrogen bonded systems by Cederbaum and co-workers.[110] The ICD has been studied for $H_2O...HCHO$, $H_2O...H_2CNH_2$, $H_2O..NH_3$, $NH_3...H_2O$, $H_2O...H_2S$, $H_2S....H_2O$ and $H_2O..H_2O$ (p-donor .....p-acceptor). Dreuw and co-workers [121] have observed ICD for the first time in real biological system. They observed ICD in the DNA repair enzymes photolyases. Photolyase function involves light-induced electron detachment from a reduced avin adenine dinucleotide ($FADH^-$), followed by its transfer to the DNA-lesion triggering repair of covalently bound nucleobase dimers.

Recently, It is shown that the energy of ICD electron and emission site can be controlled in an efficient manner by resonant Auger decay. This process is named as resonant Auger ICD (RA-ICD) decay.[37] In this process, an electron from the k-shell of a specific target atom excites resonantly to a bound unoccupied orbital. Then the core excited state follows the Auger decay for relaxation. In this Auger process, a valence electron comes to fill up the initial vacancy and another valence electron is emitted to the continuum while the initially excited electron remains as a spectator. This Auger decay is called spectator resonant Auger decay. This resonant spectator Auger decay generates a highly excited valence ionized state which then undergoes to ICD. The main advantage of resonant Auger driven ICD (RA-ICD) process is the energy of emitted ICD electron can be tune in a very efficient manner. The energy of the emitted ICD electron particularly depends on the energies and populations of the resonant Auger final states. They also depend on the parent core excited state. This offers a great opportunity to tune the energy of the emitted ICD electron in a controlled manner by adjusting the energy of the parent core excited state. Another advantage is the emission site of ICD electron

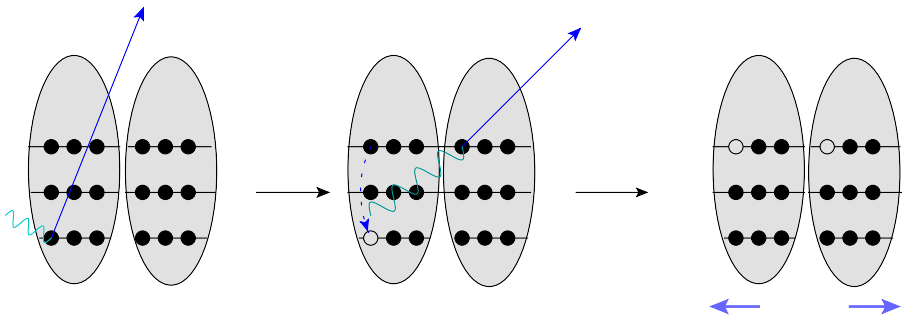

Figure 1.1: Schematic representation of ICD after inner valence ionization

can be chosen specifically by using this process. The initial parent core excitation can be placed specifically on a particular target atom. The resonant Auger decay is local in nature. Therefore, the resonant Auger decay produces two outer valence holes which are localized particularly on the initially excited target atom. The ICD electron is ejected specifically from the neighboring atom of initially excited target atom. Therefore, the site where the ICD electrons are generated can be selectively chosen.

1.10 Electron transfer mediated decay(ETMD)

Electron transfer mediated decay (ETMD)[122, 123] is highly efficient ultrafast non-radiative neutralization pathway of excited ions or molecules in environment. In this decay process, electron transfer between two subunits acts as a mediator. In ETMD, a neighbor donates an electron to an initially excited ion, while released energy transfer to the donor (ETMD2) or another neighbors (ETMD3) which emit secondary electron to the continuum. Therefore, in the ETMD process complete system acquires an extra positive charge. Being an electron transfer process ETMD is slow process compare to

the energy driven ICD process. The schematic representation of ETMD presented in Fig 1.2.

ETMD is a much faster decay process compared to the charge transfer (CT) decay. Generally, it is assumed that the neutralization of less highly excited ions proceed through charge transfer. In this process, excited ion neutralizes via electron transfer from the neighboring species. If the potential curves of ionic state and charge transfer state cross to each other then charge transfer is possible. If there is no prominent curve crossing exists then the neutralization proceeds through radiative charge transfer (RCT). Generally, it transpires in a nano-second time domain. In ETMD process, no nuclear motion is necessary for neutralization. The final state of ETMD process automatically fulfills the resonant condition for all the nuclear configurations at which the decay process is energetically favorable. The electron electron interaction is the main responsible factor for the ETMD mode. Therefore, the energy involved in this process is much higher than the CT decay which involves coupling with the electromagnetic field. These are the dominating factors which make the ETMD process much faster compared to the charge transfer decay.

Since electron transfer occurs in ETMD process, the orbital overlap between charge donor and acceptor unit plays a decisive role in the rate of the decay mechanism. The dependence of the decay rate on the orbital overlap leads to an increase of the decay rate non-linearly with decreasing the distance between the electron donor and acceptor. Therefore, nuclear dynamics has high impact on the ETMD dacay rate. The ETMD is intermolecular in nature and its decay rate strongly depends on the number of neighbors present in the system.

Theoretically, ETMD process is reported by Zobeley et al. [122] The lifetime of the inner valence excited state of is calculated. The calculated lifetime is found to be in the order of 10 femto-second (fs). It is also shown that decay rate strongly depends on the inter nuclear distance between to monomer units. At the equilibrium bond distance ICD is the main decay mode. However, ETMD becomes an operative with decreasing

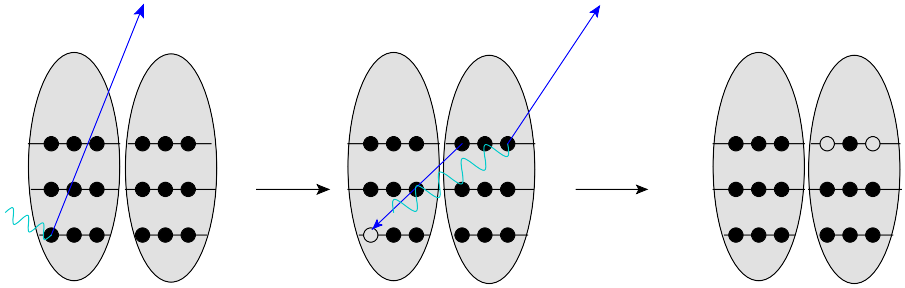

Figure 1.2: Schematic representation of ETMD after inner valence ionization

the bond distance between and atoms. Müller et al. [123] have shown that the ETMD becomes an operative in aqueous micro solvated clusters. The calculated lifetime is in the order of 20 to 100 fs for clusters with one to more water monomers. Recently, it is shown that the multiply charged Auger final states can relax very efficiently via ETMD mechanism in presence of neighbors. Cederbaum and co-workers have investigated the ETMD lifetime of excited Auger final states of atom in clusters.

1.11 Exchange ICD

The decay rate of exchange ICD [124] process is governed by the electron transfer. In exchange ICD process, inner valence vacacy of an initially excited monomer unit is filled up by an outer valence electron of the neighboring monomer. Then the excess energy is transfered to the initially excited monomer unit which emits an another outer valence electron from initially ionized unit. The two positively charged units then undergo coulomb explosion. The final state of exchange ICD process is identical to the

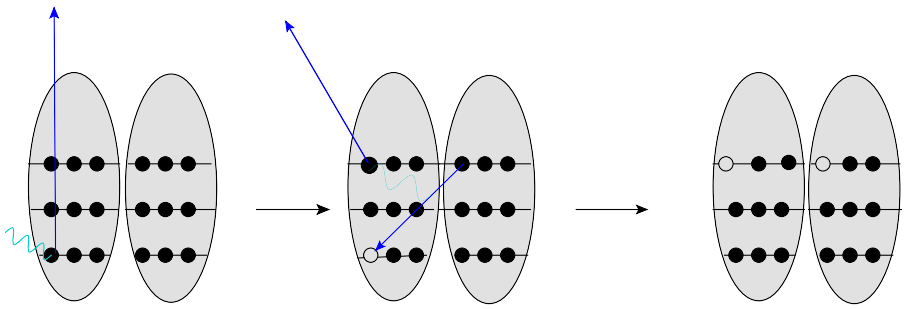

Figure 1.3: Schematic representation of Exchange ICD

virtual photon exchange ICD process. However, being an electron transfer driven process the decay rate of exchange ICD process is slow compare to the ICD process. The decay rate of exchange ICD process is quite similar to the ETMD process. Generally, exchange ICD process occurs in pico-second time domain. The schematic representation of exchange ICD process is presented in Fig 1.3.

1.12 Resonant ICD(RICD)

The resonant ICD is initiated from the ionized but from the excited state of an atom or molecule. This process is divided into two categorize, one is spectator resonant ICD and another is participator resonant ICD. The division of the resonant ICD process specifically depends on the involvement of the excited electrons in the ICD process. In a participator RICD the excited electron fills the created vacancy itself. Then the excess energy is transferred to a neighboring unit, which subsequently gets ionized . The final state is characterized by the initially excited unit to be in its ground state and the neighboring atom being ionized. In a spectator RICD the vacancy is filled by another, non-excited

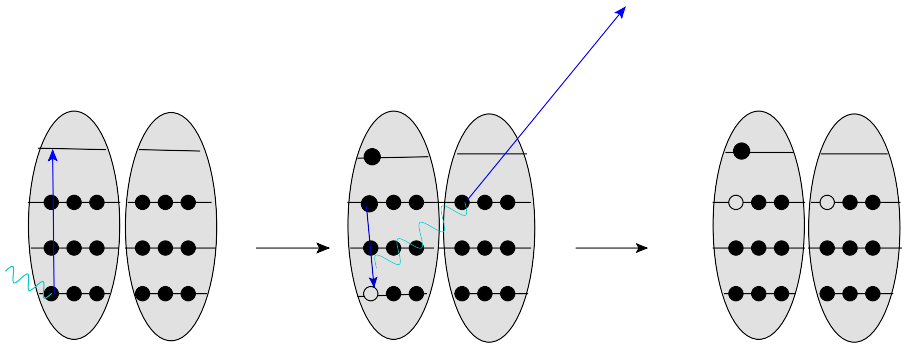

Figure 1.4: schematic representation of Spectator resonant ICD

electron of the same unit. The excess energy is transferred to the neighboring unit, which ejects an another outer valence electron. Therefore, the final state of spectator RICD is characterized by two outer valence hole placed on two different monomer units. The excited electrons act as a spectator in the entire process. The schematic representation of spectator resonant ICD process is presented in Fig 1.4. The schematic representation of participator resonant ICD process is presented in Fig 1.5.

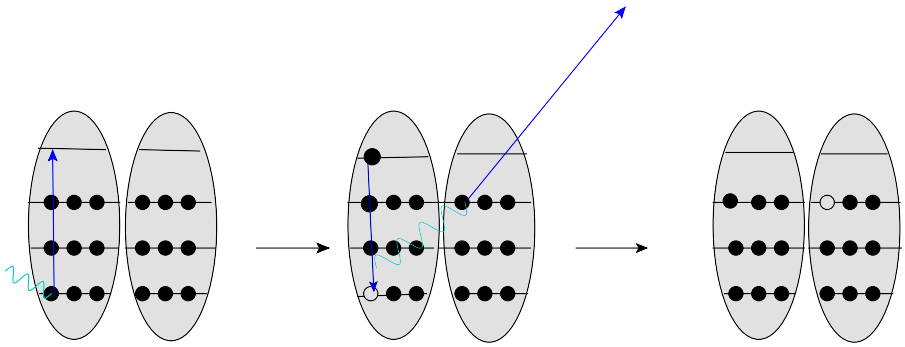

Figure 1.5: Schematic representation of Participator resonant ICD

1.13 Auger decay

The Auger decay is discovered independently by Lise Meitner and Pierre Auger. This process is initiated by creating a vacancy in the core level of an atom or molecule. In Auger decay, an electron from the outer valence level fills the vacancy in the core level and the released energy is transferred to another outer valence electron which is then emitted from the system. The emitted secondary electron (Auger electron) contains very low energy, in the order of few electron volts. Therefore, the final state of Auger decay is identified by two outer valence hole placed on the initially core excited atom. Two special kind of Auger processes are well known, one is Coster-Kronig (CK) and another is Super-Coster- Kronig (SCK) decays. In a CK decay, the vacancy lling electron originates from a higher subshell of the same shell characterized by the principal quantum number n. In a SCK decay the emitted electron also stems from the same shell.

Energetically, Auger decay is favorable when the binding energy of the single core hole excited state is higher than the double ionization threshold. The Auger process is

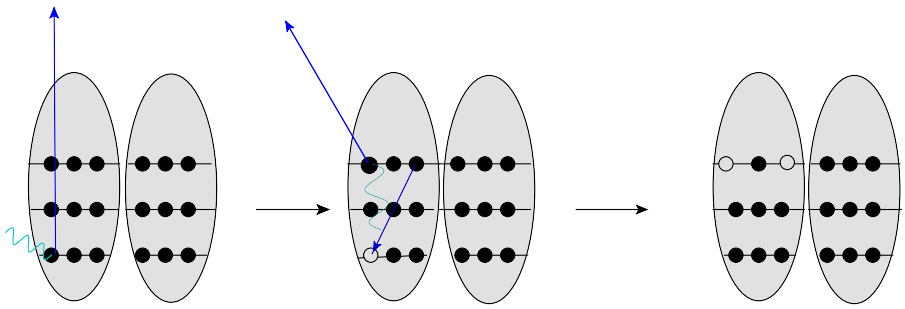

Figure 1.6: Schematic representation of Auger decay

intramolecular in nature. Therefore, the environment has very less effect on the Auger process. The decay rate of Auger process is not alter in presence of neighboring atoms or molecules. The Schematic representation of Auger decay is presented in Fig 1.6.

1.14 Objective and Scope of the thesis

The equation-of-motion coupled cluster (EOMCC) method is very well known for the accurate description of energies and properties of the bound states. It provides balanced treatment between electron correlation and relaxation effects. In this thesis our motivation is to apply this highly correlated EOMCC method for the calculation of energies and properties of the resonance states. The accurate description of resonance states using EOMCC method requires the inclusion of continuum effect. The complex absorbing potential (CAP) approach treat the continuum effect accurately. Therefore, a method which is a combination of CAP approach and EOMCC approach is very promising in the description of resonance states.

In this thesis, We have applied the CAP/EOMCC approach for the calculation of

resonance position and decay widths of shape resonances. The calculation has been done in various small systems. The results for shape resonances are compiled in the chapter II. The method has also been used in the calculation of potential energy curve for the resonance states, Which is also included in the chapter II. In chapter III the detail investigation of $^2\Pi_u$ resonance states of CO_2^- is given. The potential energy curve (PEC) for the $^2\Pi_u$ resonance states of CO_2^- is studied upon bending as well as symmetric and asymmetric stretching of the molecule.

In chapter IV we have implemented the CAP/EOMCC method for the first time to study lifetime of interatomic coulombic decay (ICD) mechanism. The lifetime has been studied for the inner valence excited state of Neon atom in neon-water clusters. It has also been applied to study the lifetime of inner valence excited state of F atom in small hydrogen bonded $(HF)_n$ clusters. To validate our method the calculated lifetime of ICD process is compared with the other theoretical methods. In chapter V we have also implemented the CAP/EOMCC method for the calculation of the decay rate of Auger process. The decay rate of Auger process is calculated using the CAP/EOMCC method for the core hole (K) and double core hole state (KK) states in various small systems. In the last chapter the same approach is used to compute how the interatomic or intermolecular coulombic decay (ICD) rate of molecule changes with changing the internuclear distance of the molecule. In the last chapter we also give the future perspective in the field of ICD using this highly correlated method.

References

[1] J. Combes, P. Duclos, M. Klein, and R. Seiler, Comm. Math. Phys. **110**, 215 (1987).

[2] L. G. Christophoru, Electron-molecule Interactions and Their Applications (Vol. 1, 1984)

[3] D. G. Truhlar, Resonances in electron-molecule scattering, van der Waals complexes, and reactive chemical dynamics(American Chemical Society, Division of Physical Chemistry, Washington DC, 1984).

[4] G. Schulz, Rev. Mod. Phys. **45**, 378 (1973); G. Schulz, Rev. Mod. Phys. **45**, 423 (1973).

[5] K. D. Jordan, Int. J. Quantum Chem. **20** 331 (1981).

[6] S. I. Chu and D. A. Telnov, Phys. Rep. **390**, 1 (2004).

[7] W. Domcke, Phys. Rep. **208**, 97 (1991).

[8] P. Burke and J. Williams, Phys. Rep. **34**, 325 (1977).

[9] J. Bayfield, Phys. Rep. **51**, 317 (1979).

[10] T. Rumph, S. Bowyer, and S. Vennes, Astron. J. **107**, 2108 (1994).

[11] T. Andersen, Phys. Rep. **394**, 157 (2004).

[12] P. Lambropoulos, P. Maragakis, and J. Zhang, Phys. Rep. **305**, 203 (1998).

[13] P. Knight, M. Lauder, and B. Dalton, Phys. Rep. **190**, 1 (1990).

[14] E. Lindroth and L. Argenti, Adv. Quantum Chem., **63**, 247 (2102).

[15] J. Simons, Acc. Chem. Res. **39**, 772 (2006)

[16] Z. Li, P. Cloutier, L. Sanche, and J. R. Wagner, J. Am. Chem. Soc. **132**, 5422 (2010).

[17] B. Boudaïffa, P. Cloutier, D. Hunting, M. A. Huels, and L. Sanche, Science **287**, 1658 (2000).

[18] A. J. F. Siegert, Phys. Rev. **56**, 750 (1939).

[19] G. Gamow, Der Bau des Atomkerns und die Radioaktivität (Hirzel, Leipzig,1932).

[20] P. Auger, J. Phys. Radium **6**, 205 (1925).

[21] V. Stumpf, P. Kolorenc, K. Gokhberg and L. S. Cederbaum, Phys. Rev. Lett.N. Moiseyev and C. Corcoran, Phys. Rev. A 20, 814 (1979); T. N. Rescigno,
110, 258302 (2013).

[22] L. S. Cederbaum, Y. C. Chiang, P. V. Demekhin, and N. Moiseyev, Phys. Rev. Lett. **106**, 123001 (2011).

[23] L. S. Cederbaum, J. Zobeley, and F. Tarantelli, Phys. Rev. Lett. **79**, 4778 (1997).

[24] R. Santra, J. Zobeley, L. S. Cederbaum, and N. Moiseyev, Phys. Rev. Lett. **85**, 4490 (2000).

[25] S. Marburger, O. Kugeler, U. Hergenhahn, and T. Möller, Phys. Rev. Lett. **90**, 203401 (2003).

[26] T. Jahnke, A. Czasch, M. S. Schöffler, S. Schössler, A. Knapp, M. Käsz, J. Titze, C. Wimmer, K. Kreidi, R. E. Grisenti, A. Staudte, O. Jagutzki, et al., Phys. Rev. Lett. **93**, 163401 (2004).

[27] R. Santra and L. S. Cederbaum, Phys. Rep. **368**, 1 (2002).

[28] U. Hergenhahn, J. Electron. Spetrosc. Relat. Phenom. **184**, 78 (2011).

[29] R. Santra and L. S. Cederbaum, Phys. Rev. Lett. **90**, 153401 (2003).

[30] Y. Morishita, X. J. Liu, N. Saito, T. Lischke, M. Kato, G. Prümper, M. Oura, H. Yamaoka, Y. Tamenori, I. H. Suzuki, and K. Ueda, Phys. Rev. Lett. **96**, 243402 (2006).

[31] F. Trinter, J. B. Williams, M. Weller, M. Waitz, M. Pitzer, J. Voigtsberger, C. Schober, G. Kastirke, C. Müller, C. Goihl, P. Burzynski, F. Wiegandt et al., Phys. Rev. Lett. **111**, 093401 (2013).

[32] K. Schnorr, A. Senftleben, M. Kurka, A. Rudenko, L. Foucar, G. Schmid, A. Broska, T. Pfeifer, K. Meyer, D. Anielski, R. Boll, D. Rolles, et al., Phys. Rev. Lett. **111**, 093402 (2013).

[33] A. I. Kuleff and L. S. Cederbaum, Phys. Rev. Lett. **98**, 083201 (2007).

[34] E. F. Aziz, N. Ottosson, M. Faubel, I. V. Hertel, and B. Winter, Nature **455**, 89 (2008).

[35] T. Jahnke, H. Sann, T. Havermeier, K. Kreidi, C. Stuck, M. Meckel, M. Schöffler, N. Neumann, R. Wallauer, S. Voss, A. Czasch, O. Jagutzki et al., Nat. Phys. **6**, 139 (2010).

[36] N. Sisourat, N. V. Kryzhevoi, P. Kolorenč, S. Scheit, T. Jahnke, and L. S. Cederbaum, Nat. Phys. **6**, 508 (2010).

[37] K. Gokhberg, P. Kolorenč, A. I. Kuleff, and L. S. Cederbaum, Nature **505**, 661 (2014).

[38] N. Vaval and L. S. Cederbaum, J. Chem. Phys. **126**, 164110 (2007).

[39] N. Moiseyev, Non-Hermitian Quantum Mechanics (Cambridge University Press, Cambridge, 2011).

[40] P. O. Löwdin, Adv. Quantum Chem. **19**, 87 (1988).

[41] J. Aguilar and J. Combes, Comm. Math. Phys. **22**, 269 (1971).

[42] E. Balslev and J. Combes, Comm. Math. Phys. **22**, 280 (1971).

[43] B. Simon, Comm. Math. Phys. **27**, 1 (1972).

[44] B. Simon, Ann. Math. **97**, 247 (1973).

[45] W. P. Reinhardt, Ann. Rev. Phys. Chem. **33**, 223 (1982).

[46] N. Moiseyev, Phys. Rep. **302**, 212 (1998).

[47] N. Moiseyev, P. Certain, and F. Weinhold, Mol. Phys. **36**, 1613 (1978).

[48] C. W. McCurdy and T. N. Rescigno, Phys. Rev. Lett. **41**, 1364 (1978).

[49] N. Moiseyev and C. Corcoran, Phys. Rev. A **20**, 814 (1979).

[50] B. Simon, Phys. Lett. **71A**, 211 (1979).

[51] N. Lipkin, N. Moiseyev, and E. Brändas, Phys. Rev. A **40**, 549–553 (1989).

[52] N. Rom, E. Engdahl, and N. Moiseyev, J. Chem. Phys. **93**, 3413 (1990).

[53] N. Moiseyev, J. Phys. B **31**, 1431 (1998).

[54] Y. Sajeev, M. Sindelka, and N. Moiseyev, Chem. Phys. **329**, 307 (2006).

[55] Y. Sajeev and N. Moiseyev, J. Chem. Phys. **127**, 034105 (2007).

[56] P. Balanarayan, Y. Sajeev, and N. Moiseyev, Chem. Phys. Lett. **524**, 84 (2012).

[57] H. Masui and Y. K. Ho, Phys. Rev. C **65**, 054305 (2002).

[58] J. Muga, J. Palao, B. Navarro, and I. Egusquiza, Phys. Rep. **395**, 357 (2004).

[59] U. V. Riss and H. D. Meyer, J. Phys. B **26**, 4503 (1993).

[60] R. Santra, Phys. Rev. A **74**, 034701 (2006).

[61] G. Jolicard and E. J. Austin, Chem. Phys. Lett. **121**, 106 (1985)

[62] G. Jolicard and E. J. Austin, Chem. Phys. **103**, 259 (1986).

[63] U. V. Riss and H. D. Meyer, J. Phys. B **31**, 2279 (1998).

[64] Y. Sajeev, V. Vysotskiy, L. S. Cederbaum, and N. Moiseyev, J. Chem. Phys. **131** , 211102 (2009).

[65] Y. Sajeev, Chem. Phys. Lett. **587**, 105 (2013).

[66] P. R. žďánská and N. Moiseyev, J. Chem. Phys. **123**, 194105 (2005).

[67] C. W. McCurdy, T. N. Rescigno, E. R. Davidson, and J. G. Lauderdale, J. Chem. Phys. **73** 2368 (1980).

[68] M. Mishra, O. Goscinski, and Y. Öhrn, J. Chem. Phys. **79**, 5994 (1983).

[69] M. Mishra, H. A. Kurtz, O. Goscinski, and Y. Öhrn, J. Chem. Phys. **79**, 1896 (1983).

[70] K. Samanta and D. L. Yeager, J. Phys. Chem. B **112**, 16214 (2008).

[71] S. B. Zhang and D. L. Yeager, Mol. Phys. **110**, 663 (2012).

[72] S. B. Zhang and D. L. Yeager, Phys. Rev. A **85**, 032515 (2012).

[73] M. Honigmann, R. J. Buenker, and H. P. Liebermann, J. Chem. Phys. **125**, 234304 (2006).

[74] M. Honigmann, H. P. Liebermann, and R. J. Buenker, J. Chem. Phys. **133**, 044305 (2010).

[75] Y. Ho, Phys. Rep. **99**, 1 (1983)

[76] R. Santra and L. S. Cederbaum and H.-D. Meyer, Chem. Phys. Lett. **303**, 413 (1999).

[77] R. Santra and L. S. Cederbaum, J. Chem. Phys. **115**, 6853 (2001).

[78] T. Sommerfeld and U. V. Riss and H.-D. Meyer, L. S. Cederbaum, B. Engels, and H. U. Suter, J. Phy. B **31**, 4107 (1998).

[79] S. Feuerbacher, T. Sommerfeld, R. Santra, and L. S. Cederbaum, J. Chem.Phys. **118**, 6188 (2003).

[80] T. Sommerfeld and R. Santra, Int. J. Quantum Chem. **82**, 218 (2001).

[81] M. Mishra, O. Goscinski, and Y. Ohrn, J. Chem. Phys. **79**, 5505 (1983).

[82] M. Ehara and T. Sommerfeld, Chem. Phys. Lett. **537**, 107 (2012).

[83] R. Santra and L. S. Cederbaum, J. Chem. Phys. **117**, 5511 (2002).

[84] C. Buth, R. Santra, and L. S. Cederbaum, Phys. Rev. A **69**, 032505 (2004).

[85] Y. Sajeev, M. K. Mishra, N. Vaval, and S. Pal, *J. Chem. Phys.* **120**, 67 (2004); Y. Sajeev, R. Santra, and S. Pal, *J. Chem. Phys.* **123**, 204110 (2005); Y. Sajeev and S. Pal, *Mol. Phys.* **103**, 2267 (2005).

[86] Y. Zhou and M. Ernzerhof, J. Phys. Chem. Lett. **3**, 1916 (2012).

[87] F. Cöster, Nucl. Phys. **7**, 421 (1958); F. Cöster and H. Kümmel, Nucl. Phys. **17**, 477 (1960).

[88] J. Cizek, J. Chem. Phys. **45**, 4256 (1966).

[89] J. Cizek, Adv. Chem. Phys. **14**, 35 (1969).

[90] A. C. Hurley, in Electron correlation in small molecules (Academic press, London, 1976).

[91] R. J. Bartlett, Annu. Rev. Phys. Chem. **32**, 359 (1981).

[92] I. Shavitt and R. J. Bartlett, ”Many-body methods in Chemistry and physics: MBPT and Coupled-Cluster theory”, Cambridge University Press, Cambridge (2009).

[93] M. Nooijen and R. J. Bartlett, J. Chem. Phys. **102**, 3629 (1995).

[94] M. Nooijen and R. J. Bartlett, J. Chem. Phys. **102**, 6735 (1995).

[95] J. Stanton and J. Gauss, J. Chem. Phys. **101**, 8938 (1994).

[96] J. F. Stanton and R.J. Bartlett, J. Chem. Phys. **98**, 7029 (1993).

[97] D. C. Comeau and R. J. Bartlett, Chem. Phys. Lett. **207**, 414 (1993).

[98] J. Geertsen, M. Rittby, and R.J. Bartlett, Chem. Phys. Lett. **164**, 57 (1989).

[99] M. Musial, S. A. Kucharski, and R.J. Bartlett, J. Chem. Phys. **118**, 1128 (2003).

[100] M. Musial and R.J. Bartlett, J. Chem. Phys. **119**, 1901 (2003).

[101] M. Musial and R.J. Bartlett, Chem. Phys. Lett. **384**, 210 (2004).

[102] R.J. Bartlett and M. Musial, Rev. Mod. Phys. **79**, 291 (2007).

[103] D.I. Lyakh, M. Musial, V.F. Lotrich, and R.J. Bartlett, Chem. Rev. **112**, 182 (2012).

[104] L. Meissner and R.J. Bartlett, J. Chem. Phys. **102**, 7490 (1995).

[105] M. Nooijen and R.J. Bartlett, J. Chem. Phys. **107**, 6812 (1997).

[106] M. Musial and R.J. Bartlett, J. Chem. Phys. **134**, 034106 (2011).

[107] T. Sommerfeld and F. Tarantelli, J. Chem. Phys. **112**, 2106 (2000).

[108] E.R. Davidson, J. Comput. Phys. **17**, 87 (1975).

[109] D.C. Grifn, D.M. Mitnik, and N.R. Badnell, J. Phys. B. **34**, 4401 (2001).

[110] S.D. Stoychev, A.I. Kuleff, and L.S. Cederbaum, J. Am. Chem. Soc. **133**, 6817 (2011).

[111] G. Öhrwall, M. Tchaplyguine, M. Lundwall, R. Feifel, H. Bergersen, T. Rander, A. Lindblad, J. Schulz, S. Peredkov, S. Barth, S. Marburger, U. Hergenhahn, S. Svensson, and O. Bjrneholm, Phys. Rev. Lett. **93**, 173401 (2004).

[112] S. Scheit, V. Averbukh, H.D. Meyer, N. Moiseyev, R. Santra, T. Sommerfeld, J. Zobeley, and L.S. Cederbaum, J. Chem. Phys. **121**, 8393 (2004).

[113] S. Scheit, V. Averbukh, H.D. Meyer, J. Zobeley, and L.S. Cederbaum, J. Chem. Phys. **124**, 154305 (2004).

[114] J. Zobeley, L.S. Cederbaum, and F. Tarantelli, J. Phys. Chem. A. **103**, 11145 (1999).

[115] I.B. Müller, and L.S. Cederbaum, J. Chem. Phys. **125**, 204305 (2006).

[116] R. Santra, J. Zobeley, L.S. Cederbaum, and F. Tarantelli, J. Electron Spectrosc. Relat. Phenom. **114**, 41 (2001).

[117] N. Sisourat, H. Sann, N.V. Kryzhevoi, P. Koloren, T. Havermeier, F. Sturm, T. Jahnke, H-K. Kim, R. Drner, and L.S. Cederbaum, Phys. Rev. Lett. **105**, 173401 (2010).

[118] V. Averbukh and L.S. Cederbaum, Phys. Rev. Lett. **96**, 053401 (2006).

[119] W. Pokapanich, N. V. Kryzhevoi, N. Ottosson, S. Svensson, L. S. Cederbaum, G. Öhrwall, and O. Björneholm, J. Am. Chem. Soc. **133**, 13430 (2011).

[120] M. Mucke, M. Braune, S. Barth, M. Frstel, T. Lischke, V. Ulrich, T. Arion, U. Becker, A. Bradshaw, and U. Hergenhahn, Nat. Phys. **6**, 143 (2010).

[121] P.H.P. Harbach, M. Schneider, S. Faraji, and A. Dreuw, J. Phys. Chem. Lett. **4**, 943 (2013).

[122] J. Zobeley, R. Santra, and L.S. Cederbaum, J. Chem. Phys. **115**, 5076 (2001).

[123] I.B. Müller and L.S. Cederbaum, J. Chem. Phys. **122**, 094305 (2005).

[124] T. Jahnke, A. Czasch, M. Schfer, S. Schssler, M. Ksz, J. Titze, K. Kreidi, R.E. Grisen- ti, A. Staudte, O. Jagutzki, LPhH Schmidt, Th Weber, H. Schmidt-Bcking, K. Ueda, and R. Drner, Phys. Rev. Lett. **99**, 153401 (2007).

Chapter 2

Equation-of-motion coupled cluster method for the study of shape resonace

In this chapter, the equation-of-motion coupled-cluster method (EOM-CC) is applied for the first time to calculate the energy and width of a shape resonance in an electron-molecule scattering. The procedure is based on inclusion of complex absorbing potential with EOM-CC theory. We have applied this method to investigate the shape resonance in $e - N_2$ *,* $e - CO$*, and* $e - C_2H_2$*. We have also applied this method to study the potential energy curve (PEC) of* $^2\Pi_g$ $e - N_2$ *and* $^2\Pi$ $e - CO$ *resonance states.*

2.1 Introduction

Resonances are useful phenomena in electron-molecule scattering [1]. They play an important role in various energy exchange processes between electronic and nuclear motion. Vibrational excitations of the molecules or molecular ions, dissociative attachment are some important processes. The resonances [2–5] of composite particles can be divided into two categories, one is shape (single-particle) and another is Feshbach (core-excited) resonances. The shape resonances are those in which electron capture process is not accompanied by electronic excitation of the target. These can be described as intermediate negative complexes [6], which decay by ejection of an electron into the neutral target molecule and a scattered electron. In general, their life time can be found in a range of $10^{-13} - 10^{-15}$ s. The structural and spectroscopic properties of such states are similar to those of bound states and that is the reason why these systems are of particular interest to the physical chemist.

Computationally, the metastable resonance states can be identified as eigenfunctions associated with complex eigenvalues. The complex energy E_{res} is called as Siegert energy. Where,

$$E_{res} = E_R - i\Gamma/2. \tag{2.1}$$

E_R is the real part of the resonance energy and Γ is the decay width. The Γ is related to the lifetime of the temporary state via, $\tau = \hbar/\Gamma$.

The main characteristic of these states is their exponential growth in the asymptotic region. Thus they are not square-integrable and Hilbert space techniques cannot be applied. They do not belong to the hermitian domain of the Hamiltonian. But, apart from their asymptotic behavior, Siegert wave functions are quite regular. They behave like a bound state in the inner molecular region. A wave function in this region is affected by physical interactions, while the asymptotic exponentially growing part describes the decay. Resonance states can also be seen as discrete states coupled with continuum.

Thus, the calculation of resonance energy requires simultaneous treatment of electron correlation and continuum effect. Thus, the calculation of these states within quantum mechanical bound states framework is beset with difficulties.

Analytic continuation of the Hamiltonian into the complex energy plane is used to absorb an outgoing electron. The analytical continuation of the Hamiltonian can be achieved through complex scaling or using complex absorbing potential. [7, 8] The complex scaling method has been successfully implemented for the atomic systems. However, it is difficult to implement for the molecular problems. The CAP [9] method is very simple to implement in any ab initio electronic structure methods. However, the complex basis function method of Moiseyev and McCurdy [10] has better mathematical foundation than the CAP method because of the partially ad hoc character of the CAP method.

The method of using a CAP is very much similar to the complex scaling theory. [11] The main advantage of this method is that it can be easily adapted with any electronic structure method. In the CAP [12–14] approach the outgoing electron is absorbed by an artificially introduced complex absorbing potential which is located in the peripheral molecular region. In this way the inner region of the wave function remains unperturbed and the 'asymptotic part' is forced into a square-integrable form. This method offers a great promise for the determination of accurate Siegert energy. [15, 16]

The CAP method has already been implemented within various electronic structure methods for the calculation of shape resonances [17]. It can be used at static-exchange level, but it becomes very much powerful and interesting when the electron-correlation effects are considered. The energy difference between (N+1) electron metastable state and the N-electron target ground state gives the kinetic energy of the projectile at which the resonance occurs. The first implementation of the CAP method has been done by Sommerfield et al. [6] for metastable anions [18] and Santra et al. [19] for resonance of cations, both in combination with the configuration interaction (CI) method. Later on, Santra and co-workers [20] have applied the CAP approach to the propagators theory

and used CAP/ADC method to compute the resonances of metastable anions. Mishra and co-workers [21] have used bivariational self consistent field (SCF) based second order propagator method for Auger and shape resonances. Recently, Sajeev et al.[16] have used CAP with the Fock space multireference coupled-cluster (FSMRCC) [16] method to study resonances of anions.

In this chapter, we have implemented CAP method within the equation-of-motion coupled-cluster theory (CAP/EOM-CC) using singles and doubles (SD) to calculate the position and width of a shape resonance. We have studied the resonance energies [22–29] and widths for the $^2\Pi_g$ state of N_2^-,$C_2H_2{}^-$ and $^2\Pi$ state of CO^-. The CAP/EOM-CCSD method allows us to treat the electron correlation accurately. we have also calculated the potential energy curves (PEC) for the low energy $^2\Pi_g$ resonance state of N_2^- and $^2\Pi$ resonance state of CO^-.

2.2 Theory

In the CAP approach CAP potential $-i\eta W$ is added to the Hamiltonian H to describe the electronic resonance state,

$$H(\eta) = H - i\eta W \tag{2.2}$$

where η is a real positive number representing the CAP strength and W is a local positive-semidefinite one-particle operator. The new Hamiltonian $H(\eta)$ satisfies the schrödinger equation

$$H(\eta)\psi(\eta) = E(\eta)\psi(\eta). \tag{2.3}$$

The presence of complex absorbing potential makes the Hamiltonian operator non hermitian but it remains complex symmetric.

If one chooses the appropriate CAP form, the addition of complex potential causes an asymptotic damping of the Siegert eigenfunction which makes the wave function square integrable. The spectrum becomes discrete. However, the artificial introduction of the

CAP potential perturbs the Hamiltonian, one can obtain the exact resonance eigenvalues and eigenfunctions in the limit $\eta \to 0$ for a complete basis set. In practical computation, one cannot solve the Siegert energy spectrum exactly since incomplete basis sets are used and one is forced to use finite η values. The complex Hamiltonian matrix $H(\eta)$ is diagonalized for a number of η values to obtain the resonance energy. The η trajectories are examined by using logarithmic velocity

$$\upsilon_i(\eta) = \eta \partial E_i / \partial \eta \tag{2.4}$$

The quantity υ_i can be used in two respects. Firstly, it is used to identify the metastable states which are characterized by a pronounced minimum $|\upsilon_i|$. Secondly, it is used to determine the optimal CAP strengths η_{opt}. In this case we have employed the condition

$$|\upsilon_i(\eta_{opt})| = min. \tag{2.5}$$

The resonance energy is not sensitive to a particular basis set unless too small basis sets are used. The complex energy at the optimal point is associated with position of the resonance (real part) and decay width (the imaginary part).

In our calculations we have used box-shaped CAP of the form

$$W(x;c) = \sum_{i=1}^{3} W_i(x_i;c_i), \tag{2.6}$$

where

$$W_i(x_i;c_i) = \{^{0,|x_i|\leq c_i,}_{(|x_i|-c_i)^2,|x_i|>c_i} \tag{2.7}$$

This CAP can be easily represented in a Gaussian basis set.[13, 14] It has been applied to the peripheral region of the target molecule to absorb the scattered electron while keeping the target unperturbed.

The exact ground state wave function of a coupled-cluster method (CC)[30–32] is

$$|\psi_{gr}\rangle = exp(T)|\phi_{ref}\rangle, \tag{2.8}$$

where $|\phi_{ref}\rangle$ is the reference wave function. Here, we have chosen closed-shell N-electron ground state Hartree-Fock determinant as a reference wave function. The cluster operator T consists of connected singles, doubles, up to n-truple excitation operators. The cluster matrix elements are determined using the equation

$$\langle\phi_e|e^{-T}He^{T}|\phi_{ref}\rangle = 0 \tag{2.9}$$

where $|\phi_e\rangle$ are the excited state determinants. The ground state energy is given by

$$\langle\phi_{ref}|e^{-T}He^{T}|\phi_{ref}\rangle = E_{gr}. \tag{2.10}$$

There are two advantages in the coupled-cluster method. First, the method is size-extensive by virtue of the exponential ansatz. Second, due to exponential nature of the wave operator, this method gives highly accurate energy and wave function even in its approximate form, within singles and doubles approximation.

The basic idea of the EOM-CC method is very simple. The ground state wave function of the single-reference coupled-cluster method is used as a starting point for the EOM-CC approach. In the EOM-CC approach, electron attached (N +1 electron) states $|\psi_k\rangle$, different from ground state $|\psi_{gr}\rangle$, are parametrized as

$$|\psi_k\rangle = R(k)|\psi_{gr}\rangle. \tag{2.11}$$

R(k) is a linear excitation operator is given by

$$R(k) = \sum_a r^a(k)a^+ + \sum_{ab}\sum_i r_i^{ab}(k)a^+b^+i + ... \tag{2.12}$$

where standard convention for indices is used, i.e., indices a,b,.., refer to the unoccupied orbitals and indices i,j,..., refer to the occupied orbitals. In equation-of-motion coupled-cluster method for singles and doubles (EOM-CCSD), the energies for electron attached states are obtained as the eigenvalues of the similarity transformed effective Hamiltonian H_{eff}.

$$H_{eff} = e^{-T}He^{T} - \langle\phi_{ref}|e^{-T}He^{T}|\phi_{ref}\rangle \tag{2.13}$$

$$H_{eff}R(k) = w_k R(k). \tag{2.14}$$

where w_k is the energy change connected with the electron attachment process. The effective Hamiltonian matrix is constructed in a 1p and 2p1h space and diagonalized to obtain the energies of electron attached states. We have applied CAP to the EOM-CCSD [33–41] method for the calculation of shape resonance. In CAP/EOM-CCSD method, the contribution of CAP term comes through the modification of H_{eff} matrix. The CAP term is added with the one-body particle-particle part of the H_{eff} matrix. The other terms of the H_{eff} matrix are modified through the appearance of complex $T(\eta)$. The new form the complex $H_{eff}(\eta)$ matrix is

$$H_{eff}(\eta) = e^{-T(\eta)}H(\eta)e^{T(\eta)} - \langle\phi_{ref}|e^{-T(\eta)}H(\eta)e^{T(\eta)}|\phi_{ref}\rangle \tag{2.15}$$

$$H_{eff}(\eta)R_\eta(k) = w_k(\eta)R_\eta(k). \tag{2.16}$$

Initially the CAP is applied to the coupled-cluster (CC) method to generate the complex $T(\eta)$ amplitudes, which are later used to generate the complex $H_{eff}(\eta)$ matrix elements. The CAP has very little effect on the ground state energy E_{gr}. After addition of CAP to the CC method the ground state energy E_{gr} remains same. Finally, the resulting complex H_{eff} matrix is diagonalized for different η values.

However to obtain the resonance energies we need to use following equation since the ground state energies are suppose to be CAP free.

$$E_{res}(\eta) = w_k(\eta) + E_{cc}(\eta) - E_{cc}(\eta = 0) \tag{2.17}$$

Thus we loose the advantage of direct difference energy in this approach. We call this approach as CAP/EOM-CCSD. Also, in this procedure this entire step needs to be done for few hundred values of η starting from $\eta = 0$. The calculation of CC for each η value is time consuming and computationally demanding since it scales as N^6. The CAP is defined only over the particle-particle block (virtual block) since it does not affect the target system. The effect of CAP is very small on the correlation energy of the

system. Hence, in the present chapter , we have also implemented an approximation for the inclusion of CAP at the (N+1) electron wave function by keeping the ground state $|\psi_{gr}\rangle$ CAP independent. We call this approach as $\mathrm{CAP/EOM-CCSD}^{'}$ method. Thus, we have

$$|\psi_k(\eta)\rangle = R_\eta(k)|\psi_{gr}\rangle. \tag{2.18}$$

We first solve the CC without any CAP potential. These cluster amplitudes $T(\eta = 0)$ are scaled with the CAP potential in using the following equations

$$D_1 = f_{aa} - f_{ii}, \tag{2.19}$$

$$t_i^a(\eta) = [t_i^a(\eta = 0) * D_1]/[D_1 + W_{aa}(\eta)], \tag{2.20}$$

$$D_2 = f_{aa} + f_{bb} - f_{ii} - f_{jj}, \tag{2.21}$$

$$t_{ij}^{ab}(\eta) = [t_{ij}^{ab}(\eta = 0) * D_2]/[D_2 + W_{aa}(\eta) + W_{bb}(\eta)], \tag{2.22}$$

with these new amplitudes $T(\eta)$ we construct the $\bar{H_N}$ matrix. We have added CAP to the one-body particle-particle ($\bar{f_{pp}}$) part of the H_{eff} matrix. So, the H_{eff} matrix can be written as

$$H_{eff}(\eta) = e^{-T(\eta)}H(\eta)e^{T(\eta)} - \langle\phi_{ref}|e^{-T}He^{T}|\phi_{ref}\rangle \tag{2.23}$$

$$H_{eff}(\eta)R_\eta(k) = w_k(\eta)R_\eta(k) \tag{2.24}$$

Thus the CC part is independent of the CAP perturbation, which means the N electron ground state is not affected by the CAP potential. The artificial nature of the CAP potential and its application only to the particle-particle interaction part justify the approximation of CAP/EOM-CCSD. The main advantage of this approximation is that it drastically reduces the η trajectory generation time since CC calculation needs to be done only once. Since, the ground state is η independent, resonance energy comes out to be the direct difference energy obtained as eigenvalues of $H_{eff}(\eta)$ for different η values.

For diagonalization purpose, we have used Davidson algorithm. In EOM-CCSD method, for the calculation of energies of the electron attached states, the dimension of the H_{eff} matrix becomes very large. The dimension becomes more than 10000 even if the $2p1h$ block for small molecules and usual basis sets is considered. A full diagonalization of such matrices by direct method is computationally expensive. This is the bottleneck of using EOM-CCSD. The Davidson algorithm helps us to use EOM-CCSD for the study of resonance problem to the systems of reasonable size. The basic concept of Davidson algorithm is that the eigenvalues are obtained through an iterative procedure which avoids the computation, storage and diagonalization of the complete matrix and stops when certain convergence criteria are satisfied. In Davidson algorithm, the dimension of the matrix is equal to the number of iterations.

We have obtained the complex energies $w_k(\eta)$ by solving eq. 2.16 for different values of η starting from 0 to 0.01 with the increment of 10^{-6}. By plotting the complex solutions in the complex energy plane with the real part and imaginary part of the energy as axes, we get the η trajectory. A resonance is obtained when the velocity

$$\upsilon_k = |\eta \partial w_k(\eta)/\partial \eta| \tag{2.25}$$

becomes minimum, indicating the stabilization point of the trajectory.

2.3 Results and Discussion

In this chapter we present the energies and widths of shape resonances using CAP/EOM-CCSD method. We have studied the resonance energies for the $^2\Pi_g$ state of N_2^-, $^2\Pi$ state of CO^- and $^2\Pi_g$ state of $C_2H_2^-$. We have also investigated the effect of basis set on the position and width of resonance. We compare the resonance parameters between N_2^- and CO^-. We have also investigated the potential energy curves for the $^2\Pi_g$ state of N_2^- and $^2\Pi$ state of CO^- using the $\mathrm{CAP/EOM-CCSD}^{'}$ method.

2.3.1 $^2\Pi_g$ shape resonance in N_2^-

The low energy electron scattering for the N_2 molecule is a well studied problem, both experimentally as well as theoretically. The $^2\Pi_g$ shape resonance in particular is very much interesting. In this section we have investigated the $^2\Pi_g$ state of N_2^- using EOM-CCSD method. This state originates from addition of one electron to the π_g LUMO of the $^1\Sigma_g^+$ ground state of neutral N_2 molecule and the associated electronic configurations are

$$^1\Sigma_g^+ : (core)^4(1\sigma_g)^2(1\sigma_u)^2(2\sigma_g)^2(1\pi_u)^4 \tag{2.26}$$

$$^2\Pi_g : (core)^4(1\sigma_g)^2(1\sigma_u)^2(2\sigma_g)^2(1\pi_u)^4(n\pi_g)^1. \tag{2.27}$$

For resonance energy calculation, we have used equilibrium bond length (2.069 a.u.). The two nitrogen atoms are placed in a cartesian coordinate system at (0.0, 0.0, $\pm$ 1.035 a.u.) and CAP box side lengths are chosen to be $c_x = c_y = \delta c$ and $c_z = 1.035 + \delta c$. The optimal value of δc is 2.5 a.u.

we have studied the $^2\Pi_g$ state of N_2^- in two different Gaussian basis sets-denoted as basis A and basis B. We benchmark our results with the other theoretical methods like Static exchange, Second order ADC, 2p-h TDA, ADC(3) and the experimental result. The basis A contains 58 contracted functions and basis B 88 functions.[29] The basis B is an extension of basis A. Basis A consists of $[5s, 4p, 2d]$ Gaussians contracted from $(11s, 7p, 2d)$ primitives. Similarly, basis B consists of $[5s, 7p, 3d]$ Gaussians contracted from $(11s, 8p, 3d)$ primitives. [29] Using these two basis sets we have computed resonance energy and width within EOM-CCSD approximation for the N_2^-. Before we discuss these results we want to mention that the results can not be compared directly with the experimental value because there is no fixed-nuclei molecule in the reality. However, the resonance energies and widths have been well reproduced within a parametrized model which describes the non local nature of the vibrational excitation mechanism. In the fixed-nuclei limit at the equilibrium geometry this model yields the parameters $E_R = 2.32$ eV and $\Gamma = 0.41$ eV. We have considered these 'experimental' values as the

most standard values for the comparison of our results.

In Table 2.1 , first row reports the results obtained with the basis A. It can be seen from Table 2.1 that static exchange method overestimates resonance position as well as width compare to the experimental and other theoretical methods. The EOM-CCSD method gives resonance position at 2.99 eV which is overestimated compared to the experimental value (2.32 eV) as well as other theoretical methods like second order ADC (2.74 eV), 2p-h TDA (2.41 eV) and ADC(3) (2.65 eV) approach. However, the EOM-CCSD method underestimates width of the resonance (0.24 eV) compared to the experimental (0.41 eV) as well as other theoretical methods. As we go from basis A to basis B resonance position is decreased where as width of the resonance is increased for all the theoretical methods except static exchange method. In basis B, the EOM-CCSD method gives resonance energy $E_R = 2.44$ eV and width $\Gamma = 0.39$ eV which is very close to the experimental value. It is interesting to note that in basis B 2p-h TDA approximation gives surprisingly good agreement with the experimental value.

Table 2.2 reports basis set convergence study for the N_2^- resonance energy. To study how the resonance energy is affected by basis set we have started with basis B and add one p function on both the nitrogen atoms.The exponent of the new p function is generated by scaling the exponent of last p function by a factor of 0.75. To reach the basis set convergence limit we have added three p functions on each nitrogen atom. Addition of first p function reduces the resonance position to 2.12 eV from 2.44 eV. However, width is increased to 0.44 eV compared to 0.39 eV. With the addition of subsequent p functions width as well as position are reduced and basis set convergence is reached. The resonance position in basis B+3P is 2.07 eV and width is 0.42 eV. It can be seen that the width is closer to the experimental value where as position is underestimated compare to the experimental value.

We have also reported the results for the complex version of multireference single- and double-excitation configuration interaction (MRD-CI) method in $5s13p1d$ CGTO [42] basis. The calculations are carried out using this method for different internuclear

Table 2.1: Energy(upper number) and width(lower number) of the $^2\Pi_g$ N_2^- shape resonance

Basis set	Static exchange [a]	second order ADC [a]	2p-h TDA [a]	ADC(3) [a]	EOM-CCSD	Experiment [a]
Basis A	3.80	2.74	2.41	2.65	2.99	2.32
	1.23	0.50	0.36	0.48	0.24	0.41
	3.80	2.61	2.26	2.54	2.44	
Basis B	1.23	0.58	0.41	0.54	0.39	

[a] See Reference 29

Table 2.2: Basis set convergence study for the $^2\Pi_g$ N_2^- shape resonance

Basis set	Energy(eV)	Width (eV)
Basis B	2.44	0.39
Basis B +1P (N 1p/ N 1p)	2.12	0.44
Basis B +2P (N 2p/ N 2p)	2.09	0.42
Basis B +3P (N 3p/ N 3p)	2.07	0.42

distances of N_2. The results are presented in Table 2.3 . Honigmann et al. [42, 43] have reported the resonance position at 1.38 eV and width of 0.414 eV at the equilibrium bond length. The position of the resonance is quite different from our result as well as the experimental value. However, width of the resonance is in good agreement with our results.

Table 2.3: Energy and width of the $^2\Pi_g$ N_2^- shape resonance

Method	Energy(eV)	Width (eV)
MRD-CI[a]	1.38	0.414
SCF[a]	1.34	0.553
EOM-CCSD	2.07	0.420
Experiment	2.32	0.410

[a] See Reference 42

2.3.2 $^2\Pi$ shape resonance in CO^-

The ground state electronic configuration of CO is

$$^1\Sigma^+ : 1\sigma^2 2\sigma^2 3\sigma^2 4\sigma^2 5\sigma^2 1\pi^4. \tag{2.28}$$

The $^2\Pi$ state is generated by adding one electron to the 2π LUMO of the $^1\Sigma^+$ ground state of neutral CO molecule. The resonance energies and widths for the $^2\Pi$ electronic state of CO^- are presented in Table 2.4. We have used equilibrium bond length (2.136 a.u.). The calculation for the $^2\Pi$ state of CO^- has been done with a 4s5p CGTO basis centered on C and another 4s5p1d CGTO basis [44] centered on O. The CO molecule is placed in a cartesian coordinate system at (0.0, 0.0, $\pm$ 1.068 a.u.). This basis set is chosen here because we can compare our results with the available theoretical results. For CAP/EOM-CC computations the CAP box side lengths chosen were $c_x = c_y = \delta c$ and $c_z = 1.068 + \delta c$, where c_x, c_y, c_z are the distances from center of the coordinate system along the x,y and z axis, respectively and δc is a non negative number, all in a.u. The value of δc is 2.5 a.u. In CAP/EOM-CC method, the resonance energy obtained is 1.32 eV and width is 0.12 eV. The Second order dilated propagator method which uses exactly same basis gives $E_R = 1.71$ eV and width $\Gamma = 0.08$ eV. We report the resonance energies and widths obtained in bi-orthogonal dilated electron propagator method with different approximations. The second order gives resonance energy $E_R = 1.68$ eV and width 0.09 eV. Third order gives resonance energy $E_R = 1.65$ eV and width 0.14 eV. Thus, we can see that the second to third order improves the width remarkably. This is very close to our results obtained using EOM-CCSD method. However, we have obtained narrower width compared to the experimental value 0.40 eV. The lack of agreement between the calculated and experimental width for the $^2\Pi$ CO^- resonance leads us to infer that this may perhaps be due to lack of adequate basis set in our calculation. Although our result for the width does not agree with the experimental value, it is in good agreement with the other theoretical methods in a similar quality basis set.

We have also studied the basis set convergence for the $^2\Pi$ shape resonance of CO^-.

Table 2.4: Energy and width of the $^2\Pi$ CO^- shape resonance

Method	Energy (eV)	Width (eV)
Experiment[a]	1.50	0.40
Theoretical approaches:		
Boomerang model [b]	1.52	0.80
Close coupling method [c]	1.75	0.28
Second order dilated electron propagator (real SCF) [d]	1.71	0.08
Results from bi-orthogonal dilated Electron propagator:[e]		
Second order (Σ^2)	1.68	0.09
Diagonal 2ph-TDA ($\Sigma^{2ph-TDA}$)	1.69	0.08
Quasi-particle third order (Σ^3_q)	1.65	0.14
Third order (Σ^3)	1.65	0.14
EOM-CCSD	1.32	0.12

[a] See Reference 45 [b] See Reference 46 [c] See Reference 47 [d] See Reference 44 [e] See Reference 48

We have chosen maug-cc-pV(D+d)Z basis set and then gradually added p function with an exponent which is scaled by a 0.75 factor with the exponent of last p function. We have added up to three p-types polarization functions on both the carbon and oxygen atoms to reach the expansion limit. The results are presented in Table 2.5. In maug-cc-pV(D+d)Z basis, the EOM-CCSD method gives resonance energy $E_R = 2.01$ eV and width $\Gamma = 0.38$ eV. When we add first p function on both the Carbon and oxygen atoms the resonance position is decreased by 0.54 eV. In this basis i.e maug-cc-pV(D+d)Z+1P we get resonance energy $E_R = 1.47$ eV and width $\Gamma = 0.44$ eV which is very close to the experimental value. Further addition of p functions lowers the resonance energy insignificantly. This indicates that the basis set limit is reached.

2.3.3 Comparison between the $^2\Pi_g$ N_2^- and $^2\Pi$ CO^- shape resonances

In this section we briefly compare the resonance parameters between CO^- and N_2^-. The results are presented in Table 2.6. We have studied resonance energies and widths for both the CO^- and N_2^- in maug-cc-pV(T+d)Z basis using the EOM-CCSD method.

Table 2.5: Basis set convergence study for the $^2\Pi$ CO^- shape resonance

Basis set	Energy(eV)	Width (eV)
maug-cc-pV(D+d)Z	2.01	0.38
maug-cc-pV(D+d)Z+1P(C 1p/ O 1p)	1.47	0.44
maug-cc-pV(D+d)Z+2P(C 2p/ O 2p)	1.44	0.44
maug-cc-pV(D+d)Z+3P(C 3p/ O 3p)	1.42	0.44

Table 2.6: Energy and width of the $^2\Pi_g$ N_2^- and $^2\Pi$ CO^- shape resonances

Molecular ions	Energy (eV)	Width (eV)
N_2^-	2.63	0.42
CO^-	1.90	0.46

For both cases we have used equilibrium bond lengths. For N_2^- we have obtained the resonance energy $E_R = 2.63$ eV and width $\Gamma = 0.42$ eV. It can be seen from Table 2.6 that the resonance energy $E_R = 1.90$ eV obtained for CO^- is lower than N_2^- and width $\Gamma = 0.46$ eV has higher value. Our results for the N_2^- and CO^- follow the correct trend. Physically, these results are expected because the CO resonance contains p-wave as well as d-wave character, however, these are not present in N_2 resonance. The polarization effects are similar in both CO and N_2. The potential energy barrier which plays an important role for the shape resonance is weaker in CO than in N_2. The behavior of the CO molecule is qualitatively similar to the N_2 molecule, however the coupling between the partial waves is much stronger in CO.

2.3.4 $^2\Pi_g$ shape resonance in $C_2H_2^-$

In this section we have studied the $^2\Pi_g$ shape resonance of $C_2H_2^-$. The $C_2H_2^-$ $^2\Pi_g$ state is analogous with the $^2\Pi$ state of CO^- and $^2\Pi_g$ state of N_2^-, and consequently expected to be a short-lived shape resonance. The $^2\Pi_g$ state originates from adding an electron to the π_g^* LUMO of the $^1\Sigma_g^+$ ground state of neutral acetylene molecule. The electronic

configuration for the $^2\Pi_g$ state of $C_2H_2^-$ is

$$^2\Pi_g : (core)^4(2\sigma_g)^2(2\sigma_u)^2(3\sigma_g)^2(1\pi_u)^4(n\pi_g)^1. \tag{2.29}$$

The resonance energies and widths for the $^2\Pi_g$ state of $C_2H_2^-$ are presented in Table 2.7. We have used C-C bond distance 2.2828 a.u. and C-H bond distance 1.9994 a.u. In the CAP/EOM-CCSD method, CAP box side lengths are chosen to be $c_x = c_y = \delta c$ and $c_z = 1.141 + \delta c$. The value of δc is 2.85 a.u. The basis set consists of the Dunning primitive set $(9s5p)$ contracted to give $[5s3p]$ functions (Dunning 1970). For each carbon atom, one d-polarization function (exponent 0.75) and one p-type function (exponent 0.040) have been added. The hydrogen atoms are described by two s groups in a [4,1] contraction. For each hydrogen atom, one p-type function with exponent 0.048 has been added. Then the basis set contains total 56 contracted functions. We have denoted this basis as basis C. We have used this basis to calculate the $^2\Pi_g$ shape resonance of $C_2H_2^-$. The CAP/EOM-CCSD method gives resonance energy $E_R = 2.61$ eV and width $\Gamma = 0.76$ eV. Our result is in good agreement with the experimental values. It can be seen from Table 2.7 that the trapped electron method underestimates the resonance energy compared to the other experimental and theoretical values. The CI method [54] gives resonance position at 2.92 eV which is slightly higher than our results and other theoretical values. However it predicts width of 1.10 eV which is in good agreement with other experimental results. Using the Vibrational Excitation technique, the vertical electron affinity of acetylene was determined as 2.60 eV. Electron impact method confirm the location of the resonance between 2.50 eV to 2.70 eV. The theoretical investigations on the $^2\Pi_g$ resonance of $C_2H_2^-$ are rare. The Multiple-Scattering Xα method gives resonance position at 2.60 eV and width of 1.0 eV.

We have also studied the basis set convergence for the $^2\Pi_g$ state of $C_2H_2{}^-$. We start with basis C and then gradually add p function on both the carbon atoms to reach the expansion limit. We have added up to three p-type polarization functions on both the carbon atoms of $C_2H_2{}^-$. The exponent value for the new p-type function is scaled by a

Table 2.7: Energy and width of the $^2\Pi_g$ $C_2H_2^-$ shape resonance

Method	Energy (eV)	Width (eV)
Experiment		
Trapped Electron [a]	1.80/1.85	-
Vibrational Excitation [b]	2.60	$>$ 1.00
Electron impact [c]	2.50	
Theoretical approaches:		
Multiple-Scattering Xα [d]	2.60	1.00
CI [e]	3.29/2.92	1.10/1.10
EOM-CCSD	2.61	0.76

[a] See Reference 49 and 50 [b] See Reference 51 [c] See Reference 52 [d] See Reference 53 [e] See Reference 54

factor half with the exponent of last p function. The results for the basis set convergence study are presented in Table 2.8. The addition of first p function lowers the resonance energy value by 0.74 eV. In this basis i.e C+1P we get resonance energy $E_R = 1.87$ eV and width $\Gamma = 0.81$ eV which is very close to the result obtained in the trapped electron method. Further addition of p function lowers the resonance energy by 0.05 eV. After addition of three p-types functions we get the converged result.

Table 2.8: Basis set convergence study for the $^2\Pi_g$ $C_2H_2^-$ shape resonance

Basis	Energy (eV)	Width (eV)
Basis C +1P(C 1p/ C 1p)	1.87	0.81
Basis C + 2P(C 2p / C 2p)	1.82	0.79
Basis C + 3P(C 3p/ C 3p)	1.79	0.80

2.3.5 Potential energy curve for the $^2\Pi_g$ resonance state of N_2^-

In this section, we have calculated the potential energy curve (PEC) for the lower energy $^2\Pi_g$ state of N_2^-. In Fig 2.1 we provide the PEC for the $^2\Pi_g$ resonance state of N_2^-. The calculated resonance energies (E_R) and widths (Γ) for the $^2\Pi_g$ state of N_2^- are presented in Table 2.9 for different internuclear distances. The calculations have been carried out in four different basis sets. The first one consists of [5s7p] contracted Gaussian type orbitals (CGTO)[29]. For each nitrogen atom, one p type (exponent=0.03) function has been added. So, the basis set contains total [5s8p] functions on each nitrogen atom. We have denoted this basis as basis A. The second one denoted as basis B, the third one denoted as basis C and the fourth one is denoted as basis D. The basis B contains [5s10p] functions [6] and the basis C contains [5s10p2d] functions [6].The basis D consists of d-aug-cc-pVDZ basis and two extra p type functions have been added. The exponent of the new p function is generated by scaling the exponent of the last p function of the d-aug-cc-pVDZ basis by a ratio 1.5. Here, we have chosen the four different basis sets to show the basis set dependence on the PEC of the $^2\Pi_g$ resonance state of N_2^-.

The $\mathrm{CAP/EOM-CCSD'}$ computations are performed at $N-N$ internuclear distance between 1.80 a.u.- 2.80 a.u. In $\mathrm{CAP/EOM-CCSD'}$ calculations, the two nitrogen atoms are placed in a cartesian coordinate system at (0.0,0.0, $\pm$ R/2). where R is the internuclear distance between two nitrogen atoms in the Z axis. The CAP box side lengths are chosen to be $c_x = c_y = \delta c$ and $c_z = \delta c + R/2$. In order to obtain the the optimum box size for which the absorbing potential is best fitted to the basis set and the

size of the target system, the $\mathrm{CAP/EOM-CCSD}'$ calculations are performed for the various CAP box sizes. The velocity of the trajectory at the stabilization point is smallest for a box size $\delta c = 2.50$ a.u. compared to the other box size.

In Table 2.9 we report the position and width of resonance for different bond lengths in four different basis sets using the $\mathrm{CAP/EOM-CCSD}'$ method. It can be seen that in all four basis sets width of resonance is maximum at 1.80 a.u. and decreases uniformly with increasing the bond length and becomes zero at 2.80 a.u. Similar trend is also observed for position of the resonance. As we go from basis A to basis B, we get the higher resonance position for bond length upto 2.60 a.u. However, we get the higher width value for bond length upto 2.07 a.u. Beyond equilibrium bond length the width of the resonance is smaller in basis B compared to basis A. This shows the importance of addition of 2p functions. In basis C, which is similar to basis B with just additional 2d functions, there is not much change in position or width of resonance. This shows that addition of d function does not have much effect on the resonance position or width. In basis D we get results which are similar to basis B. It can be seen that in all the four basis sets qualitative trends are same.

Table 2.9: Calculated resonance energies (E_R) and decay widths (Γ) for the $^2\Pi_g$ state of N_2^-

Internuclear distance (a.u.)	Basis A		Basis B		Basis C		Basis D	
	E_R(eV)	Γ (eV)	E_R(eV)	Γ (eV)	E_R (eV)	Γ (eV)	E_R (eV)	Γ (eV)
1.80	1.98	0.78	2.36	0.84	2.36	0.87	2.43	0.81
1.90	1.93	0.65	2.25	0.68	2.34	0.71	2.45	0.65
2.00	1.98	0.60	2.28	0.57	2.26	0.59	2.36	0.39
2.07	1.98	0.44	2.36	0.48	2.28	0.48	2.36	0.35
2.20	1.92	0.39	2.06	0.29	2.01	0.32	1.98	0.29
2.30	1.74	0.30	1.82	0.27	1.74	0.21	1.60	0.18
2.40	1.33	0.17	1.46	0.16	1.41	0.08	1.33	0.11
2.50	1.27	0.04	1.38	0.11	1.36	0.05	1.05	0.09
2.60	1.25	0.02	1.27	0.08	1.30	0.05	0.97	0.05
2.70	1.25	0.01	0.97	0.02	1.30	0.02	0.95	0.04
2.80	1.25	0.00	0.95	0.00	1.30	0.00	0.93	0.00

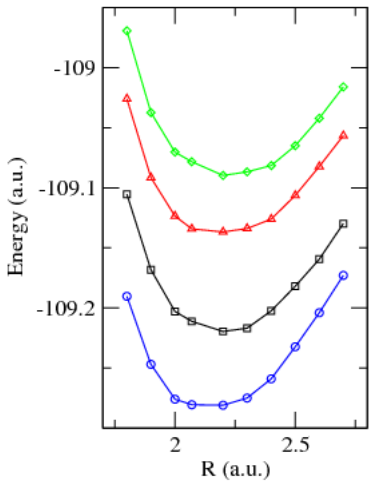

Figure 2.1: Potential energy curve (PEC) for the $^2\Pi_g$ state of N_2^-, Diamond symbol indicates the PEC in basis B, triangle symbol indicates the PEC in basis A, square symbol indicates the PEC in basis D, circle symbol indicates the PEC in basis C

2.3.6 Potential energy curve for the $^2\Pi$ state of CO^-

In this section, we have calculated the potential energy curve (PEC) for the $^2\Pi$ state of CO^-. The PEC for the $^2\Pi$ state of CO^- are presented in Fig 2.2. Two basis sets are used to study the PEC's of CO^- . The first one consists of d-aug-cc-pVDZ basis and the second one consists of d-aug-cc-pVDZ+1P basis. The d-aug-cc-pVDZ+1P basis is constructed by adding one p function on carbon and oxygen atom each. The exponent of new p function is generated by scaling the exponent of last p function in d-aug-cc-pVDZ basis by a factor 0.66. In the PEC calculation, the CO molecule is placed in a cartesian coordinate system at (0.0,0.0,$\pm$ R/2 a.u.) and the CAP box side lengths are chosen to

Table 2.10: Calculated resonance energies (E_R) and decay widths (Γ) for the $^2\Pi$ state of CO^-

Internuclear distance(a.u.)	d-aug-cc-pVDZ		d-aug-cc-pVDZ+1P	
	E_R(eV)	Γ (eV)	E_R (eV)	Γ (eV)
1.80	1.41	1.09	1.38	0.68
1.90	1.36	0.97	1.32	0.60
2.00	1.46	0.92	1.33	0.56
2.13	1.49	0.78	1.30	0.52
2.20	1.49	0.54	1.36	0.48
2.30	1.38	0.48	0.98	0.36
2.40	1.25	0.24	0.89	0.30
2.50	0.87	0.21	0.72	0.12
2.60	0.70	0.08	0.57	0.10
2.70	0.68	0.05	0.35	0.05
2.80	0.70	0.00	0.35	0.00

be $c_x = c_y = \delta c$ and $c_z = \delta c + R/2$. Where R is the internuclear distance between carbon and oxygen atom. The optimum value of δc is 3.5 a.u. The calculated resonance energies (E_R) and decay widths (Γ) for the $^2\Pi$ resonance state of CO^- as a function of internuclear separation are presented in Table 2.10.

From Table 2.10 it can be seen that in both the basis sets position and width Γ of resonance is reduced with the bond length. The width of resonance approaches to zero at 2.80 a.u. As we go from basis d-aug-cc-pVDZ to basis d-aug-cc-pVDZ+1P, in which we have extra p function, position and width of resonance is reduced. From Fig 2.2 it can be seen that PEC in both the basis sets have similar trend.

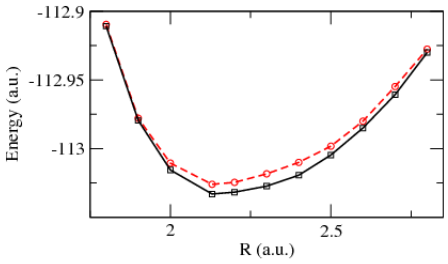

Figure 2.2: Potential energy curve (PEC) for the $^2\Pi$ state of CO^-, square symbol indicates the PEC in d-aug-cc-pVDZ+1P basis and circle symbol indicates the PEC in d-aug-cc-pVDZ basis

2.3.7 Conclusion

In this chapter we have shown how the highly correlated method like EOM-CCSD, which is already known to be suitable for accurate calculation of properties of electronically excited, bound states, can be extended for the treatment of resonance states in electron molecule collision. we have implemented complex absorbing potential within the EOM-CCSD method for the calculation of resonance energies. We have applied our method to study the $^2\Pi_g$ N_2^-,$C_2H_2^-$ and $^2\Pi$ CO^- shape resonances. We compare our results with different theoretical as well as experimental results. Our results for the resonance energy are in good agreement with the experimental and other theoretical methods. The present results clearly indicate the utility of the CAP/EOM-CCSD approach for the study of metastable electronic states. Since resonance energy is related to the electron affinity, the electron correlation play an important role for the accurate calculation of resonance

energy. From our study of the effect of basis set it can be seen that basis set, in particular, diffuse basis functions are very important for the accurate calculation of resonance energy.

References

[1] D. E. Golden, *Adv. At. Mol. Phys.* **14**, 1 (1978); G. J. Schulz, *Rev. Mod. Phys.* **45**, 423 (1973); P. G. Burke, *Adv. At. Mol. Phys.* **4**, 173 (1968).

[2] V. I. Kukulin, V. M. Kransnopol'sky, and J. Horacek, *Theory of Resonances (Kluwer, Dordrecht, 1989).*

[3] D. G. Truhlar, *in Modern Theoretical Chemistry, edited by G. A. Segal (Plenum, New York, 1977), Vol. 8.*

[4] A. U. Hazi and H. S. Taylor, *Phys. Rev. A* **1**, 1109 (1970).

[5] N. Moiseyev and F. Weinhold, *Phys. Rev. A* **20**, 27 (1979); M. N. Medikeri and M. K. Mishra, *Adv. Quantum Chem.* **27**, 223 (1996).

[6] T. Sommerfeld, U. V. Riss, H. D. Meyer, L. S. Cederbaum, B. Engels, and H. U. Suter, *J. Phys. B* **31**, 4107 (1998).

[7] G. Jolicard and E. J. Austin, *Chem. Phys. Lett.* **121**, 106 (1985).

[8] W. P. Reinhardt, *Annu. Rev. Phys. Chem.* **33**, 223 (1982); N. Moiseyev, *Phys. Rep.* **302**, 211 (1998).

[9] U. V. Riss and H. D. Meyer, *J. Phys. B* **26**, 4503 (1993); R. Santra and L. S. Cederbaum, *Phys. Rep.* **368**, 1 (2002); J. G. Muga, J. P. Palao, B. Navarro, and I. L. Egusquiza, *Phys. Rep.* **395**, 357 (2004).

[10] N. Moiseyev and C. Corcoran, *Phys. Rev. A* **20**, 814 (1979); T. N. Rescigno, C. W. McCurdy, and A. E. Orel, *Phys. Rev. A* **17**, 1931 (1978); C. W. McCurdy and T. N. Rescigno, *Phys. Rev. Lett.* **41**, 1364 (1978).

[11] N. Rom, N. Lipkin, and N. Moiseyev, *Chem. Phys.* **151**, 199 (1991).

[12] N. Moiseyev, *J. Phys. B* **31**, 1431 (1998); U. V. Riss and H. D. Meyer, *J. Phys. B* **31**, 2279 (1998).

[13] R. Santra and L. S. Cederbaum, *J. Chem. Phys.* **115**, 6853 (2001).

[14] R. Santra, L. S. Cederbaum, and H. D. Meyer, *Chem. Phys. Lett.* **303**, 413 (1999).

[15] R. A. Donnelly and J. Simons, *J. Chem. Phys.* **73**, 2858 (1980); Y. K. Ho, *Phys. Rep.* **99**, 1 (1983).

[16] Y. Sajeev, M. K. Mishra, N. Vaval, and S. Pal, *J. Chem. Phys.* **120**, 67 (2004); Y. Sajeev, R. Santra, and S. Pal, *J. Chem. Phys.* **123**, 204110 (2005); Y. Sajeev and S. Pal, *Mol. Phys.* **103**, 2267 (2005).

[17] T. sommerfeld and R. Santra, *Int. J. Quantum Chem.* **82**, 218 (2001).

[18] T. Sommerfeld, U. V. Riss, H. D. Meyer, and L. S. cederbaum, *Phys. Rev. Lett.* **79**, 1237 (1997).

[19] R. Santra and L. S. cederbaum, *J. Chem. Phys.* **117**, 5511 (2002).

[20] S. Feuerbacher, T. Sommerfeld, R. Santra, and L. S. Cederbaum, *J. Chem. Phys.* **118**, 6188 (2003).

[21] M. Mishra, O. Goscinski, and Y. öhrn, *J. Chem. Phys.* **79**, 5505 (1983).

[22] M. N. Medikeri and M. Mishra, *Int. J. Quantum Chem., Symp.* **S28**, 29 (1994).

[23] M. Berman, O. Walter, and L. S. Cederbaum, *Phys. Rev. Lett.* **50**, 1979 (1983).

[24] M. Berman, H. Estrada, L. S. Cederbaum, and W. Domcke, *Phys. Rev. A* **28**, 1363 (1983).

[25] B. I. Schneider and L. A. Collins, *Phys. Rev. A* **30**, 95 (1984).

[26] W. M. Huo, T. L. Gibson, M. A. P. Lima, and V. Mckoy, *Phys. Rev. A* **36**, 1632 (1987).

[27] C. J. Gilan, C. J. Noble, and P. G. Burke, *J. Phys. B* **21**, L53 (1988).

[28] B. M. Nestmann and S. D. Peyerimhoff, *J. Phys. B* **18**, 615 (1985); **18**, 4309 (1985).

[29] H. D. Meyer, *Phys. Rev. A* **40**, 5605 (1989).

[30] J. Cizek, *J. Chem. Phys.* **45**, 4256 (1966).

[31] J. Cizek, *Adv. Chem. Phys.* **14**, 35 (1969).

[32] R. J. Bartlett, *Annu. Rev. Phys. Chem.* **32**, 359 (1981).

[33] M. Nooijen and R. J. Bartlett, *J. Chem. Phys.* **102**, 3629 (1995).

[34] M. Nooijen and R. J. Bartlett, *J. Chem. Phys.* **102**, 6735 (1995).

[35] J. Stanton and J. Gauss, *J. Chem. Phys.* **101**, 8938 (1994).

[36] J. F. Stanton and R.J. Bartlett, *J. Chem. Phys.* **98**, 7029 (1993).

[37] D. C. Comeau and R. J. Bartlett, *Chem. Phys. Lett.* **207**, 414 (1993).

[38] J. Geertsen, M. Rittby, and R.J. Bartlett, *Chem. Phys. Lett.* **164**, 57 (1989).

[39] M. Musial, S. A. Kucharski, and R.J. Bartlett, *J. Chem. Phys.* **118**, 1128 (2003).

[40] M. Musial and R.J. Bartlett, *J. Chem. Phys.* **119**, 1901 (2003).

[41] M. Musial and R.J. Bartlett, *Chem. Phys. Lett.* **384**, 210 (2004).

[42] M. Honigmann, R. J. Buenker, and H. P. Liebermann, *J. Chem. Phys.* **125**, 234304 (2006).

[43] M. Honigmann, R. J. Buenker, and H. P. Liebermann, *J. Chem. Phys.* **131**, 034303 (2009).

[44] R. A. Donnelly, *Int. J. Quantum Chem., Symp.* **S19**, 337 (1985).

[45] H. Erhardt, L. Langhans, F. Linder, and H. S. Taylor, *Phys. Rev. A* **173**, 222 (1968).

[46] M. Zubek and C. Szmytkowski, *J. Phys. B* **10**, L27 (1977)

[47] N. Chandra, *Phys. Rev. A* **16**, 80 (1977).

[48] S. Mahalakshmi, A. Venkatnathan, and M. K. Mishra, *J. Chem. Phys.* **115**, 4549 (2001).

[49] D. F. Dance and I. C. Walker, *Chem. Phys. Lett.* **18**, 601 (1973).

[50] E. H. Van Veen and F. L. Plantenga, *Chem. Phys. Lett.* **38**, 493 (1976).

[51] K. H. Kochem, W. Sohn, K. Jung, H. Erhardt, and E. S. Chang, *J. Phys. B* **18**, 1253 (1985).

[52] L. Andric and R. I. Hall, *J. Phys. B* **21**, 355 (1988).

[53] J. A. Tossel, *J. Phys. B* **18**, 387 (1985).

[54] V. Krumbach, B. M. Nestmann, and S. D. Peyerimhoff, *J. Phys. B* **22**, 4001 (1989).

Chapter 3

CAP/EOM-CCSD method for the potential energy curve of CO_2^- anion

In this chapter, the equation-of-motion coupled cluster (EOM-CC) method employing the complex absorbing potential (CAP) has been used to investigate the low energy electron scattering by CO_2. We have studied the potential energy curve (PEC) for the $^2\Pi_u$ resonance states of CO_2^- upon bending as well as symmetric and asymmetric stretching of the molecule. Specifically, we have stretched the $C-O$ bond length from 1.1 $\AA$ to 1.5 $\AA$ and the bending angles are changed between 180° to 132°. Upon bending, the low energy $^2\Pi_u$ resonance state is split into two components, i.e. $^2A_1$, $^2B_1$ due to the Renner-Teller effect (RT), which behave differently as the molecule is bent.

3.1 Introduction

Since its discovery, the low energy electron scattering of CO_2 has continued to fascinate the imagination of chemists and physicists because of its role in atmospheric chemistry, gas lasers and low temperature plasma. It is well known that CO_2 can not permanently bind an electron and that all CO_2^- states are metastable in nature. Despite the long standing interest in electron scattering in CO_2, there are a number of questions unresolved. One of the open intriguing questions is the connection between the short-lived scattering states with the long-lived CO_2^- anions in the mass spectroscopy region.

The electron scattering in CO_2^- is mainly governed by two low lying anionic states, one is $^2\Sigma_g^+$ symmetry [1, 2] virtual state and another is $^2\Pi_u$ resonance state.[3–7] Both the $^2\Pi_u$ resonance states and $^2\Sigma_g^+$ virtual states have very short lifetime. Generally, the $^2\Pi_u$ resonance states have lifetime in the femto-second (fs) region. In compare to the short lived $^2\Pi_u$ resonance state, the existence of long-lived CO_2^- anion [8, 9] has also been proved. The double electron transfer to the CO_2^+ ion, [10, 11] electron collisions with cyclic anhydrides [12] are the some techniques where long lived CO_2^- is produced.

The resonance states are identified by complex eigenvalues within the formalism of Siegert and Gamow, [13, 14]

$$E_{res} = E_R - i\Gamma/2, \tag{3.1}$$

where E_R is the resonance position and Γ is the decay width. The Γ is related to the lifetime of the temporary anionic state via, $\tau = \hbar/\Gamma$.

The resonance states are metastable [15, 16] in nature and can be described as the coupling of a discrete state with a continuum. The resonance states are part of the continuum and are represented by a non-square integrable wave function (non-L^2). Thus the calculation of resonance states requires a method which is able to address the continuum nature as well its many body nature. Two principal classes of approaches are well known for computing the resonance energy E_r and the decay width Γ. First, scattering methods

which precisely address the continuum nature of the wave function and second, so-called L^2 methods that transform the continuum problem to a bound state problem. There are two L^2 methods which are very well known in literature, one is the complex absorbing potential approach (CAP) [17–25] the other is the complex scaling approach. [26, 27] Here, our focus is on the complex absorbing potential approach. The main advantage of the CAP method is that it is easy to implement within any bound state $ab\,initio$ electronic structure method.

The CAP method has been applied in the context of various theoretical methods. Historically, Jolicard and Austin [28] implemented the CAP method for the first time to calculate the resonance parameters subject to a model potential. The CAP method has been established on firm ground by Riss and Meyer.[20] The first implementation of CAP in the context of bound state electronic structure theory was done by Sommerfeld et al. [18] for metastable anions and Santra et al. [23] for metastable cations, both in combination with the configuration interaction method (CI). Later, Santra and co-workers [24] introduced the CAP method within the Green's function approach. Sajeev et al. [29] introduced a CAP potential within the Fock space multireference coupled cluster (FSMRCC) framework to study anion resonances. Ehara et al. [30] implemented the CAP potential within the symmetry-adapted cluster-configuration interaction (SAC-CI) method for metastable anions. Recently, Ghosh et al. [31–34] have introduced CAP within the EOM-CC framework for both anionic and cationic resonance states. Kyrlov and co-workers [35] have also applied CAP within the EOM-CC framework for the study of shape resonance.

Both electron correlation and relaxation effects play a substantial role in the accurate description of resonance states. The equation-of-motion coupled-cluster method treats the dynamic and non-dynamic electron correlation in a very efficient manner while fulfuling the size-extensivity criteria in the ground state. Another advantage is that the EOM-CCSD method [36–42] gives the direct, intensive energy difference. This makes the EOM-CC method appropriate for the description of resonance states.

Electron scattering on CO_2 has been studied quite elaborately both experimentally and theoretically. Detailed studies of resonant vibrational excitation of CO_2 have been performed experimentally by Allan.[43, 44] $Ab\ initio$ calculations on CO_2^- have been studied by Morgan et al.[45] using the R matrix method. In their calculations, they have focused on the angular dependence of the virtual state pole. Rescigno et al. [3, 6] have studied scattering on CO_2 focusing on the $^2\Pi_u$ shape resonance state pole. Recently, McCurdy et al. [7] have performed an extensive study on the vibrational excitation cross section [46, 47] of CO_2 by electron impact in the vicinity of $^2\Pi_u$ resonance.

In this chapter, we have implemented the CAP method within the equation-of-motion coupled cluster theory (CAP/EOM-CC) using singles and doubles (SD) to calculate the position and width of the $^2\Pi_u$ shape resonance in CO_2^-. We have studied the potential curve for the $^2\Pi_u$ resonance state of CO_2^- as a function of the symmetric and asymmetric stretches of the $C-O$ bond and the bending angle.

3.2 Theory

In this section, we briefly discuss the CAP/EOM-CCSD method for computing the resonance energy E_R and decay width Γ. In the CAP approach, the idea is to add an absorbing potential, $-i\eta W$, to the physical Hamiltonian, H, yielding a non-hermitian Hamiltonian

$$H(\eta) = H - i\eta W, \tag{3.2}$$

where η is a strength parameter and W is a real, soft box like potential. The addition of CAP makes the wave function square integrable. The complex Hamiltonian matrix is diagonalized for a number of η values to obtain the resonance energy. The complex resonance energy (E_r) is identified from the η trajectories of the eigenvalues of $H(\eta)$. The distinct minimum of the velocity

$$\upsilon_i(\eta) = \eta \partial E_i / \partial \eta. \tag{3.3}$$

gives the resonance energy. The best approximation for the E_r is obtained from the optimal η_{opt} value. The optimal η_{opt} value is obtained by employing the condition,

$$|\upsilon_i(\eta_{opt})| = min. \tag{3.4}$$

In the EA-EOM-CCSD approach,[34] the wave function for the μ th electron attached ($N+1$ electron) states can be written as

$$\Psi(\mu) = R^{N+1}(\mu)|\Psi_0\rangle \tag{3.5}$$

where

$$|\Psi_0\rangle = e^T|\phi_0\rangle \tag{3.6}$$

is the N electronic ground state wave function for the Coupled cluster (CC) method. [48–51] The $R^{N+1}(\mu)$ is a linear excitation operator for the state μ defined as

$$R^{N+1}(\mu) = \sum_a r^a(\mu) a_a^+ + 1/2 \sum_i \sum_{ab} r_i^{ab}(\mu) a_a^+ a_b^+ a_i. \tag{3.7}$$

In eq. 3.6, $|\phi_0\rangle$ is the N-electron closed-shell Hartree-Fock determinant and T represents the cluster operator. The cluster operator T consists of singles, doubles,..., excitation operators. The cluster operator T can be defined as following manner

$$T = \sum_{ia} t_i^a a_a^+ a_i + 1/4 \sum_{ab} \sum_{ij} t_{ij}^{ab} a_a^+ a_b^+ a_i a_j + ..., . \tag{3.8}$$

where the standard convention for the indices is used, i.e., indices a,b,..., refer to the unoccupied orbitals and indices i,j,.., refer to the occupied orbitals. The cluster matrix elements t are generated by using the equation

$$\langle \phi_e | (H_N e^T)_c | \phi_0 \rangle = 0, \tag{3.9}$$

where $|\phi_e\rangle$ are the excited determinants and c in eq. 3.9 indicates only the connected diagrams are considered.

In the equation-of-motion coupled cluster method for singles and doubles (EOM-CCSD), the difference between the energies of μ th electron attached states and ground state ($w_\mu = E_\mu - E_g$) are calculated

$$[\bar{H_N}, R^{N+1}(\mu)]|\phi_0\rangle = w_\mu R^{N+1}(\mu)|\phi_0\rangle \forall \mu, \tag{3.10}$$

on projecting onto the basis of excited determinants $|\phi^a\rangle$ and $|\phi_i^{ab}\rangle$ with respect to $|\phi_0\rangle$, gives the matrix form,

$$\bar{H_N} R^{N+1}(\mu) = w_\mu R^{N+1}(\mu). \tag{3.11}$$

Where

$$\bar{H_N} = e^{-T} H_N e^T - \langle\phi_0|e^{-T} H_N e^T|\phi_0\rangle \tag{3.12}$$

is the similarity transformed Hamiltonian of the coupled-cluster (CC) method and w_μ is the energy change connected with the electron attachment process. In the EA-EOM-CCSD approach, $\bar{H_N}$ is constructed in a $1p$ and $2p1h$ space and diagonalized to obtain the electron attachment energies.

Once the CAP is added into the CAP/EOM-CCSD method, it becomes part of the one body particle-particle ($\bar{f_{pp}}$) part of $\bar{H_N}$. The other terms of the $\bar{H_N}$ matrix are altered via the appearance of the complex $T(\eta)$. Thus, the new form of the $\bar{H_N}$ matrix is

$$\bar{H_N}(\eta) = e^{-T(\eta)} H_N(\eta) e^{T(\eta)} - \langle\phi_0|e^{-T(\eta)} H_N(\eta) e^{T(\eta)}|\phi_0\rangle \tag{3.13}$$

Here, initially, we have applied the CAP to the coupled cluster (CC) method to evolve the complex $T(\eta)$ amplitudes, which are used latter to construct the $\bar{H_N}(\eta)$ matrix. After addition of CAP, the ground state wave function for the CC method can be expressed as

$$|\Psi_0(\eta)\rangle = e^{T(\eta)}|\phi_0\rangle \tag{3.14}$$

Finally, we have diagonalized the resulting complex $\bar{H_N}(\eta)$ matrix for the different η values. However to obtain the resonance energies we need to use following equation since the ground state energies are suppose to be CAP free.

$$E_{res}(\eta) = w_{\mu}(\eta) + E_{CC}(\eta) - E_{CC}(\eta = 0) \tag{3.15}$$

The resonance states can be identified from the η trajectories that shows stabilization cusps.

Recently, Kyrlov and co-workers[35] have applied the CAP within the EOM-CC framework. However, their approach is different from our approach. They use $E_{res}(\eta)$ as $[E_{N+1}(\eta) - E_N(\eta)]$. Further to calculate both $E_{N+1}(\eta)$ and $E_N(\eta)$ they add CAP at the SCF level. The SCF orbitals, T amplitudes, R operator are complex in nature. Therefore, the SCF ground state is perturbed in their approach. However, we have applied the CAP into the CC level or a perturvative in calculating $E_{N+1}(\eta)$. Therefore, in our approach SCF ground state is unperturbed.

3.3 Computational details

The one-particle basis set used in the CAP/EOM-CCSD [31–33] calculation is a combination of valence basis sets with some number of diffuse functions. The diffuse functions are required to describe the outgoing electron. Here, we start with the aug-cc-pVTZ [52] basis. We have removed the f functions form the aug-cc-pVTZ basis set and then add one extra s function and one diffuse p function on each carbon and oxygen atom in CO_2.

The exponent of the new p function is generated by scaling the exponent of the last p function of the aug-cc-pVTZ basis by a ratio 3.165. The exponent of the new s function is generated by scaling the exponent of the last s function of the aug-cc-pVTZ basis by a ratio 3.165.

The first step in the CAP/EOM-CCSD computations is an SCF calculation for the neutral CO_2. The SCF calculation has been performed by using the GAMESS-US suite

of programs.[53] The required matrix elements of the EOM-CCSD and CAP matrices have been computed using our own codes. For diagonalization purpose, we have implemented the non hermitian version of Davidson algorithm[54, 55] in our EOM-CC code.

The potential W is the soft-box potential and it can be defined as

$$W(x;c) = \sum_{i=1}^{3} W_i(x_i;c_i), \tag{3.16}$$

where

$$W_i(x_i;c_i) = \{^{0,|x_i|\leq c_i,}_{(|x_i|-c_i)^2,|x_i|>c_i} \tag{3.17}$$

Here, $c_i, i = 1,3$ are the real, non-negative parameters which define the size of a rectangular box. The target molecule is placed in the center of the box. The matrix elements of $W(x;c)$ are calculated within a Gaussian basis set.

In order to keep the neutral N electron ground scattering target system unperturbed, we eliminate the effect of CAP on the SCF ground state,

$$\hat{W} \rightarrow \hat{Q}\hat{W}\hat{Q}, \tag{3.18}$$

where

$$\hat{Q} = \sum_{i} |\phi_i\rangle\langle\phi_i|. \tag{3.19}$$

The redefinition is easily achieved by employing the condition

$$\langle\phi_p|\hat{W}|\phi_q\rangle = 0, \tag{3.20}$$

where $|\phi_p\rangle$ or $|\phi_q\rangle$ is an occupied orbital.

3.4 Results and Discussions

Here, we investigate the potential energy curve (PEC) of the metastable low energy $^2\Pi_u$ resonance state of CO_2^- using the CAP/EOM-CCSD method. We have studied the PEC for the $^2\Pi_u$ resonance state of CO_2^- as a function of the symmetric and asymmetric

stretch of $C-O$ and the $O-C-O$ bond angle. In the CAP/EOM-CCSD calculations, the CO_2 molecule is placed in a cartesian system at $(0.0, 0.0, \pm Ra.u.)$, where R is the bond distance between the carbon and oxygen atom. In the CAP/EOM-CC computations, for the symmetric and asymmetric stretch the CAP box side lengths are chosen to be $c_x = c_y = \delta c$ and $c_z = \delta c + R$, where c_x,c_y,c_z are the distances from the center of the coordinate system along the x,y, and z axis, respectively, and δc is a non-negative number, all in a.u. However, in case of bending, the CAP box side lengths are chosen to be $c_x = \delta c + r_x$, $c_y = \delta c$ and $c_z = \delta c + r_z$, where r_x and r_z are the C-O bond lengths along the x and z axis, respectively.

We have performed CAP/EOM-CCSD calculations for the symmetric and asymmetric stretch in two different δc values. The δc values are 2.5 a.u. and 3.5 a.u. respectively. However, We have performed CAP/EOM-CCSD calculations for the bending in three different δc values. The δc values are 2.0 a.u., 2.5 a.u. and 3.5 a.u. respectively. We have shown for all the box sizes the resonance energies and decay widths follow the similar trend for the symmetric stretch, asymmetric stretch and bending of the CO_2 molecule.

3.4.1 Potential energy curve of the $^2\Pi_u$ resonance state of the CO_2^-

In this subsection, we discuss the PEC for the low energy $^2\Pi_u$ resonance state of CO_2^- using the CAP/EOM-CCSD method. The electron scattering in CO_2^- is dominated by the $^2\Pi_u$ resonance state. The $^2\Pi_u$ state is generated by adding an electron to the empty π^* orbital of the neutral CO_2. The equilibrium bond distance between carbon and oxygen ($C-O$) in CO_2 molecule is 1.161 $\mathring{A}$. The ground state electronic configuration of CO_2 is

$$^1\Sigma_g^+ : (core)^6\sigma_g^2\sigma_u^2\sigma_g^2\sigma_u^2\pi_u^4\pi_g^4. \tag{3.21}$$

The orbital symmetry of the CO_2 molecule changes upon bending. The orbital symmetry changes in the following manner: $\sigma_g \rightarrow a_1$, $\sigma_u \rightarrow b_2$, $\pi_g \rightarrow a_2 + b_2$, $\pi_u \rightarrow a_1 + b_1$.

Since, the linear CO_2 molecule contains two low lying empty valence orbitals of σ_g and π_u symmetry, one can expect two low lying anionic states. One is the $^2\Pi_u$ resonance state and another is the $^2\Sigma_g^+$ virtual state. In C_{2v} symmetry, the $^2\Pi_u$ resonance state of CO_2 further corresponds to the $^2A_1$ (lower energy) and $^2B_1$ (higher energy) states and the virtual $^2\Sigma_g^+$ state corresponds to the $^2A_1$ state. Here, we concentrate on the $^2A_1$ component of the $^2\Pi_u$ resonance state.

In PEC calculation, the $C-O$ bonds are symmetrically stretched from 1.1 $\mathring{A}$ to 1.5 $\mathring{A}$ and the bond angle is changed between 180° to 132° in steps of 3°. The calculated resonance energies E_R and decay widths Γ for the $^2\Pi_u$ resonance state of CO_2^- are collected in Table 3.1 for the different $C-O$ bond lengths. The results for the $^2A_1$ component of $^2\Pi_u$ state are collected in Table 3.2 for the different $\angle O-C-O$ bond angles.

In linear geometry, the PEC curve for the $^2\Pi_u$ state is shown in Fig 3.1 at different $C-O$ bond lengths. Starting from the equilibrium $C-O$ bond length the resonance position E_R decreases substantially with increasing the $C-O$ bond length. The decay width Γ also decreases with increasing the $C-O$ bond length. Finally, the $^2\Pi_u$ resonance state becomes a bound state at a distance $\rangle$ 1.45 $\mathring{A}$. At this distance the PEC of $^2\Pi_u$ CO_2^- crosses the PEC of ground state and the decay width vanishes.

Among the two $^2A_1$ states, the lowest $^2A_1$ state which is originated from the virtual $^2\Sigma_g^+$ state quickly turn into a bound state on bending the molecule. The lowest $^2A_1$ state becomes bound at an angle 147°. In contrast, the second $^2A_1$ state does not become bound on bending the molecule. The second $^2A_1$ state becomes stable only on stretching. The PEC for $^2A_1$ resonance states as a function of $O-C-O$ bond angle are presented in Fig 3.2.

Starting from the linear geometry, the bending of the CO_2 molecule causes the width of the $^2A_1$ component of the $^2\Pi_u$ resonance state to increase rapidly while decreasing the resonance energy. It is worth discussing why the width of the $^2A_1$ resonance state increases upon bending of the molecule. The symmetric stretching of the CO_2 molecule

in a linear geometry does not change the symmetry of the molecule. Thus, it does not significantly change the angular momentum character of the resonance state. In linear geometry, the lowest l component of the resonance state is a p-wave in nature but not the dominant-one which is f-wave in nature. The degeneracy of the $^2\Pi_u$ resonance state is lost when we bend the CO_2 molecule and as an s-wave component is mixed into the $^2A_1$ resonance state. There is no angular momentum barrier associated with an s-wave. So, the mixing of the s-wave into the $^2A_1$ resonance state plays a significant role in increasing the resonance width upon bending the molecule.

Another important point is that in a linear geometry the CO_2 molecule has zero dipole moment. As we bend the CO_2 molecule, it acquires a dipole moment. This is another aspect of symmetry breaking and mixing of the s-wave into the resonance state which contributes to an increase in width with increasing bending angle. At small bending angles, the dipole moment is less and its consequences are not great. However, the dipole moment increases with increasing the bending angle and it plays a crucial role in changing the behavior of the resonance state.

We also investigate how the $^2\Pi_u$ resonance state behaves subject to the asymmetric stretch of the C-O bond. In our calculations, we have stretched the one C-O bond from 1.2 $\mathring{A}$ to 1.5 $\mathring{A}$ and the other is shrunk from 1.1 $\mathring{A}$ to 0.80 $\mathring{A}$ simultaneously. The results are reported in Table 3.3. From Table 3.3 it can be seen that in asymmetric stretching the resonance energy for the $^2\Pi_u$ resonance state and its decay width increases rapidly. The important aspect concerning the behavior of the $^2\Pi_u$ resonance state is that the dipole moment becomes non-zero when we stretch the CO_2 molecule asymmetrically. The dipole moment increases rapidly with the asymmetric stretch of the molecule. The long range dipole potential progressively weakens the short-range attractive potential created by the angular momentum barrier. Thus, the dipole moment plays the crucial role in increasing the width for asymmetric stretch.

We compare our results with the experimental method and the other theoretical methods available in the literature at the equilibrium bond length. The results are collected

in Table 3.4. The experimental method [43] gives resonance energy around 3.60 eV, which shows close agreement with the EOM-CCSD results. The Static exchange method [56] gives resonance position at E_R=5.26 eV and decay width Γ=0.70 eV, the $ADC(2)$ method gives resonance position E_R= 4.21 eV and decay width Γ= 0.21 eV at the equilibrium bond length. Thus, we can see that the Static exchange to $ADC(2)$ [56] the resonance position is reduced by 1.05 eV and decay width is also reduced by 0.49 eV. The result obtained with the $ADC(2)$ method [56] is very close to our results obtained using the EOM-CCSD method.

Table 3.1: Calculated resonance energies E_R and decay widths (Γ) for the $^2\Pi_u$ resonance state of CO_2^- at different $C-O$ bond length

Bond distance(Angstrom)	$\delta c = 2.5$a.u		$\delta c = 3.5$a.u	
	E_R(eV)	Γ(eV)	E_R(eV)	Γ(eV)
1.10	5.56	0.32	5.55	0.19
1.13	4.90	0.28	4.91	0.18
1.16	4.18	0.19	4.17	0.15
1.19	3.70	0.16	3.67	0.12
1.23	2.97	0.14	2.97	0.09
1.27	2.31	0.12	2.32	0.08
1.30	1.86	0.11	1.86	0.08

Table 3.2: Calculated resonance energies E_R and decay widths (Γ) for the $^2A_1$ component (lower energy) of $^2\Pi_u$ resonance state of CO_2^- at different $O-C-O$ bond angles

Bond angle (deg)	δc=2.0 a.u		δc=2.5 a.u		δc=3.5 a.u	
	E_R(eV)	Γ(eV)	E_R(eV)	Γ(eV)	E_R(eV)	Γ(eV)
180	4.19	0.23	4.18	0.19	4.17	0.15
177	4.18	0.23	4.18	0.20	4.17	0.15
174	4.18	0.24	4.17	0.20	4.16	0.15
171	4.16	0.25	4.16	0.21	4.15	0.16
168	4.14	0.25	4.14	0.22	4.13	0.16
165	4.11	0.26	4.11	0.23	4.10	0.17
162	4.09	0.28	4.09	0.24	4.07	0.17
159	4.07	0.30	4.06	0.25	4.03	0.19
156	4.02	0.32	4.02	0.27	4.01	0.20
153	3.99	0.33	3.98	0.28	3.95	0.21
150	3.96	0.34	3.95	0.29	3.92	0.22
147	3.90	0.36	3.90	0.30	3.88	0.22
144	3.87	0.38	3.86	0.32	3.83	0.22
141	3.82	0.39	3.80	0.33	3.79	0.23
138	3.80	0.41	3.79	0.35	3.79	0.23
135	3.76	0.42	3.75	0.35	3.74	0.23
132	3.70	0.43	3.70	0.36	3.69	0.24

Table 3.3: Calculated resonance energies E_R and decay widths (Γ) for the $^2\Pi_u$ resonance state of CO_2^- in asymmetric stretching of $C-O$ bond length

Bond distance(Angstrom)	δc=2.5 a.u		δc=3.5 a.u	
	E_R(eV)	Γ(eV)	E_R(eV)	Γ(eV)
1.10,1.20	4.45	0.23	4.42	0.19
0.95,1.35	5.18	0.32	5.15	0.21
0.90, 1.40	5.54	0.36	5.52	0.23
0.80, 1.50	6.49	0.54	6.44	0.36

Table 3.4: Calculated resonance energies E_R and decay widths (Γ) for the $^2\Pi_u$ resonance state of CO_2^- at equilibrium bond length

Method	E_R(eV)	Γ(eV)
Experiment[a]	3.60	....
Static exchange [b]	5.26	0.70
ADC(2) [b]	4.21	0.21
EOM-CCSD	4.18	0.19

[a] See reference 43. [b] see reference 56.

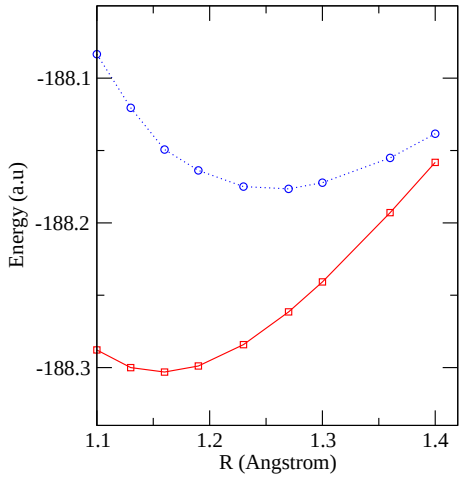

Figure 3.1: Potential energy curve (PEC) for $^2\Pi_u$ resonance state and ground state of CO_2. Circles indicate the PES for the $^2\Pi_u$ resonance state

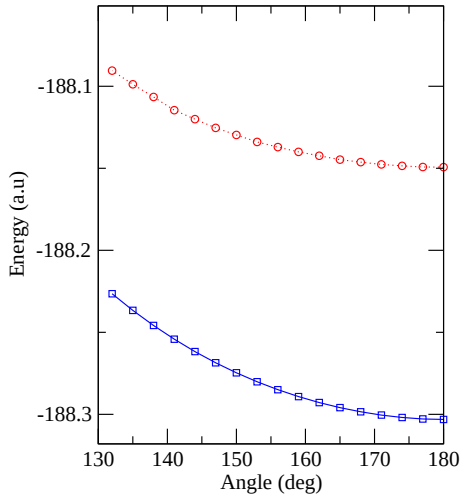

Figure 3.2: Potential energy curve for the $^2A_1$ resonance state and ground state of CO_2. Circles indicate the PEC for the $^2A_1$ resonance state and squres indicate the PEC for ground state CO_2

3.5 Conclusion

In this chapter we have implemented the CAP/EOM-CCSD method to investigate the potential energy curve (PEC) of $^2\Pi_u$ resonance state of CO_2^-. We have studied the PEC of the resonance state as a function of the $C-O$ bond length and $\angle O-C-O$ bond angle. In linear geometry both the short-lived states, $^2\Sigma_g^+$and $^2\Pi_u$ resonance states become bound when the CO_2 molecule is stretched. The $^2\Pi_u$ resonance state becomes bound at $C-O$ bond length $\rangle$ 1.45 $\mathring{A}$. When the CO_2 molecule departs from linearity, the $^2\Pi_u$ resonance state splits into two components, i.e., $^2A_1$, $^2B_1$, due to the Renner-Teller (RT) [57] effect. Upon bending the molecule, the $^2A_1$ component of the $^2\Pi_u$ resonance state is mixed with the $^2A_1$ component of $^2\Sigma_g^+$ virtual state. Thus, the $^2A_1$ component of the $^2\Sigma_g^+$ virtual state acquire some Π character. The $^2A_1$ component of the $^2\Sigma_g^+$ state becomes bound at a bending angle $\langle$ 147°. So, the PEC of CO_2^- can be viewed as three effective vibronically coupled electronic states problem.

References

[1] M. A. Morrison, *Phys. Rev. A* **25**, 1445 (1982)

[2] S. Mazevet, M. A. Morrison, L. A. Morgan, and R. k. Nesbet, *Phys. Rev. A* **64**, 40701 (2001).

[3] T. N. Rescigno, D. A. Byrum, W. A. Isaacs, and C. W. McCurdy, *Phys. Rev. A* **60**, 2186 (1999).

[4] M. A. Morrison, N. F. Lane, and L. Collins, *Phys. Rev. A* **15**, 2186 (1977).

[5] C. H. Lee, C. Winstead, and V. McKoy, *Chem. Phys.* **111**, 5056 (1999).

[6] T. N. Rescigno, W. A. Isaacs, A. E. Orel, H. D. Meyer, and C. W. McCurdy, *Phys. Rev. A* **65**, 32716 (2002).

[7] C. W. McCurdy, W. A. Isaacs, H. D. Meyer, and T. N. Rescigno, *Phys. Rev. A* **67**, 42708 (2003).

[8] A. Dreuw, T. Sommerfeld, and L. S. Cederbaum, *Theor. Chem. Acc.* **100**, 60 (1998); A. Dreuw and L. S. Cederbaum, *J. Phys. B* **32**, L665 (1999).

[9] T. Sommerfeld, H. D. Meyer, and L. S. Cederbaum, *Phys. Chem. Chem. Phys.* **6**, 42 (2004); T. Sommerfeld, *J. Phys. B* **36**, L-127 (2003).

[10] D. Schr öder, C. A. Schalley, J. N. Harvey, and H. Schwartz, *Int. J. Mass Spectrom.* **185**, 25 (1999).

[11] M. K. Raarup, H. H. Andersen, and T. Andersen, *J. Phys. B* **32**, L659 (1999).

[12] C. D. Cooper and R. N. Compton, *Chem. Phys. Lett.* **14**, 29 (1972).

[13] A. J. F. Siegert, *Phys. Rev.* **56**, 750 (1939).

[14] G. Gamow, *Der Bau des Atomkerns und die Radioaktivität* **(**S. Hirzel, Leipzig, 1932).

[15] A. U. Hazi and H. S. Taylor, *Phys. Rev. A* **1**, 1109 (1970)

[16] N. Moiseyev and F. Weinhold, *Phys. Rev. A* **20**, 27 (1979).

[17] J. Zobeley, L. S. Cederbaum, and F. Tarantelli, *J. Chem. Phys.* **108**, 9737 (1998)

[18] T. Sommerfeld, U. V. Riss, H. -D. Meyer, L. S. Cederbaum, B. Engels, and H. U. Suter, *J. Phys. B* **31**, 4107 (1998).

[19] W. P. Reinhardt, *Annu. Rev. Phys. Chem.* **33**, 223 (1982);

[20] U. V. Riss and H. D. Meyer, *J. Phys. B* **26**, 4503 (1993)

[21] J. G. Muga, J. P. Palao, B. Navarro, and I. L. Egusquiza, *Phys. Rep.* **395**, 357 (2004).

[22] N. Moiseyev, *J. Phys. B* **31**, 1431 (1998); U. V. Riss and H. D. Meyer, *J. Phys. B* **31**, 2279 (1998).

[23] R. Santra and L. S. Cederbaum, *J. Chem. Phys.* **117**, 5511 (2002).

[24] S. Feuerbacher, T. Sommerfeld, R. Santra, and L. S. Cederbaum, *J. Chem. Phys.* **118**, 6188 (2003).

[25] R. Santra and L. S. Cederbaum, *Phys. Rep.* **368**, 1 (2002)

[26] N. Moiseyev, *Phys. Rep.* **302**, 212 (1998).

[27] N. Rom, N. Lipkin, and N. Moiseyev, *Chem. Phys.* **151**, 199 (1991).

[28] G. Jolicard and E. J. Austin, *Chem. Phys. Lett.* **121**, 106 (1985).

[29] Y. Sajeev, M. K. Mishra, N. Vaval, and S. Pal, *J. Chem. Phys.* **120**, 67 (2004); Y. Sajeev, R. Santra, and S. Pal, *J. Chem. Phys.* **123**, 204110 (2005); Y. Sajeev and S. Pal, *Mol. Phys.* **103**, 2267 (2005).

[30] M. Ehara and T. Sommerfeld, *Chem. Phys. Lett.* **537**, 107 (2012)

[31] A. Ghosh, N. Vaval, and S. Pal, *J. Chem. Phys.* **136**, 234110 (2012)

[32] A. Ghosh, A. Karne, S. Pal, and N. Vaval, *Phys. Chem. Chem. Phys.* **15**, 17915 (2013)

[33] A. Ghosh, S. Pal, and N. Vaval *J. Chem. Phys.* **139** 064112 (2013); A. Ghosh, S.pal, and N. Vaval, *Mol. Phys.* **112**, 669 (2014).

[34] Y. Sajeev, A. Ghosh, N. Vaval, and S. Pal, *Int. Rev. Phys. Chem.*,*2014* DOI:10.1080/0144235X.2014.935585

[35] T.C. Jagau, D. Zuev, K.B. Bravaya, E. Epifanovsky, and A.I. Krylov, *J. Phys. Chem. Lett.* **5**, 310 (2014); D. Zuev, T. C. Jagau, K. B. Bravaya, E. Epifanovsky, Y. Shao, E. Sundstrom, M. H. -Gordon and A. I. Krylov, *J. Chem. Phys.* **141**, 024102 (2014).

[36] M. Nooijen and R. J. Bartlett, *J. Chem. Phys.* **102**, 3629 (1995); M. Nooijen and R. J. Bartlett, *J. Chem. Phys.* **102**, 6735 (1995).

[37] J. F. Stanton and R. J. Bartlett, *J. Chem. Phys.* **98**, 7029 (1993).

[38] D. C. Comeau and R. J. Bartlett, *Chem. Phys. Lett.* **207**, 414 (1993).

[39] J. Geertsen, M. Rittby, and R. J. Bartlett, *Chem. Phys. Lett.* **164**, 57 (1989).

[40] L. Meissner and R. J. Bartlett, *J. Chem. Phys.* **102**, 7490 (1995).

[41] M. Nooijen and R. J. Bartlett, *J. Chem. Phys.* **107**, 6812 (1997).

[42] M. Musial and R. J. Bartlett, *J. Chem. Phys.* **134**, 034106 (2011).

[43] M. Allan, *Phys. Rev. Lett.* **87**, 033201 (2001).

[44] M. Allan, *J. Phys. B* **35**, L387 (2002)

[45] L. A. Morgan, *Phys. Rev. Lett.* **80**, 1873 (1998).

[46] W. Vanroose, Z. Zhang, C. W. McCurdy, and T. N. Rescigno, *Phys. Rev. Lett.* **92**, 053201 (2004)

[47] I. I. Fabrikant, H. Hotop, *Phys. Rev. Lett.* **94**, 063201 (2005)

[48] J. Čižek, *J. Chem. Phys.* **45**, 4256 (1966).

[49] J. Čižek, *Adv. Chem. Phys.* **14**, 35 (1969).

[50] R. J. Bartlett and M. Musial, *Rev. Mod. Phys.* **79**, 291 (2007).

[51] D. I. Lyakh, M. Musial, V. F. Lotrich, and R. J. Bartlett, *Chem. Rev.* **112**, 182 (2012).

[52] T. H. Dunning, Jr. *J. Chem. Phys.* **90**, 1007 (1989).

[53] M. W. Schmidt, K. K. Baldridge, J. A. Boatz, S. T. Elbert, M. S. Gordon, J. H. Jensen, S. Koseki, N. Matsunaga, K. A. Nguyen, S. Su, T. L. Windus, M. Dupuis, and J. A. Montgomery, 'GAMESS: General atomic and molecular electronic structure system,' *J. Comput. Chem.* **14**, 1347 (1993).

[54] T. Sommerfeld and F. Tarantelli, *J. Chem. Phys.* **112**, 2106 (2000).

[55] E. R. Davidson, *J. Comput. Phys.* **17**, 87 (1975).

[56] T. Sommerfeld and T. Posset, *J. Chem. Phys.* **119**, 7714 (2003).

[57] B. Wu, L. Xia, Y. -F. Wang, H. -k. Li, X. -j. Zeng, and S. X. Tian, *Phys. Rev. A* **85**, 052709 (2012)

Chapter 4

Study of Interatomic coulombic decay using Equation-of-motion coupled cluster (EOMCC) method

In this chapter, we have explored about the Interatomic or Intermolecular coulombic decay (ICD) process. ICD is an efficient and ultrafast radiation less decay mechanism which can be initiated by removal of an electron from the inner-valence shell of an atom or molecule. Generally, the ICD mechanism is prevailed in weakly bound clusters. A very promising approach, known as CAP/EOM-CC, consists of the combination of complex absorbing potential (CAP) with the equation-of-motion coupled-cluster (EOM-CC) method, is applied for the first time to study the nature of the ICD mechanism. We have applied this technique to determine the lifetime of an auto-ionized, inner-valence excited state of the $Ne(H_2O)$, $Ne(H_2O)_2$ and $Ne(H_2O)_3$ systems. The lifetime is found to be very short and decreases significantly with the number of neighboring water molecules.

We have also applied this method to study the interatomic coulombic decay (ICD) mechanism in small hydrogen bonded clusters. The lifetime of F 2s inner-valence ionized state of $(HF)_n$, (n=2-3) clusters were calculated using this method. The lifetime is found to be very short and decreases substantially with increasing the number of HF monomer.

4.1 Introduction

Electronically excited molecules and atoms can relax by emitting a photon or an electron. These particles carry essential information on the electronic structure of their emitter. In general, energetically low lying states (outer-valence) decay radiatively and high lying excited or ionized states decay by electron emission. When the excitation occurs due to the ionization of electron from the core orbital, then the excited molecule follows the radiative decay or Auger decay [1, 2] for the relaxation. In Auger decay, an electron from the higher energy level fills the vacancy in the core level and the released energy can be transfered to another electron, which is then ejected from the system. The ejected electron is called the Auger electron. The Auger electron has specific energy depending on the element from which the electron is ejected. The Auger decay process is intraatomic in nature. So, it is expected that the environment has weak influence on this process. Interaction with environment does not change the decay width of the Auger decay.

The situation is changed dramatically when the excited molecule or atom is embedded in a chemical environment. In this case, another ultrafast non-radiative decay mechanism is possible. After removing an electron from the inner valence orbital of a particular monomer, the inner-valence hole is filled up by an outer valence electron of the same monomer and the excess energy gained by this process is transferred to a neighboring monomer, where a secondary electron is emitted from the outer valence orbital. So, the final state is characterized by two outer valence holes, placed on two different monomers. This decay process is called interatomic coulombic decay (ICD) [3–13] mechanism. The ICD is a very fast and efficient relaxation mechanism occuring in a weakly bound cluster initiated by an inner valence hole. In ICD mechanism [14–16] efficient energy transfer takes place between neighboring monomers. This decay differs from the Auger decay as the electron is not coming out from the excited or ionized atom

but from its neighbor. It transpires typically on a femto-second(fs) time scale. Without the neighbor the excited or ionized monomer will decay by slow photon emission.

Energetically, ICD is possible because the localization of two positive holes on two different monomers diminishes the coulomb repulsion and accordingly lower the double ionization potential (DIP) value. The lowering of the DIP is so prominent that it becomes lower than the inner valence IP. So, the system gains energy in going from an inner valence hole to a double ionized outer valence state. That makes the ICD mechanism a spontaneous decay process and it becomes faster than any other decay mechanism. The intermolecular nature of the ICD mechanism is manifested by the associated decay width which strongly depends on the internuclear distance between the monomers and also on the number of neighboring monomers.[17]

ICD can be viewed as a long-range correlation effect. Consequently, electron correlation and relaxation effect play a crucial role in the accurate description of all these states. The equation-of-motion coupled-cluster (EOM-CC) method provides the uniform treatment of electron correlation and relaxation effect for the initial and final states. The EOM-CC method includes dynamic and non-dynamic electron correlation very efficiently in a size extensive manner. That makes the EOM-CC method as a suitable method for the study of ICD mechanism.

The ionization of water clusters is of supreme interest in different areas spanning biology, chemistry and astrophysics. Understanding the changes in electronic structure that occur in these ionic clusters is important in fields as diverse as cloud nucleation in the earth's atmosphere, radiation biology and interstellar chemistry. The ICD emits a low energy electron from the molecular neighbor of the initially excited molecular ion. Recently, it has been established that the low energy electron can efficiently breakup the DNA-constituents.[11] So, the ICD process might act as a source of an electron that can cause radiation damage in biological system.

In this chapter we have devoted our work to study the ICD process in neon-water clusters using the equation-of-motion coupled-cluster singles and doubles (EOM-CCSD)

augmented by a complex absorbing potential (CAP). This method is termed as CAP/EOM-CCSD.[18] Using this method we have calculated the lifetime of an inner valence 2s hole of the Ne atom in NeH_2O, $Ne(H_2O)_2$, $Ne(H_2O)_3$ clusters. We have also applied this method to study the lifetime of an inner-valence 2s hole of the F atom in small hydrogen bonded $(\mathrm{HF})_2, (\mathrm{HF})_3$ clusters.

4.2 THEORY

In this section, we briefly discuss the CAP/EOM-CCSD method for computing the position and lifetime of the decaying states (resonance states). The resonance states are recognized by complex eigenvalues within the formalism of Siegert[19] and Gamow,[20]

$$E_r = E_R - i\Gamma/2, \tag{4.1}$$

where E_R represents the resonance position and Γ is the decay width. Γ is inversely related to the lifetime of the resonance state via, $\tau = \hbar/\Gamma$.

Resonance states are electronically metastable states and are represented by non-square integrable (non-L^2) wave function. They can also be defined as discrete states embedded in and coupled to the continuum. So, the calculation of resonance states require a method which can treat the continuum as well as electron correlation simultaneously. Regarding the continuum, there are two L^2-methods which are very popular for computing the resonance energy E_R and width Γ. One is the complex absorbing potential (CAP)[21–29] approach and other is the complex scaling method.[30] The latter is related to the complex basis function method. [31, 32] Here, our focus is on the complex absorbing potential approach. CAP/EOM-CC approach has been used recently to calculate the position and width of a shape resonance. [18] Related Fock space coupled-cluster method based on both CAP and complex scaling has also been used to calculate the shape resonance energies and widths. [33]

In the CAP approach, a CAP potential $-i\eta W$ is added to the physical Hamiltonian

to describe the electronic resonance state,

$$H(\eta) = H - i\eta W, \tag{4.2}$$

where η is the CAP strength and W is a real soft box like potential. After addition of CAP [34–37] the wave function becomes square integrable. The resonance energy E_r is obtained from the η -trajectories of the eigenvalues of $H(\eta)$. The pronounced local minimum of velocity υ_i as a function of η

$$\upsilon_i(\eta) = \eta \partial E_i / \partial \eta. \tag{4.3}$$

gives the resonance energy. The best approximation for the E_r is obtained from the optimal η value. The optimal η value is obtained by satisfying the condition

$$|\upsilon_i(\eta_{opt})| = min. \tag{4.4}$$

In IP-EOM-CCSD [38, 39]approach, the wave function for the μth ionized state can be written as

$$|\psi_\mu\rangle = R^{N-1}(\mu)|\psi_0\rangle \tag{4.5}$$

where

$$|\psi_0\rangle = e^T|\phi_0\rangle \tag{4.6}$$

is the N electron ground state wave function for the coupled-cluster (CC) method. [40–42] The $R^{N-1}(\mu)$ is the ionization operator and it can be defined as

$$R^{N-1}(\mu) = \sum_i r_i(\mu) a_i + 1/2 \sum_{ij} \sum_a r^a_{ij}(\mu) a^+_a a_i a_j \tag{4.7}$$

In eq. 4.6, $|\phi_0\rangle$ is the N electron closed-shell Hartree-Fock determinant and T represents the cluster operator

$$T = \sum_{ia} t^a_i a^+_a a_i + 1/4 \sum_{ab} \sum_{ij} t^{ab}_{ij} a^+_a a^+_b a_i a_j. \tag{4.8}$$

where i,j,...denote the occupied spin orbitals and a,b...are the unoccupied orbitals in the reference determinant $|\phi_0\rangle$.

In the equation-of-motion coupled-cluster method,[43–48] the energies of the ground state and excited states of $(N-1)$ electron system are calculated by solving

$$\bar{H_N} R^{N-1}(\mu)|\phi_0\rangle = w_\mu R^{N-1}(\mu)|\phi_0\rangle. \tag{4.9}$$

In matrix form eq.4.9 can be written as

$$\bar{H_N} R^{N-1}(\mu) = w_\mu R^{N-1}(\mu). \tag{4.10}$$

Where

$$\bar{H_N} = e^{-T} H_N e^T - \langle\phi_0|e^{-T} H_N e^T|\phi_0\rangle \tag{4.11}$$

is the similarity transformed Hamiltonian of the coupled-cluster (CC) theory and w_μ is the energy change connected with the ionization process. In IP-EOM-CCSD approach, $\bar{H_N}$ is constructed in a $1h$ and $2h1p$ space and diagonalized to obtain the ionization energies. The Davidson algorithm [49, 50] is used to diagonalize the $\bar{H_N}$ matrix.

Once the CAP is added,i.e., in the CAP/EOM-CCSD method, first the CAP is applied with the CC method to generate the complex $T(\eta)$ amplitudes. The wave function for the CC method can be written as

$$\psi_0(\eta) = e^{T(\eta)}|\phi_0\rangle. \tag{4.12}$$

Then, the CAP is added with the one body particle-particle part of the $\bar{H_N}$ matrix. Now, the complex $\bar{H_N}$ matrix can be defined as

$$\bar{H_N}(\eta) = e^{-T(\eta)} H_N(\eta) e^{T(\eta)}. \tag{4.13}$$

Finally, the resulting complex $\bar{H_N}$ matrix is diagonalized for the different η values.

The complex eigenvalues are obtained by diagonalization of the $\bar{H_N}$ matrix. We have varied the η values starting from 0 to 0.01 with an increment of 10^{-6}. we have plotted

the complex eigenvalues in the complex energy plane. The resonance energy is identified with the appearance of minimum velocity

$$\upsilon_\mu(\eta) = \eta \partial w_\mu / \partial \eta. \tag{4.14}$$

for each resonance state.

4.3 RESULTS AND DISCUSSION

In this chapter, we have calculated the lifetime of the Ne 2s inner valence 2s hole in neon-water clusters using the CAP/EOM-CCSD method described in the preceding section. Our main objective of this chapter to study how the lifetime of the Neon 2s state changes in the presence of neighboring atoms or molecules. To study the dependence of the ICD lifetime on the environment we have chosen the three neon-water systems NeH_2O, $Ne(H_2O)_2$, $Ne(H_2O)_3$. The ICD process in neon-water clusters can be seen as follows: The Ne2s vacancy is localized on the Ne atom. A Ne2p electron falls into the Ne2s vacancy and the released energy is used to eject an O 2p electron from a neighboring H_2O monomer. In our calculation, we have used the aug-cc-pVTZ basis set [51] for the Ne atom. The aug-cc-pVDZ and cc-pVDZ basis sets [52] are used for the O and H atom respectively. We have computed and used the optimized geometry obtained at CCSD(T) level for NeH_2O and $Ne(H_2O)_2$. The cc-pVDZ basis set is used for the geometry optimization. Because of its size, the calculation of the geometry of $Ne(H_2O)_3$ has been done on the MP2 level. The results for the resonance energy E_R and decay width Γ of the neon 2s states in the clusters are collected in Table 4.1. In our calculation, we have used GAMESS [53] software package to evaluate the two electron integrals. The required matrix elements for the EOM-CCSD and CAP matrices have been computed using our own codes. The geometry optimization for all these molecules has been performed using ACS-II [54]software package.

we have also calculated the lifetime of the F 2s inner-valence hole of F atom in

the small hydrogen bonded HF clusters using the CAP/EOM-CCSD mehod. We have studied the two HF clusters $(\mathrm{HF})_2$, $(\mathrm{HF})_3$. In an isolated HF molecule, the cationic state which is produced by emitting an electron from the 2s inner-valence level of F atom can decay radiatively. The decay channel corresponding to the electron emission is not energetically allowed. However, the analogous cationic state in HF clusters can decay via electron emission. The decay process can be view as follows: the F 2s vacancy is localized on one of the HF monomer. An electron from the 2p level of F atom of the same monomer comes to fill up the F 2s vacancy and the excess energy is used to eject an electron of F 2p level from the neighboring HF monomer. In our calculation, we have used aug-cc-pVTZ basis set for both the F and H atoms in $(\mathrm{HF})_2$ cluster. However, in case of $(\mathrm{HF})_3$, aug-cc-pVDZ basis set has been used for both the F and H atoms. We have computed and used the optimized geometry at MP2 level for $(\mathrm{HF})_2$, $(\mathrm{HF})_3$ clusters. The geometry optimization has been performed using Gaussian 09 software package.[55]

4.3.1 NeH_2O SYSTEM

In this subsection, we discuss the lifetime of an inner valence 2s resonance state of the Ne atom in NeH_2O . The optimized geometry for the NeH_2O system is presented in Fig 4.1. The bond distance between the Ne and O atom is 2.91 $\mathring{A}$. For the CAP/EOM-CCSD computation the CAP box side lengths are chosen to be $c_x = 2.0+\delta c$, $c_y = \delta c$ and $c_z = 6.0 + \delta c$, all in a.u. The computed optimal value of the δc is 4.0 a.u. The complex resonance energy for the NeH_2O system is $E_r = 1.755 - i(1.4 \times 10^{-4})$ a.u. The decay width Γ for the NeH_2O system is 7.6 meV, which corresponds to a lifetime of 86 fs.

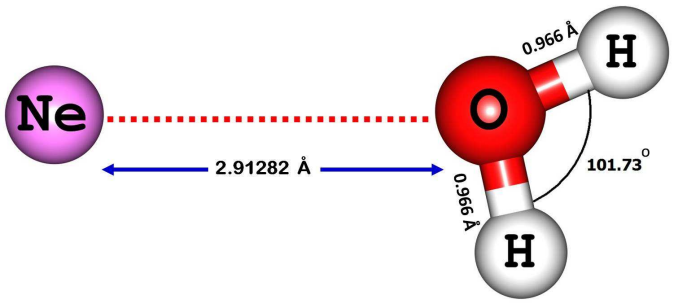

Figure 4.1: NeH_2O system, optimized at CCSD(T)/cc-pVDZ level

4.3.2 $Ne(H_2O)_2$ SYSTEM

The optimized geometry for the $Ne(H_2O)_2$ system is presented in Fig 4.2. The bond distance between the Ne and O atom is 2.93 $\mathring{A}$. In the CAP/EOM-CCSD computation, the CAP box side lengths chosen for the $Ne(H_2O)_2$ system were $c_x = 2.0 + \delta c$, $c_y = \delta c$ and $c_z = 8.0 + \delta c$, all in a.u. The optimal value of δc is 4.0 a.u. The calculated resonance energy for the $Ne(H_2O)_2$ system is $E_r = 1.753 - i(4.6 \times 10^{-4})$ a.u. The decay width Γ for the $Ne(H_2O)_2$ is 25.0 meV corresponding to a lifetime of 26 fs. It is seen that adding a second neighbor by going from NeH_2O to $Ne(H_2O)_2$ the lifetime decreases by about factor 3.

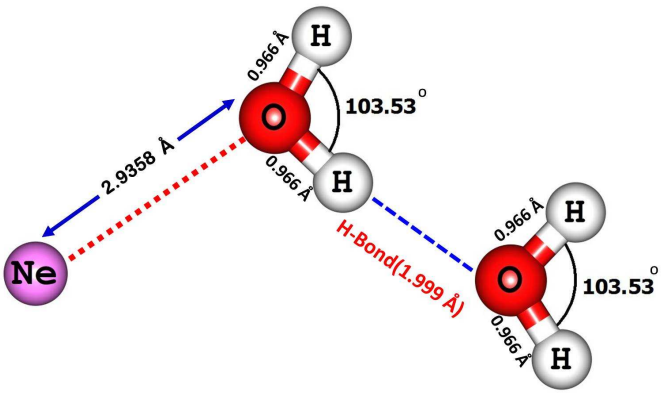

Figure 4.2: $\mathrm{Ne(H_2O)_2}$ system, optimized at CCSD(T)/cc-pVDZ level

Table 4.1: Calculated resonance energies (E_R) and decay widths (Γ) for the 2s inner valence hole of Ne atom in neon-water clusters

system	E_R(a.u.)	Γ (a.u.)	Γ (meV)	lifetime(fs)
NeH_2O	1.755	2.8×10^{-4}	7.6	86
$Ne(H_2O)_2$	1.753	9.2×10^{-4}	25.0	26
$Ne(H_2O)_3$	1.752	15.2×10^{-4}	41.3	16

4.3.3 $Ne(H_2O)_3$ SYSTEM

The optimized geometry for the $Ne(H_2O)_3$ system is presented in Fig 4.3. For this larger system, the geometry is optimized at the MP2 level in cc-pVTZ basis set. The bond distance between the Ne and O atom is 3.27 $\mathring{A}$. For the CAP/EOM-CCSD computations the CAP box side lengths are chosen to be $c_x = 6.0 + \delta c$, $c_y = 2.0 + \delta c$ and $c_z = 8.0 + \delta c$, all in a.u. The optimal value of δc is 3.0 a.u. To be consistent with the other calculations we have used same basis set for the calculation of the lifetime of $Ne(H_2O)_3$ as for other clusters. The result for the $Ne(H_2O)_3$ system is presented in Table 4.1. We have obtained the complex resonance energy $E_r = 1.752 - i(7.6 \times 10^{-4})$ a.u. The decay width Γ for the $Ne(H_2O)_3$ is 41.3 meV, and the lifetime has dropped to 16 fs. We stress that as we go from NeH_2O with a single neighbor to $Ne(H_2O)_3$ with three neighbors, the lifetime

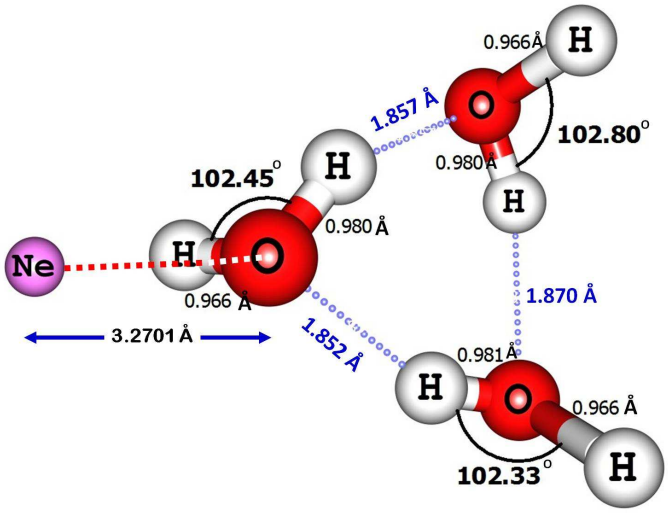

Figure 4.3: $\mathrm{Ne(H_2O)_3}$ system, optimized at MP2/cc-pVTZ level

is reduced by factor as large as 5.

4.3.4 $(\mathrm{HF})_2$ system

In this subsection, we have discussed about the lifetime of 2s inner-valence hole of F atom in $(\mathrm{HF})_2$ cluster. Since, the two HF monomer subunits in $(\mathrm{HF})_2$ are not equivalent, two energetically different inner-valence states are expected in the independent-particle model. Thus, the two resonance states 'main line' arise from F 2s ionization of $(\mathrm{HF})_2$ system. The optimized geometry for the $(\mathrm{HF})_2$ is presented in Fig 4.4. The hydrogen bond distance in $(\mathrm{HF})_2$ system is 1.81 $\mathring{A}$. In the CAP/EOM-CCSD calculations, the CAP box side lengths are chosen to be $c_x = 2.5 + \delta c$, $c_y = 0.5 + \delta c$ and $c_z = \delta c$, where c_x, c_y, c_z are the distances from the center of the coordinate system along the x,y,z axis, respectively, all in a.u. The optimal value of δc is 4.5 a.u. The results for the resonance energies E_R and decay widths Γ of the F 2s inner-valence state in $(\mathrm{HF})_2$ cluster are collected in Table 4.2. We compare our results with CAP/CI results available in literature. The resonance energy E_R for the σ orbital localized at the hydrogen donating F atom is

Table 4.2: Calculated resonance energies (E_R) and decay widths (Γ) for the 2s inner valence hole of F atom in $(\mathrm{HF})_2$ using aug-cc-pVTZ basis set

Method	E_R(eV)	Γ (meV)	lifetime(fs)
CAP/EOM-CCSD	39.1	20.7	31
	40.8	33.0	20
CAP/CI[a]	38.6	18.0	37
	40.5	30.0	22

[a] See reference 27.

39.1 eV with the decay width of 20.7 meV. The CAP/CI method gives resonance energy $E_R = 38.6$ eV and width $\Gamma = 0.41$ eV. For the 2σ orbital associated with the hydrogen accepting F atom the resonance position is at 40.8 eV with width of 33.0 meV. For the same state CAP/CI [27] gives position at 40.5 eV with width of 30.0 meV. It can be seen that the lifetime associated with the inner-valence hole at hydrogen accepting F atom is less compared to the F atom at the hydrogen donating end. Our results are in good agreement with the CAP/CI results.[27]

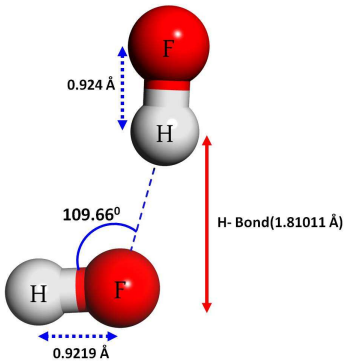

Figure 4.4: $(HF)_2$ system, optimized at MP2/cc-pVTZ level

4.3.5 $(HF)_3$ system

The $(HF)_3$ cluster has a cyclic structure with C_{3h} symmetry. The optimized geometry for the $(HF)_3$ system is presented in Fig 4.5. The hydrogen bond distance in $(HF)_3$ cluster is 1.72 $\mathring{A}$. In this subsection, we have discussed about the lifetime of 2s inner-valence hole of F atom in $(HF)_3$ cluster. Three inner-valence resonane states appear from F 2s ionization of $(HF)_3$ system. In the CAP/EOM-CCSD calculations, the CAP box side lengths chosen for the $(HF)_3$ system were $c_x = 14.0 + \delta c$, $c_y = 2.8 + \delta c$ and $c_z = 21.0 + \delta c$, all in a.u. The optimal value of δc is 2.0 a.u. The computed resonance energies E_R and decay widhs Γ of the F 2s inner-valence states in $(HF)_3$ cluster are collected in Table 4.3. The lifetime obtained for the $(HF)_3$ is the order of 140-180 meV, which corresponding to the lifetime of 3.6-4.6 fs. Our results show excellent agreement with the previous theoretical results. Cederbaum and co-workers have predicted the lifetime of the F 2s inner valence state in $(HF)_3$ cluster is about 0.1-0.15 eV, which corresponding to the lifetime of 4.5-6.5 fs.

Table 4.3: Calculated resonance energies (E_R) and decay widths (Γ) for the 2s inner valence hole of F atom in $(\mathrm{HF})_3$ using aug-cc-pVDZ basis set

E_R(eV)	Γ (meV)	lifetime(fs)
40.5	140	4.60
40.7	160	4.06
41.6	180	3.60

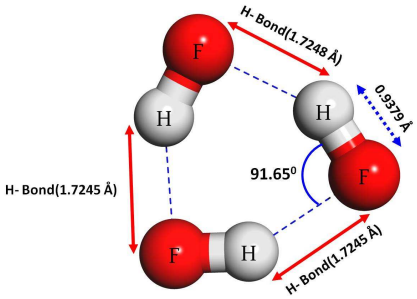

Figure 4.5: $(\mathrm{HF})_3$ system, optimized at MP2/cc-pVTZ level

4.4 CONCLUSION

In this chapter, we have implemented the equation-of-motion coupled-cluster (EOM-CC) method along with complex absorbing potential (CAP) approach to study the ICD in weakly bound neon-water clusters. One can view these clusters as Ne microsolvated in water.[56] Specifically, we have applied this method to study the lifetime of an inner valence 2s hole of Ne atom in NeH_2O, $Ne(H_2O)_2$, $Ne(H_2O)_3$ clusters. We expect to have different O-H bond lengths for inner valence ionized species compared to the neutral cluster. However, our study is for the vertical ionization and not for the adiabatic calculation. The computed lifetime for the NeH_2O system is 86 fs. The lifetime obtained for the $Ne(H_2O)_2$ system is 26 fs and drops further to 16 fs if an additional neighbor is added to obtain $Ne(H_2O)_3$. As a characteristic feature of ICD,[17] the lifetimes decrease

strongly with an increasing number of neighbors. The reason for the over proportional change of lifetime is the changes of electronic structure as we go from NeH_2O system to $Ne(H_2O)_3$ system. Another possible reason is with increasing the number of water molecules the basis set becomes large. This provides the better treatment of electron correlation for the large neon-water cluster. Since the bond distances between the Ne and O atoms in different neon-water clusters are large enough we feel that energy transfer in ICD process is governed by virtual photon exchange [57] pathway. It is illuminating to compare these lifetimes to the respective lifetime of 2s ionized isolated Ne. The isolated Ne can only decay by photon emission and its lifetime is .2 ns,[58] i.e., due to presence of 3 neighbors, the ionized Ne atom decays by 10^5 order of magnitude faster than without neighbors. We have also applied the CAP/EOM-CCSD approach to study the ICD in small hydrogen bonded HF cluster. Specifically, we have applied this method to study the lifetime of an inner-valence 2s hole of F atom in $(\mathrm{HF})_2, (\mathrm{HF})_3$ clusters. In $(\mathrm{HF})_2$ cluster, the estimated lifetime to be the order of 20.7-33.0 meV, which corresponding to the lifetime of 31-20 fs. The lifetime decreases strongly when we go from $(\mathrm{HF})_2$ to $(\mathrm{HF})_3$. The computed lifetime for the $(\mathrm{HF})_3$ cluster drops to be the order of 140-180 meV, which corresponding to the lifetime of 3.6-4.6 fs. We stress that as we go from $(\mathrm{HF})_2$ with one neighbor to $(\mathrm{HF})_3$ with two neighbors, the lifetime reduced by factor as large as 6. The reason behind the changes of lifetime is the number of decay channels increase as we go from $(\mathrm{HF})_2$ to $(\mathrm{HF})_3$. Another possible reason is the hydrogen bond distance shrink by about 0.10 $\mathring{A}$ when we go from $(\mathrm{HF})_2$ to $(\mathrm{HF})_3$. This makes the ICD mechanism more faster for the $(\mathrm{HF})_3$ system. This documents nicely the enormous impact of ICD.

References

[1] P. Auger, *J. Phys. Radium* **6**, 205 (1925).

[2] L. S. Cederbaum, Y. C. Chiang, P. V. Demekhin, and N. Moiseyev, *Phys. Rev. Lett* **106**, 123001 (2011).

[3] L. S. Cederbaum, J. Zobeley, and F. Tarantelli, *Phys. Rev. Lett.* **79**, 4778 (1997)

[4] N. Moiseyev, R. Santra, J. Zobeley, and L. S. Cederbaum, *J. Chem. Phys.* **114**, 7351 (2001).

[5] R. Santra, J. Zobeley, L. S. Cederbaum and N. Moiseyev, *Phys. Rev. Lett.* **85**, 4490 (2000)

[6] J. Zobeley, L. S. Cederbaum, and F. Tarantelli, *J. Phys. Chem. A* **103**, 11145 (1999).

[7] G. Öhrwall, M. Tchaplyguine, M. Lundwall, R. Feifel, H. Bergersen, T. Rander, A. Lindblad, J. Schulz, S. Peredkov, S. Barth, S. Marburger, U. Hergenhahn, S. Svensson, and O. Björneholm, *Phys. Rev. Lett.* **93**, 173401 (2004)

[8] S. Scheit, V. Averbukh, H. D. Meyer, N. Moiseyev, R. Santra, T. Sommerfeld, J. Zobeley, and L. S. Cederbaum, *J. Chem. Phys.* **121**, 8393 (2004).

[9] S. Scheit, V. Averbukh, H. D. Meyer, J. Zobeley, and L. S. Cederbaum, *J. Chem. Phys.* **124**, 154305 (2004).

[10] S. Barth, S. Joshi, S. Marburger, V. Ulrich, A. Lindblas, G. Öhrwall, O. Björneholm, and U. Hergenhahn, *J. Chem. Phys.* **122**, 241102 (2005).

[11] T. Jahnke, H. Sann, T. Havermeier, K. Kreidi, C. Stuck, M. Meckel, M. Schffler, N. Neumann, R. Wallauer, S. Voss, A. Czasch, O. Jagutzki, A. Malakzadeh, F. Afaneh, Th. Weber, H. Schmidt-Böcking, and R. Dörner, *Nature Phys.*, **6**, 139 (2010);

[12] M. Mucke, M. Braune, S. Barth, M. Förstel, T. Lischke, V. Ulrich, T. Arion, U. Becker, A. Bradshaw, and U. Hergenhahn, *Nature Phys.* **6**, 143 (2010); T. Jahnke, A. Czasch, M. S. Schöffler, S. Schössler, A. Knapp, M. Käsz, J. Titze, C. Wimmer, K. Kreidi, R. E. Grisenti, A. Staudte, O. Jagutzki, U. Hergenhahn, H. Schmidt-Böcking, and R. Dörner, *Phys. Rev. Lett.* **93**, 163401 (2004).

[13] N. Sisourat, N. V. Kryzhevoi, P. Kolorenč, S. Scheit, T. Jahnke, and L. S. Cederbaum, *Nature Phys.* **6**, 508 (2010).

[14] P. V. Demekhin, S. D. Stoychev, A. I. Kuleff, and L. S. Cederbaum, *Phys. Rev. Lett.* **107**, 273002 (2011).

[15] I. B. Müller and L. S. Cederbaum, *J. Chem. Phys.* **125**, 204305 (2006).

[16] V. Averbukh, I. B. Müller, and L. S. Cederbaum, *Phys. Rev. Lett.* **93**, 263002 (2004).

[17] R. Santra and L. S. Cederbaum, *Phys. Rep.* **368**, 1 (2002).

[18] A. Ghosh, N. Vaval, and S. Pal, *J. Chem. Phys.* **136**, 234110 (2012).

[19] A. J. F. Siegert, *Phys. Rev.* **56**, 750 (1939).

[20] G. Gamow, *Der Bau des Atomkerns und die Radioaktivität* **(**S. Hirzel, Leipzig, 1932).

[21] T. Sommerfeld, U. V. Riss, H. D. Meyer, L. S. Cederbaum, B. Engels, and H. U. Suter, *J. Phys. B* **31**, 4107 (1998).

[22] G. Jolicard and E. J. Austin, *Chem. Phys. Lett.* **121**, 106 (1985).

[23] W. P. Reinhardt, *Annu. Rev. Phys. Chem.* **33**, 223 (1982); N. Moiseyev, *Phys. Rep.* **302**, 211 (1998).

[24] U. V. Riss and H. D. Meyer, *J. Phys. B* **26**, 4503 (1993); J. G. Muga, J. P. Palao, B. Navarro, and I. L. Egusquiza, *Phys. Rep.* **395**, 357 (2004).

[25] N. Moiseyev, *J. Phys. B* **31**, 1431 (1998); U. V. Riss and H. D. Meyer, *J. Phys. B* **31**, 2279 (1998).

[26] R. Santra and L. S. Cederbaum, *J. Chem. Phys.* **115**, 6853 (2001).

[27] R. Santra, L. S. Cederbaum, and H. D. Meyer, *Chem. Phys. Lett.* **303**, 413 (1999).

[28] R. Santra and L. S. Cederbaum, *J. Chem. Phys.* **117**, 5511 (2002).

[29] S. Feuerbacher, T. Sommerfeld, R. Santra, and L. S. Cederbaum, *J. Chem. Phys.* **118**, 6188 (2003).

[30] N. Rom, N. Lipkin, and N. Moiseyev, *Chem. Phys.* **151**, 199 (1991).

[31] N. Moiseyev and C. Corcoran, *Phys. Rev. A* **20**, 814 (1979); T. N. Rescigno, C. W. McCurdy, Jr., and A. E. Orel, *Phys. Rev. A* **17**, 1931 (1978).

[32] C. W. McCurdy, Jr., and T. N. Rescigno, *Phys. Rev. Lett.* **41**, 1364 (1978).

[33] Y. Sajeev, M. K. Mishra, N. Vaval, and S. Pal, *J. Chem. Phys.* **120**, 67 (2004); Y. Sajeev, R. Santra, and S. Pal, *J. Chem. Phys.* **123**, 204110 (2005); Y. Sajeev and S. Pal, *Mol. Phys.* **103**, 2267 (2005).

[34] N. Vaval and L. S. Cederbaum, *J. Chem. Phys.* **126**, 164110 (2007).

[35] Y. Sajeev and N. Moiseyev, *J. Chem. Phys.* **127**, 034105 (2007)

[36] Y. Sajeev, V. Vysotskiy, L. S. Cederbaum, and N. Moiseyev, *J. Chem. Phys.* **131**, 211102 (2009).

[37] M. Ehara and T. Sommerfeld, *Chem. Phys. Lett.* **537**, 107 (2012).

[38] M. Musial, S. A. Kucharski, and R.J. Bartlett, *J. Chem. Phys.* **118**, 1128 (2003).

[39] M. Musial and R.J. Bartlett, *J. Chem. Phys.* **119**, 1901 (2003); M. Musial and R.J. Bartlett, *Chem. Phys. Lett.* **384**, 210 (2004).

[40] J. Čižek, *J. Chem. Phys.* **45**, 4256 (1966).

[41] J. Čižek, *Adv. Chem. Phys.* **14**, 35 (1969).

[42] R. J. Bartlett, *Annu. Rev. Phys. Chem.* **32**, 359 (1981).

[43] M. Nooijen and R. J. Bartlett, *J. Chem. Phys.* **102**, 3629 (1995).

[44] M. Nooijen and R. J. Bartlett, *J. Chem. Phys.* **102**, 6735 (1995).

[45] J. F. Stanton and J. Gauss, *J. Chem. Phys.* **101**, 8938 (1994).

[46] J. F. Stanton and R. J. Bartlett, *J. Chem. Phys.* **98**, 7029 (1993).

[47] D. C. Comeau and R. J. Bartlett, *Chem. Phys. Lett.* **207**, 414 (1993).

[48] J. Geertsen, M. Rittby, and R.J. Bartlett, *Chem. Phys. Lett.* **164**, 57 (1989).

[49] T. Sommerfeld and F. Tarantelli, *J. Chem. Phys.* **112**, 2106 (2000).

[50] E. R. Davidson, *J. Comput. Phys.* **17**, 87 (1975).

[51] R. A. Kendall, T. H. Dunning, Jr., and R. J. Harrison, *J. Chem. Phys.* **96**, 6796 (1992).

[52] T. H. Dunning, Jr., *J. Chem. Phys.* **90**, 1007 (1989).

[53] M. W. Schmidt, K. K. Baldridge, J. A. Boatz, S. T. Elbert, M. S. Gordon, J. H. Jensen, S. Koseki, N. Matsunaga, K. A. Nguyen, S. Su, T. L. Windus, M. Dupuis, and J. A. Montgomery, 'GAMESS: General atomic and molecular electronic structure system,' *J. Comput. Chem.* **14**, 1347 (1993).

[54] J. F. Stanton, J. Gauss, S. A. Perera, J. D. Watts, A. D. Yau, M. Nooijen, N. Oliphant, P. G. Szalay, W. J. Lauderdale, S. R. Gwaltney, S. Beck, A. Balkov, D. E. Bernholdt, K. K. Baeck, P. Rozyczko, H. Sekino, C. Huber, J. Pittner, W. Cencek, D. Taylor, and R. J. Bartlett, Integral packages included are VMOL (J. Almlf and P. R. Taylor); VPROPS (P. Taylor); ABACUS (T. Helgaker, H. J. Aa. Jensen, P. Jrgensen, J. Olsen, and P. R. Taylor); HONDO/GAMESS (M. W. Schmidt, K. K. Baldridge, J. A. Boatz, S. T. Elbert, M. S. Gordon, J. J. Jensen, S. Koseki, N. Matsunaga, K. A. Nguyen, S. Su, T. L. Windus, M. Dupuis, J. A. Montgomery). ACES II a program product of the Quantum Theory Project, University of Florida, 2006.

[55] M. J. Frisch, G. W. Trucks, H. B. Schlegel, G. E. Scuseria, M. A. Robb, J. R. Cheeseman, G. Scalmani, V. Barone, B. Mennucci, G. A. Petersson, H. Nakatsuji, M. Caricato, X. Li, H. P. Hratchian, A. F. Izmaylov, J. Bloino, G. Zheng, J. L. Sonnenberg, M. Hada, M. Ehara, K. Toyota, R. Fukuda, J. Hasegawa, M. Ishida, T. Nakajima, Y. Honda, O. Kitao, H. Nakai, T. Vreven, J. A. Montgomery, Jr., J. E. Peralta, F. Ogliaro, M. Bearpark, J. J. Heyd, E. Brothers, K. N. Kudin, V. N. Staroverov, R. Kobayashi, J. Normand, K. Raghavachari, A. Rendell, J. C. Burant, S. S. Iyengar, J. Tomasi, M. Cossi, N. Rega, J. M. Millam, M. Klene, J. E. Knox, J. B. Cross, V. Bakken, C. Adamo, J. Jaramillo, R. Gomperts, R. E. Stratmann, O. Yazyev, A.J. Austin, R. Cammi, C. Pomelli, J. W. Ochterski, R. L. Martin, K. Morokuma, V. G. Zakrzewski, G. A. Voth, P. Salvador, J. J.

Dannenberg, S. Dapprich, A. D. Daniels, Ö. Farkas, J. B. Foresman, J. V. Ortiz, J. Cioslowski, and D. J. Fox, Gaussian, Inc., Wallingford CT, 2009.

[56] I. B. Müller and L. S. Cederbaum, *J. Chem. Phys.* **122**, 094305 (2005).

[57] T. Jahnke, A. Czasch, M. Schöffler, S. Schössler, M. Käsz, J. Titze, K. Kreidi, R. E. Grisenti, A. Staudte, O. Jagutzki, L. Ph. H. Schmidt, Th. Weber, H. Schmidt-Böcking, K. Ueda, and R. Dörner *Phys. Rev. Lett.* **99** 153401 (2007)

[58] D. C. Griffin, D. M. Mitnik, and N. R. Badnell, *J. Phys. B* **34**, 4401 (2001).

Chapter 5

Equation-of-motion coupled cluster method for the core hole and double core hole Auger decay

In this chapter, we have explored about the Auger decay. The recent development of Linac coherent light source high intense x-ray laser makes it possible to create double core ionization in the molecule. The generation of double core hole state and its decay is identified by Auger spectroscopy. The decay of this double core hole (DCH) states can be used as a powerful spectroscopic tool in chemical analysis. In this present work, we have implemented a promising approach, known as CAP/EOM-CC method, for the first time to calculate the decay rate of core hole (k) and double core hole (kk) state. We have applied this method to calculate the lifetime of auto-ionized core hole and double core hole excited states in various systems. The calculated lifetime is found to be very short for the double core hole (kk) state and the decay rate is faster compare to the single core hole (k) Auger decay.

The recent development of short pulse, intense, x-ray free electron laser (XEFL) [1, 2] allow to create multiple vacancies in the core level of molecules through the sequential absorption of multiple photon. However, at the same time it is possible to generate multiple vacancies in the core level using synchroton radiation (SR). In contrast to the XEFL, SR creates vacancies through the single photon absorption. The creation of double vacancies in the core level produce a high lying excited cationic state which lie above the double ionization threshold as a result it can relax via Auger decay. In Auger decay,[3, 4] an electron from the outer valence level fills the vacancy in the core level and the released energy is transferred to another outer valence electron which is then emitted from the system. The emitted secondary electron (Auger electron) contains very low energy, in the order of few electron volts. The presence of different atomic sites in the molecule open up two different possibilities for the double core hole (DCH) states,[5, 6] one is with two core hole states placed on one single atom and another with two core hole states placed on two different atoms. The decay of double core hole state of molecule through Auger decay can be rationalized as follows: In the first Auger transition, DCH (KK) state decay to the core valence valence (KLL) state with the emission of one Auger electron and then the (KLL) state again decay to the quadrupole valence valence (LLLL) state in the second Auger transition with the emission of another Auger electron. The other possibilities are direct Auger decay or double Auger decay. In the direct Auger decay, two outer valence electrons simultaneously fill the core level vacancy with the emission of an Auger electron. In double Auger decay, an outer valence electron fills the core hole vacancy with the emission of two Auger electrons.

The Auger decay for the core hole state of molecule has been studied quite elaborately in both theoretically and experimentally. However, theoretical works on DCH Auger decay are limited. Inhester et al. [7] have studied the decay rate of DCH Auger decay of first row hydrides using the configuration interaction (CI) method. Averbukh

and co-workers [8] have calculated the lifetime of DCH Auger decay using the Fano-ADC approach. Very recently, Ehara and co-workers [9] have studied the DCH state of molecules. In their work, complete active space self-consistent field (CASSCF) and configuration interaction (CASCI) have been employed to calculate the energies of DCH state. Wentzel's formulla has been used to calculate the Auger intensity. The Auger decay of DCH state has also been confirmed experimentally. [10]

Auger decay plays a significant role in the detection of chemical environment. The energy required to removal of an electron from the core level depends specifically on the atomic species. Thus, the chemical environment is identified by the Auger spectroscopy through the shifts of line or position. This is the way for the chemical analysis using electronic spectroscopy. The energy shift or position shift is more pronounced in case of double core hole Auger decay and it is expected to be a more powerful spectroscopic tool compare to the traditional single core hole Auger spectroscopy for the analysis of local chemical environment. [11, 12] The improvement of energy shift or position shift may helpful for the future spectroscopic studies of electronic structure in a better way. Further, in biological medium the neutralization of excited ions occurs through Auger decay plays an important role in cellular DNA damage. [13, 14] Therefore, the accurate description of Auger decay might be helpful in the development of new radiooncology scheme. It is well known that both electron correlation and relaxation effects play an important role in the description of core hole and double core hole states. The EOM-CC method [15] includes both electron correlation [16] (dynamic as well as non-dynamic) and relaxation effect effectively and also fulfill the size extensivity criteria in the ground state. It also gives direct intensive energy difference. Therefore, the EOMCC approach is very promising to describe the Auger decay for core hole and double core hole states.

The starting point for the EOM-CC method [15] is a coupled cluster (CC) ground state wave function. In CC method, the ground state wave function can be defined as $|\psi_0\rangle = e^T|\phi_0\rangle$,

where $|\phi_0\rangle$ is the N-electron close shell reference determinant .e.g., the restricted

Hartree-Fock determinant (RHF) and T is the cluster operator. In the coupled cluster singles and doubles (CCSD) approximation, T operator can be defined as follows

$$T = \sum_{ia} t_i^a a_a^+ a_i + 1/4 \sum_{ab} \sum_{ij} t_{ij}^{ab} a_a^+ a_b^+ a_i a_j + ..., . \tag{5.1}$$

where the standard convention for the indices is used, i.e., indices a,b,..., refer to the virtual spin orbitals and indices i,j,.., refer to the occupied spin orbitals.

Within the EOM-CCSD formalism, [17–19] the wave function for the ionized, double ionized states, $|\psi_\mu\rangle$, can be expressed as

$$|\psi_\mu\rangle = R(\mu)|\psi_0\rangle, \tag{5.2}$$

where $R(\mu)$ is ionization, double ionization, etc, operator

$$R(\mu) = r_0(\mu) + R_1(\mu) + R_2(\mu) + R_3(\mu) + ... \tag{5.3}$$

The $R(\mu)$ can be defined via creation -annihilation operator depending on the considered process as follows

$$R(\mu)^{IP} = \sum_i r_i(\mu) a_i + 1/2 \sum_a \sum_{ij} r_{ij}^a(\mu) a_a^+ a_j a_i + ... \tag{5.4}$$

$$R(\mu)^{DIP} = 1/2 \sum_{ij} r_{ij}(\mu) a_i a_j + 1/6 \sum_a \sum_{ijk} r_{ijk}^a(\mu) a_a^+ a_k a_j a_i + ... \tag{5.5}$$

The $R_1(\mu)$ operator does not contribute to the expansion of $R(\mu)^{DIP}$ operator. The r_0 operator is zero for IP, DIP, etc.

The Schrödinger equation for IP, DIP states can be expressed as

$$H_N R(\mu)|\psi_0\rangle = \Delta E_\mu R(\mu)|\psi_0\rangle \tag{5.6}$$

where $\mathrm{H_N}$ is the normal ordered Hamiltonian and it can be expressed as

$$H_N = H - \langle\phi_0|H|\phi_0\rangle \tag{5.7}$$

The final form of EOM-CC equation is

$$\bar{H_N} R(\mu)|\phi_0\rangle = w_\mu R(\mu)|\phi_0\rangle \tag{5.8}$$

where w_μ is the energy change connected with the considered process. The $\bar{H_N}$ is the similarity transformed Hamiltonian, in terms of connected diagrams and it can be defined as

$$\bar{H_N} = e^{-T} H e^{T} - \langle\phi_0|e^{-T} H e^{T}|\phi_0\rangle \tag{5.9}$$

In a matrix form eq 6.10 is

$$\bar{H_N} R(\mu) = w_\mu R(\mu) \tag{5.10}$$

The $\bar{H_N}$ matrix is diagonalized in the sub space of 1h and 2h1p space to get the required ionization potential (IP) values.

The double ionization potential (DIP) values are obtained through non-symmetric diagonalization of $\bar{H_N}$ matrix in the subspace of 2h and 3h1p space.

In this work, we take the CCSD model for both the GS as well as IP part (solve R_1 and R_2 equation). However, in case of DIP-EOMCC, GS we take the CCSD model (n^6) and DIP part is as in the full CCSDT one (so we solve R_2 and R_3 equations).

In the CAP/ EOMCC method,[20, 21] the CAP term (-iη W) [22–24] should be added to the coupled cluster (CC) method where η represents the CAP strength and W is a real soft box like potential. After addition of CAP to the CC method, the ground state wave function $|\psi_0\rangle$ for the CC method can be defined as $|\Psi_0(\eta)\rangle = e^{T(\eta)}|\phi_0\rangle$.

Then, the CAP term is added to the one body particle-particle ($\bar{f_{pp}}$) part of $\bar{H_N}$. The other terms of the $\bar{H_N}$ matrix are altered via the appearance of the complex $T(\eta)$. Thus, the new form of the $\bar{H_N}$ matrix is

$$\bar{H_N}(\eta) = e^{-T(\eta)} H_N(\eta) e^{T(\eta)} - \langle\phi_0|e^{-T(\eta)} H_N(\eta) e^{T(\eta)}|\phi_0\rangle \tag{5.11}$$

$$\bar{H_N}(\eta) R_\eta(\mu) = w_\mu(\eta) R_\eta(\mu) \tag{5.12}$$

Finally, the resulting complex $\bar{H_N}(\eta)$ matrix is diagonalized for the different η values. The resonance energies are obtained using the following equation

$$E_{res}(\eta) = w_\mu(\eta) + E_{CC}(\eta) - E_{CC}(\eta = 0) \tag{5.13}$$

In this chapter, we approximate $T(\eta)$ as $T(\eta = 0)$. The CAP is added directly to the one body particle-particle ($\bar{f_{pp}}$) part of $\bar{H_N}$. Thus, the new form of the $\bar{H_N}$ matrix is

$$\bar{H_N}(\eta) = e^{-T(\eta=0)} H_N(\eta) e^{T(\eta=0)} - \langle\phi_0|e^{-T} H_N e^{T}|\phi_0\rangle \tag{5.14}$$

$$\bar{H_N}(\eta) R_\eta(\mu) = w_\mu(\eta) R_\eta(\mu) \tag{5.15}$$

Finally, the resulting complex $\bar{H_N}(\eta)$ matrix is diagonalized in 1h and 2h1p space for the calculation of core hole Auger decay. The double core hole Auger decay is calculated diagonalizing the complex $\bar{H_N}(\eta)$ matrix in 2h and 3h1p space. The resonance states can be identified from the η trajectories that shows stabilization cusps. The justification of our approximation is discussed elaborately in ref 25.[25]

The Auger decay rate for the single core hole state (K) state of Ne, $\mathrm{H_2O}$, HF systems are calculated using our CAP/ EOMCC method. All the calculated values are compared with the available theoretical and experimental values in literature. The SCF calculations are done with the help of GAMESS-US software package.[26] In the calculation of Ne, $\mathrm{H_2O}$, HF molecules aug-cc-pVQZ basis set [27] is chosen for the Ne, O and F atoms. The cc-pVTZ basis set is chosen for the H atom. The cartesian coordinate used for the $\mathrm{H_2O}$, HF molecules are compiled in Table 5.1 and Table 5.2. The decay rate (Γ) for the Auger decay of core hole states have been calculated in various CAP box sizes for all the systems. The results are presented in Table 5.3. The results for the decay rate of single core hole state is compared with the various theoretical approaches such as configuration interaction (CI),[7] Fano-ADC approach, [8] etc. Our results show excellent agreement with the various theoretical methods as well as experimental results. The decay rate for

Table 5.1: Cartesian coordinate used for H_2O molecule in Å

atom	X	Y	Z
O	0.0000	0.0000	0.0000
H	0.0000	0.0000	0.9584
H	0.9280	0.0000	-0.2391

Table 5.2: Cartesian coordinate used for HF molecule in Å

atom	X	Y	Z
F	0.0000	0.0000	0.4584
H	0.0000	0.0000	-0.4584

the double core hole (KK) states are calculated in Ne, HF systems. The calculated decay rate for the double core hole (KK) states in various CAP box sizes are presented in Table 5.4. The lifetime for the double core hole state(kk) is also compare with the available theoretical methods. From Table 5.4 we can see decay for the double core hole (DCH) state is much faster compare to the single core hole state. The possible reason behind the enhanced rate of DCH is that it deforms the valence electron density more heavily compare to the single core hole state.

Table 5.3: Calculated decay widths (Γ) for the single core (k) ionized states in 10^{-3} a.u

		Theory		Experiment
	CAP-EOMCC		Other methods	
		CAP Box		
Ne	11.8	2.60/2.60/2.60	8.8[a] , 10.3 [b]	
	9.7	2.70/2.70/2.70		
	8.2	2.80/2.80/2.80		
HF	7.9	3.00/3.00/3.87	7.3 [c], 8.3[d]	
	6.2	3.20/3.20/4.06		
	4.2	3.50/3.50/4.37		
H_2O	7.6	4.75 /3.00/4.81	5.6 [c], 6.8 [d], 5.4 [e]	5.8 ± 0.2[f]
	6.5	4.95/3.20/5.01		
	5.4	5.25/3.50/ 5.31		

[a] see ref 28. [b] see ref 29. [c] see ref 7. [d] see ref 30 [e] see ref 8. [f] see ref 31.

Table 5.4: Calculated decay widths (Γ) for the double ionized states in 10^{-3} a.u

	Theory			
	States	CAP-EOMCC		Other methods
			CAP Box	
Ne^{2+}	$1s^{-2}{}^1S$	24.0	2.6/2.6/2.6	25.8 [a], 26.0[b], 29.5 [c]
	$1s^{-1}2s^{-1}{}^1S$	19.3		
	$1s^{-1}2p^{-1}{}^1P$	18.5		
	$1s^{-2}{}^1S$	20.4	2.7/2.7/2.7	
	$1s^{-1}2s^{-1}{}^1S$	15.8		
	$1s^{-1}2p^{-1}{}^1P$	15.3		
	$1s^{-2}{}^1S$	17.4	2.8/2.8/2.8	
	$1s^{-1}2s^{-1}{}^1S$	13.1		
	$1s^{-1}2p^{-1}{}^1P$	12.6		
HF^{2+}	$1\sigma^{-2}$	17.4	3.00/3.00/3.87	21.8 [a]
	$1\sigma^{-1}2\sigma^{-1}$	13.5		
	$1\sigma^{-1}3\sigma^{-1}$	13.4		
	$1\sigma^{-1}1\pi^{-1}$	12.1		
	$1\sigma^{-2}$	15.0	3.20/3.20/4.06	
	$1\sigma^{-1}2\sigma^{-1}$	10.0		
	$1\sigma^{-1}3\sigma^{-1}$	10.1		
	$1\sigma^{-1}1\pi^{-1}$	9.2		

[a] see ref 7. [b] see ref 28. [c] see ref 29.

In summary, we have successfully implemented the CAP/EOMCC method for the first time to calculate the Auger decay of core hole and double core hole states of molecules. We have shown the decay rate of DCH states are $\sim$ 2 to 3 times faster compare to the single core hole Auger decay. Our results show excellent agreement with the available literature values. This is the first time Auger decay for the multiple ionized states has been studied using such a highly correlated method like CAP-EOMCC. To apply our approach for the large biomolecules will be the direction of our future work. We hope our approach will help to develop efficient description and models how radiation damage occurs after multiple core ionization in large system.

References

[1] M. M. Seibert et al., *Nature* **470** 78 (2011).

[2] H. N. Chapman et al., *Nature* **470**, 73 (2011).

[3] P. Auger, *J. Phys. Radium* **6**, 205(1925).

[4] L. S. Cederbaum, Y. -C. Chiang, P. V. Demekhin, and N. Moiseyev, **106**, 123001 (2011).

[5] L. S. Cederbaum, F. Tarantelli, A. Sgamellotti, and J. Schirmer, *J. Chem. Phys.* **85** 6513 (1986).

[6] L. S. Cederbaum, F. Tarantelli, A. Sgamellotti, and J. Schirmer, *J. Chem. Phys.* **86**, 2168 (1987).

[7] L. Inhester, G. Groenhof, and H. Grubmüller, *J. Chem. Phys.* **138**, 164304 (2013).

[8] P. Kolorenč and V. Averbukh, *J. Chem. Phys.* **135**, 134314 (2011)

[9] M. Tashiro, K. Ueda, and M. Ehara, *J. Chem. Phys.* **135**, 154307 (2011).

[10] J. H. D. Eland, M. Tashiro, P. Linusson, M. Ehara, K. Ueda, and R. Feifel, *Phys. Rev. Lett.* **105**, 213005 (2010).

[11] M.Tashiro, M. Ehara, H. Fukuzawa, K. Ueda, C. Buth, N. V. Kryzhevoi, and L. S. Cederbaum, *J. Chem. Phys.* **132**, 184302 (2010).

[12] N. H. Turner and J. A. Schreifels, *Anal. Chem.* **72**, 99R-110R (2000).

[13] B. Boudaïffa, P. Cloutier, D. Hunting, M. A. Huels, and L. Sanche, *Science* **287**, 1658 (2000).

[14] V. Stumpf, P. Kolorenč, K. Gokhberg, and L. S. Cederbaum, *Phys. Rev. Lett.* **110**, 258302 (2013).

[15] R. J. Bartlett and M. Musial, *Rev. Mod. Phys.* **79**, 291 (2007).

[16] D. Mukherjee and S. Pal, *Adv. Quantum Chem.* **20**, 291 (1989).

[17] M. Musial, S. A. Kucharski, and R. J. Bartlett, *J. Chem. Phys.* **118**, 1128 (2003).

[18] M. Musial, A. Perera, R. J. Bartlett, *J. Chem. Phys.* **134**, 114108 (2011).

[19] H. Pathak, A. Ghosh, B. K. Sahoo, B. P. Das, N. vaval, and S. Pal, *Phys. Rev. A* **90**, 010501(R) (2014).

[20] A. Ghosh, N. Vaval, and S. Pal, *J. Chem. Phys.* **136**, 234110 (2012).

[21] A. Ghosh, S. Pal, and N. Vaval, *J. Chem. Phys.* **139**, 064110 (2013).

[22] R. Santra and L. S. Cederbaum, *Phys. Rep* **368** 1 (2002).

[23] U. V. Riss and H. D. Meyer, *J. Phys. B* **26**, 4503 (1993).

[24] N. Moiseyev, *J. Phys. B* **31**, 1431 (1998).

[25] Y. Sajeev, R. Santra, and S. Pal, *J. Chem. Phys.* **122**, 234320 (2005).

[26] M. W. Schmidt, K. K. Baldridge, J. A. Boatz, S. T. Elbert, M. S. Gordon, J. H. Jensen, S. Koseki, N. Matsunaga, K. A. Nguyen,S. Su, T. L. Windus, M. Dupuis, J. A. Montgomery, *J. Comput. Chem.* **14**, 1347 (1993).

[27] R. A. Kendall, T. H. Jr. Dunning, and R. J. Harrison, *J.Chem. Phys.* **96**, 6796 (1992).

[28] C. P. Bhalla, N. O. Folland, and M. A. Hein, *Phys. Rev. A* **8**, 649(1973).

[29] M. H. Chen, *Phys. Rev. A* **44**, 239 (1991)

[30] F. Larkins, *J. Electron Spectrosc. Relat. Phenom.* **67**, 159 (1994).

[31] R. Sankari, M. Ehara, H. Nakatsuji, Y. Senba, K. Hosokawa, H. Yoshida, A. D. Fanis, Y. Tamenori, S. Aksela, and K. Ueda, *Chem. Phys. Lett.* **380**, 647 (2003)

Chapter 6

The potential curve for the lifetime of Interatomic coulombic decay(ICD) mechanism using equation-of-moton coupled cluster (EOMCC) method

In this chapter, we have applied the CAP/EOMCCSD method to compute how the interatomic or intermolecular coulombic decay (ICD) rate of molecule changes with changing the internuclear distance of the molecule. The calculation of ICD decay rate in different internuclear distances is a step towards understanding the dynamics in challenging systems involving inner valence excited states. In this chapter, the summary of the thesis is presented. We have also discuss the future perspective in this field.

6.1 Introduction

The Interatomic coulombic decay (ICD) is a highly efficient relaxation pathway of electronically excited atoms or molecules in environment. The ICD has been predicted theoretically by Cederbaum et al. [1] in 1997. The electronically excited states which can relax via ICD mechanism can be generated in various ways e.g. following the Auger decay [2] of core excited state or through creating a vacancy in the inner valence state or outer valence state. The important characteristic of ICD [3–6] is its fast decay. Generally, it occurs in femto-second time scale. The ICD is a completely environmental phenomena. The efficient energy exchange with the neighboring atoms or molecules plays the key role in this decay process. Thus, the ICD decay [7–12] rate strongly depends on the number of environmental species as well as internuclear distances between them. Energetically, ICD is possible when the binding energy of the excited state lies above the double ionization threshold of the corresponding cluster.

Electronically excited states of atoms or molecules can also relax in various radiative decay mechanism, such as photon emission, radiative charge transfer (RCT), etc. However, these are slow processes. Generally, they occur in nano-second (ns) time scale. Another non-radiative decay mechanism is operative for the core excited states of atoms or molecules is called Auger decay. In Auger decay, a core level vacancy of a particular atom or molecule is replaced by two outer valence vacancy of the same atom or molecule. Auger decay is also a very fast decay process. It occurs in femto-second or even atto-second time domain. The electronically excited states preferably undergoes ICD mechanism when the intramolecular auto-ionization is not energetically favorable.

Historically, ICD has been studied in various weakly bound systems, such as hydrogen bonded clusters,[13] van der Waals clusters,[4] etc. The existence of ICD has also been proved in most weakly bound He_2 cluster in nature.[14] Recently, Cederbaum and co-workers [15] have shown that the site and energy of the ICD electron can efficiently

controlled by spectator resonance Auger decay. It has also been proved that complex absorbing potential approach is highly efficient to calculate the lifetime of inner valence excited states. Santra et al.[16, 17] have applied the CAP/CI approach to calculate the lifetime of ICD decay mode. The CAP/ADC method [18] has also been developed to measure the ICD decay rate. Recently, a highly efficient CAP/EOMCC method [19] has been developed by Vaval and co-workers and it has been applied successfully to calculate the lifetime of 2s inner valence excited states of Ne atom in $\mathrm{Ne(H_2O)_n}$ (n=1,3) clusters. Very recently, the ICD mechanism has been observed experimentally for the NeNe [20, 21] and $(\mathrm{H_2O})_2$ systems.[22, 23]

Recently, it has been proved that the low energy electrons of the order of 2-3 electron volts (eV) are highly efficient to break the single DNA stand and the electrons of the order of 5-6 eV are extremely useful to break the double DNA stand.[24, 25] One of the most amazing feature of ICD is it automatically produces low energy electrons of the order of 4-5 eV. Thus, the ICD might be act as an important source of low energy electrons which can cause severe damage to the single and double DNA stand. Therefore, the accurate description of ICD mechanism is highly important to convert this decay mode to a useful radiotherapy scheme.

The ICD process mainly depends on the initial ionized excited state and the double ionized final state. Therefore, to describe the ICD process effectively, the accurate description of both the ionized states are extremely important. The accurate measurement of initial ionized excited state is possible using the EOMCC method. One of the most amazing feature of EOMCC method is the capability of including electron correlation and relaxation effects in an effective manner. The electron correlation and relaxation effects play the substantial role in the accurate description of ionized excited state . Another advantage is that it gives direct intensive energy difference. Therefore, the EOMCC approach is very promising to calculate the lifetime of ICD process in an accurate manner.

In this chapter, we have applied the well known CAP/EOMCCSD approach for the

first time to study the potential curve for the lifetime of 2s inner valence excited state of Ne atom in NeNe, NeMg, NeAr systems. The results have been compared with the other theoretical results available in literature.

6.2 Theory

In this section, we briefly discuss about the CAP/EOMCCSD method. The CAP approach [26–30] is known to be a very powerful approach to describe the resonance states effectively. The main idea of CAP approach is to absorb the outgoing electron without disturbing the target system. In this way, the wave function of the outgoing electron becomes square integrable. In the CAP approach, the modified Hamiltonian can be defined as

$$H(\eta) = H - i\eta W, \tag{6.1}$$

where η represents the CAP strength and W is the real soft box like potential. The addition of CAP makes the Hamiltonian operator non-Hermitian. The resonance energies are obtained through solving the complex eigenvalue problem corresponding to the matrix representation of $H(\eta)$.

The resonance energy is obtained when

$$|\eta \partial E/\partial \eta| \tag{6.2}$$

becomes minimum.

According to Siegert and Gamow, the resonance energy can be expressed as

$$E_r = E_R - i\Gamma/2, \tag{6.3}$$

where E_R represents the resonance position and Γ is the decay width. Γ is inversely related to the lifetime of the resonance state via, $\tau = \hbar/\Gamma$.

The starting point for the EOMCC method is a coupled cluster (CC) ground state wave function. In CC method, the ground state wave function can be defined as

$$|\psi_0\rangle = e^T|\phi_0\rangle, \tag{6.4}$$

where ϕ_0 is the N-electron close shell reference determinant .e.g., the restricted Hartree-Fock determinant (RHF) and T is the cluster operator. In the coupled cluster singles and doubles (CCSD) approximation, T operator can be defined as follows

$$T = \sum_{ia} t_i^a a_a^+ a_i + 1/4 \sum_{ab} \sum_{ij} t_{ij}^{ab} a_a^+ a_b^+ a_i a_j + ..., . \tag{6.5}$$

where the standard convention for the indices is used, i.e., indices a,b,..., refer to the virtual spin orbitals and indices i,j,.., refer to the occupied spin orbitals.

In the EOMCCSD approach, [31–33] the wave function for the μ th ionized states ψ_μ can be expressed as

$$|\psi_\mu\rangle = R(\mu)|\psi_0\rangle, \tag{6.6}$$

where $R(\mu)$ is the ionization operator.

The $R(\mu)$ operator can be defined via creation -annihilation operator as follows

$$R(\mu)^{IP} = \sum_i r_i(\mu) a_i + 1/2 \sum_a \sum_{ij} r_{ij}^a(\mu) a_a^+ a_j a_i + ... \tag{6.7}$$

The Schrödinger equation for the ionized states can be expressed as

$$H_N R(\mu)|\psi_0\rangle = \Delta E_\mu R(\mu)|\psi_0\rangle \tag{6.8}$$

where $\mathrm{H_N}$ is the normal ordered Hamiltonian and it can be written as

$$H_N = H - \langle\phi_0|H|\phi_0\rangle \tag{6.9}$$

The final form of EOMCC equation is

$$\bar{H_N} R(\mu)|\phi_0\rangle = w_\mu R(\mu)|\phi_0\rangle \tag{6.10}$$

where w_μ is the energy change connected with the ionization process. The $\bar{H_N}$ is the similarity transformed Hamiltonian, in terms of connected diagrams and it can be defined as

$$\bar{H_N} = e^{-T} H e^{T} - \langle \phi_0 | e^{-T} H e^{T} | \phi_0 \rangle \tag{6.11}$$

In a matrix form eq 6.10 is

$$\bar{H_N} R(\mu) = w_\mu R(\mu) \tag{6.12}$$

The $\bar{H_N}$ matrix is diagonalized in the sub space of 1h and 2h1p space to get the required ionization potential (IP) values.

In the CAP/ EOMCC method, the CAP term should be added to the coupled cluster (CC) method. After addition of CAP to the CC method, the ground state wave function $|\psi_0\rangle$ for the CC method can be written as

$$|\Psi_0(\eta)\rangle = e^{T(\eta)} |\phi_0\rangle \tag{6.13}$$

The $T(\eta)$ amplitudes become complex. These complex $T(\eta)$ amplitudes have been used latter to construct the $\bar{H_N}(\eta)$ matrix.

Then, the CAP term is added to the one body particle-particle ($\bar{f_{pp}}$) part of $\bar{H_N}$. The other terms of the $\bar{H_N}$ matrix are altered via the appearance of the complex $T(\eta)$. Thus, the new form of the $\bar{H_N}$ matrix is

$$\bar{H_N}(\eta) = e^{-T(\eta)} H_N(\eta) e^{T(\eta)} - \langle \phi_0 | e^{-T(\eta)} H_N(\eta) e^{T(\eta)} | \phi_0 \rangle \tag{6.14}$$

$$\bar{H_N}(\eta) R_\eta(\mu) = w_\mu(\eta) R_\eta(\mu) \tag{6.15}$$

Finally, the resulting complex $\bar{H_N}(\eta)$ matrix is diagonalized for the different η values. However to obtain the resonance energies we need to use following equation since the ground state energies are suppose to be CAP free.

$$E_{res}(\eta) = w_\mu(\eta) + E_{CC}(\eta) - E_{CC}(\eta = 0) \tag{6.16}$$

In this chapter, we have made an approximation $T(\eta) \approx T(\eta = 0)$. Thus, the CAP is not added at the CC level. The CAP is added directly to the one body particle-particle ($\bar{f_{pp}}$) part of $\bar{H_N}$. Therefore, the new form of the $\bar{H_N}$ matrix is

$$\bar{H_N}(\eta) = e^{-T(\eta=0)} H_N(\eta) e^{T(\eta=0)} - \langle \phi_0 | e^{-T} H_N e^{T} | \phi_0 \rangle \tag{6.17}$$

Finally, the resulting complex $\bar{H_N}(\eta)$ matrix is diagonalized for the different η values to get the resonance energies. The resonance states can be identified from the η trajectories that shows stabilization cusps.

The artificial nature of the CAP potential and its application only to the particle-particle part justify our approximation. The CAP has very less effect on the ground state energy.The main advantage of this approximation is that it reduces the η trajectory generation time. In this approach CC calculation needs to be done only once. Since, the ground state is η independent, resonance energy we get as the direct difference energy obtained as eigenvalues of $\bar{H_N}(\eta)$ for different η values

$$\bar{H_N}(\eta) R_\eta(\mu) = w_\mu(\eta) R_\eta(\mu). \tag{6.18}$$

6.3 Computational details

The aug-cc-pCVTZ basis [34] set has been used to calculate the lifetime of ICD process in NeNe, NeMg, NeAr systems. The first step in the CAP/EOMCCSD computations is an SCF calculation for the neutral NeNe, NeMg, NeAr systems. The SCF calculation has been performed by using the GAMESS-US suite of programs. [35] The required matrix elements of the EOMCCSD and CAP matrices have been computed using our own codes. For diagonalization purpose, we have implemented the non hermitian version of Davidson algorithm in our EOMCC code.

The potential W is the soft-box potential and it can be defined as

$$W(x;c) = \sum_{i=1}^{3} W_i(x_i;c_i), \tag{6.19}$$

where

$$W_i(x_i;c_i) = \{^{0,|x_i|\leq c_i,}_{(|x_i|-c_i)^2,|x_i|>c_i} \tag{6.20}$$

Here, $c_i, i = 1,3$ are the real, non-negative parameters which define the size of a rectangular box. The target molecule is placed in the center of the box. The matrix elements of $W(x;c)$ are calculated within a Gaussian basis set.

6.4 Results and discussion

In this chapter, we have implemented the CAP/EOMCCSD method to study the potential curves for the lifetime of 2s inner valence excited state of Ne atom in NeNe, NeMg, NeAr systems. The lifetime has been studied in various internuclear distances. In the CAP/EOMCCSD calculations, the all the molecules are placed in a cartesian coordinate system at $(0.0, 0.0, \pm R/2 a.u.)$, where R is the bond distance between the two atoms. In the CAP/EOMCC computations, the CAP box side lengths are chosen to be $c_x = c_y = \delta c$ and $c_z = \delta c + R/2$, where c_x,c_y,c_z are the distances from the center of the coordinate system along the x,y, and z axis, respectively, and δc is a non-negative number, all in a.u. The δc value we have chosen for the NeNe is 3.0 a.u and for the NeMg system value is 5.0 a.u. The δc value for the NeAr system is 4.0 a.u.

The ICD decay process in NeNe can be explained as follows : the Ne 2s vacancy is localized on one of the Ne atom. An electron from the 2p level of the same Ne atom comes to fill up the Ne 2s vacancy and the excess energy is used to eject an electron of Ne 2p level from the neighboring Ne atom. Therefore, the final state of ICD process in NeNe is characterized by $Ne^{+}(2p^{-1})Ne^{+}(2p^{-1})$ state. The ICD channel is open in NeNe system because the energy of $\mathrm{Ne}^{+}(2\mathrm{s}^{-1})\mathrm{Ne}$ state lies above the energy of $Ne^{+}(2p^{-1})Ne^{+}(2p^{-1})$ state. At equilibrium bond length of neutral NeNe molecule, the energy of $\mathrm{Ne}^{+}(2\mathrm{s}^{-1})\mathrm{Ne}$

Table 6.1: Calculated decay widths (Γ) for the $^2\Sigma_u^+$ inner valence hole of Ne atom in NeNe

Bond distance(Å)	Γ (meV)	lifetime(fs)
2.8	9.52	69
2.9	8.27	79
3.0	7.21	91
3.1	6.72	98
3.2	6.53	100
3.3	6.35	103
3.4	6.20	106

state is 48.38 electron volts(eV). Here, we have calculated the lifetime of $^2\Sigma_u^+$ inner valence excited state of neon dimer in various inter nuclear distances. Starting from 2.8 Å we have symmetrically stretch the Ne-Ne bond distance up to 3.5 Å. The lifetimes for the $^2\Sigma_u^+$ inner valence excited state in various internuclear distances are presented in Table 6.1. Starting from the Ne-Ne bond distance 2.8 Å the lifetime increases rapidly when we stretch the Ne-Ne bond distance. Another important aspect is the ICD decay channel is open for the $^2\Sigma_u^+$ inner valence excited state at bond distance $\rangle$ 2.70 Å. When the Ne-Ne bond distance is $\langle$ 2.70 Å the ICD decay channel for the $^2\Sigma_u^+$ state is energetically forbidden. The schematic representation of lifetimes for the $^2\Sigma_u^+$ inner valence excited state of neon dimer in various internuclear distances are presented in Fig 6.1.

The lifetime for the $^2\Sigma_u^+$ state is compared with the other theoretical approaches available in literature. The computed lifetime for the $^2\Sigma_u^+$ state at equilibrium bond distance (3.2 Å) is 100 femto-second (fs). The calculated lifetime using the CAP/ADC method is 92 fs.[18] The d-aug-cc-pV5Z basis set has been used in the CAP/ADC calculation. The CAP/CI method gives lifetime for the $^2\Sigma_u^+$ state is 64 fs. The basis set used in the CAP/CI calculation [17] is d-aug-cc-pVDZ augmented by three diffuse s, p, and d functions each. In a recent experiment it has been found that the 2s inner valence excited state of Ne atom in neon dimer can have lifetime in the order of (150$\pm$ 50) fs.[21] Therefore, the result obtained in CAP/EOMCCSD method show excellent agreement with the experimental

result.

The 2s inner valence excited state of Ne atom in NeMg can relax through ICD mechanism to a $\mathrm{Ne^{+}(2p^{-1})Mg^{+}(3s^{-1})}$ final state. In this process, one 2p electron fills up the 2s vacancy of Ne atom and released energy ejected another 3s outer valence electron from the Mg atom. At equilibrium bond length (4.4 Å) the energy of the $\mathrm{Ne^{+}(2s^{-1})Mg}$ state is 48.3 eV. The energy of the $\mathrm{Ne^{+}(2p^{-1})Mg^{+}(3s^{-1})}$ state is 32.29 eV. The energy of $\mathrm{Ne^{+}(2p^{-1})Mg^{+}(3s^{-1})}$ state is 16 eV lower in comparison with $\mathrm{Ne^{+}(2s^{-1})Mg}$ state. Therefore, the ICD decay channel is energetically open for the $\mathrm{Ne^{+}(2s^{-1})Mg}$ state. The $\mathrm{Ne^{+}(2s^{-1})Mg}$ state can also relax to a final state $\mathrm{NeMg^{2+}(3s^{-2})}$ through Electron transfer mediated decay mechanism(ETMD). The energy of the $\mathrm{NeMg^{2+}(3s^{-2})}$ state is 22.5 eV. The two decay channel is open for the $\mathrm{Ne^{+}(2s^{-1})Mg}$ state due to very low energy of 3s orbital of Mg atom. However, the only decay channel is open for NeNe is ICD. The calculation of lifetime separately for ICD and ETMD process is not possible using the CAP/EOMCCSD method. Here, We have calculated the total lifetime of $\mathrm{Ne^{+}(2s^{-1})Mg}$ state in various internuclear distances. Starting from Ne-Mg bond distance 4.0 Å, the lifetime of $\mathrm{Ne^{+}(2s^{-1})Mg}$ state is calculated up to the bond distance 5.0 Å. The calculated lifetime for various internuclear distances are presented in Table 6.2. Starting from equilibrium bond distance, the lifetime of $\mathrm{Ne^{+}(2s^{-1})Mg}$ state increases strongly with increasing the Ne-Mg bond distance. The schematic representation of lifetimes for the 2s inner valence excited state of NeMg in various internuclear distances are presented in Fig 6.2.

We have also calculated the lifetime of 2s inner valence excited state of Ne atom in NeAr cluster in various internuclear distances between Ne and Ar atom. The calculated lifetime in various internuclear distances are presented in Table 6.3. The schematic representation of lifetimes for the 2s inner valence excited state of NeAr in various internuclear distances are presented in Fig 6.3. The two decay channel is open for the $\mathrm{Ne^{+}(2s^{-1})Ar}$ state. It can decay to the final $\mathrm{Ne^{+}(2p^{-1})Ar^{+}(3p^{-1})}$ state through ICD process. The ICD decay channel is open because $\mathrm{Ne^{+}(2p^{-1})Ar^{+}(3p^{-1})}$ state (at equilibrium bond length

Table 6.2: Calculated decay widths (Γ) for the 2s inner valence hole of Ne atom in NeMg

Bond distance(Å)	Γ (meV)	lifetime(fs)
4.0	30.24	22
4.2	24.25	27
4.4	17.25	38
4.6	9.87	66
4.8	3.83	171

Table 6.3: Calculated decay widths (Γ) for the 2s inner valence hole of Ne atom in NeAr

Bond distance(Å)	Γ (meV)	lifetime(fs)
2.8	124.15	5
3.0	114.12	6
3.2	84.90	8
3.4	47.63	14
3.5	37.40	17
3.6	33.89	19
3.8	26.22	25

3.5 Å) has energy 5 eV lower compare to the $\mathrm{Ne^{+}(2s^{-1})Ar}$ state. Further, $\mathrm{Ne^{+}(2s^{-1})Ar}$ state can relax to $\mathrm{NeAr^{2+}(3p^{-2})}$ state via ETMD pathway. Here, we have calculated the total lifetime of $\mathrm{Ne^{+}(2s^{-1})Ar}$ state using the CAP/EOMCCSD method. However, at equilibrium bond length of NeAr system ETMD process is suppressed by ICD decay mode.

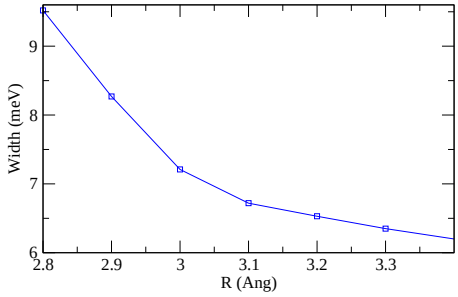

Figure 6.1: Potential curve of calculated decay widths (Γ) for the $^2\Sigma_u^+$ inner valence state of Ne atom in NeNe

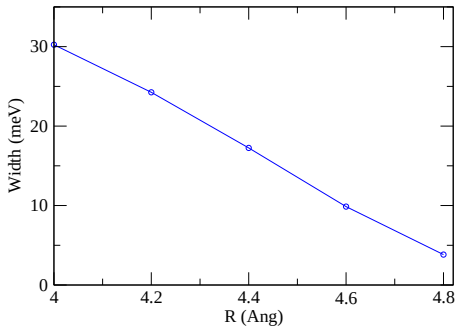

Figure 6.2: Potential curve of calculated decay widths (Γ) for the 2s inner valence hole of Ne atom in NeMg

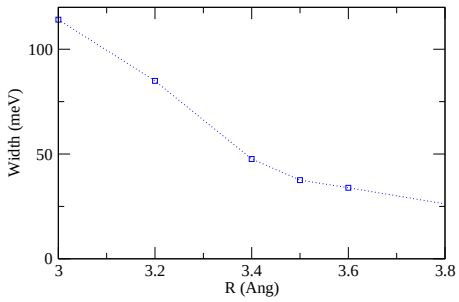

Figure 6.3: Potential curve of calculated decay widths (Γ) for the 2s inner valence hole of Ne atom in NeAr

6.5 Conclusion

In this chapter we have implemented the highly correlated CAP/EOMCCSD approach for the first time to describe the ICD process in weakly bound van der Waals clusters. The method has been implemented to study the lifetime of 2s inner valence excited state of Ne atom in NeNe, NeMg, NeAr systems in various internuclear distances. The ICD decay rate decreases rapidly when we stretch the NeNe, NeMg, NeAr systems from their equilibrium bond length. The reason behind decreasing the decay rate is that with increasing the bond distance between two atoms energy transfer process becomes slow down which decreases the ICD decay rate. Another important aspect is at equilibrium bond length when we go from NeNe to NeMg the decay rate increases. Further, the decay rate increases when we go from NeMg to NeAr. The reason for increasing the decay rate when we go from NeMg to NeAr is that the equilibrium bond length for the NeMg system is 4.4 Å. However, the equilibrium bond length for NeAr system is 3.5 Å. Therefore, the bond distance between two atoms play an important role to make difference in ICD decay rate. The reason for the change of lifetime is the changes of electronic structure as we go from NeNe to NeMg. In case of NeMg the double ionization threshold is much less compare to the NeNe.

In this thesis, the CAP/EOMCC method has been developed and successfully implemented for the description of shape resonance as well as various non-radiative decay phenomena such as ICD, Auger decay, etc. However, the highly correlated CAP/EOMCC approach has been implemented for the smaller systems to describe these various phenomena. To apply our approach for the large bio-molecules will be the direction of our future work. We hope our approach might be helpful in further development of efficient radiooncology scheme to understand the radiation damage in biological systems in a more accurate manner.

References

[1] L.S. Cederbaum, J. Zobeley, and F. Tarantelli *Phys. Rev. Lett.* **79** 4778 (1997).

[2] L. S. Cederbaum, Y. C. Chiang, P. V. Demekhin, and N. Moiseyev, *Phys.Rev. Lett.* **106**, 123001 (2011).

[3] N. Moiseyev, R. Santra, J. Zobeley, and L. S. Cederbaum, *J. Chem. Phys.* **114**, 7351 (2001).

[4] R. Santra, J. Zobeley, L. S. Cederbaum and N. Moiseyev, *Phys. Rev. Lett.* **85**, 4490 (2000)

[5] S. Scheit, V. Averbukh, H. D. Meyer, N. Moiseyev, R. Santra, T. Sommerfeld, J. Zobeley, and L. S. Cederbaum, *J. Chem. Phys.* **121**, 8393 (2004).

[6] S. Scheit, V. Averbukh, H. D. Meyer, J. Zobeley, and L. S. Cederbaum, *J. Chem. Phys.* **124**, 154305 (2004).

[7] S. Barth, S. Joshi, S. Marburger, V. Ulrich, A. Lindblas, G. Öhrwall, O. Björneholm, and U. Hergenhahn, *J. Chem. Phys.* **122**, 241102 (2005).

[8] P. V. Demekhin, S. D. Stoychev, A. I. Kuleff, and L. S. Cederbaum, *Phys. Rev. Lett.* **107**, 273002 (2011).

[9] I. B. Müller and L. S. Cederbaum, *J. Chem. Phys.* **125**, 204305 (2006).

[10] V. Averbukh, I. B. Müller, and L. S. Cederbaum, *Phys. Rev. Lett.* **93**, 263002 (2004).

[11] R. Santra and L. S. Cederbaum, *Phys. Rep.* **368**, 1 (2002).

[12] V. Averbukh and L. S. Cederbaum, *Phys. Rev. Lett.* **96**, 053401 (2006).

[13] S. D. Stoychev, A. I. Kuleff, and L. S. Cederbaum, *J. Am. Chem. Soc.* **133**, 6817 (2011).

[14] N. Sisourat, N. V. Kryzhevoi, P. Kolorenč, S. Scheit, T. Jahnke, and L. S. Cederbaum, *Nat. Phys.* **6**, 508 (2010).

[15] K. Gokhberg, P. Kolorenc, A. I. Kuleff, and L. S. Cederbaum, *Nature* **505**, 661 (2014).

[16] R. Santra, L. S. Cederbaum, and H. D. Meyer, *Chem. Phys. Lett.* **303**, 413 (1999).

[17] R. Santra and L.S. Cederbaum, *J. Chem. Phys.* **115**, 6853 (2001).

[18] N. Vaval and L. S. Cederbaum, *J. Chem. Phys.* **126**, 164110 (2007).

[19] A. Ghosh, S. Pal, and N. Vaval, *J. Chem. Phys.* **139**, 064112 (2013).

[20] T. Jahnke, A. Czasch, M. S. Schöffler, S. Schössler, A. Knapp, M. Käsz, J. Titze, C. Wimmer, K. Kreidi, R. E. Grisenti, A. Staudte, O. Jagutzki, U. Hergenhahn, H. Schmidt-Böcking, and R. Dörner, *Phys. Rev. Lett.* **93**, 163401 (2004).

[21] K. Schnorr, A. Senftleben, M. Kurka, A. Rudenko, L. Foucar, G. Schmid, A. Broska, T. Pfeifer, K. Meyer, D. Anielski, R. Boll, D. Rolles, M. Kübel, M.F. Kling, Y.H. Jiang, S. Mondal, T. Tachibana, K. Ueda, T. Marchenko, M. Simon, G. Brenner, R. Treusch, S. Scheit, V. Averbukh, J. Ullrich, C.D. Schröter, and R. Moshammer, *Phys. Rev. Lett.* **111**,093402 (2013).

[22] T. Jahnke, H. Sann, T. Havermeier, K. Kreidi, C. Stuck, M. Meckel, M. Schöffler, N. Neumann, R. Wallauer, S. Voss, A. Czasch, O. Jagutzki, A. Malakzadeh, F. Afaneh, Th. Weber, H. Schmidt-Böcking, and R. Dörner, *Nat. Phys.*, **6**, 139 (2010);

[23] M. Mucke, M. Braune, S. Barth, M. Förstel, T. Lischke, V. Ulrich, T. Arion, U. Becker, A. Bradshaw, and U. Hergenhahn, *Nat. Phys.* **6**, 143 (2010);

[24] F. Trinter, M. S. Schöffler, H.-K. Kim, F. P. Sturm, K. Cole, N. Neumann, A. Vredenborg, J. Williams, I. Bocharova, R. Guillemin, M. Simon, A. Belkacem, A. L. Landers, Th. Weber, H. Schmidt-Böcking, R. Dörner, and T. Jahnke, *Nature* **505**, 664 (2014).

[25] B. Boudaïffa, P. Cloutier, D. Hunting, M. A. Huels, and L. Sanche, *Science* **287** (5458), 1658 (2000).

[26] T. Sommerfeld, U. V. Riss, H. D. Meyer, L. S. Cederbaum, B. Engels, and H. U. Suter, *J. Phys. B* **31**, 4107 (1998).

[27] G. Jolicard and E. J. Austin, *Chem. Phys. Lett.* **121**, 106 (1985).

[28] W. P. Reinhardt, *Annu. Rev. Phys. Chem.* **33**, 223 (1982); N. Moiseyev, *Phys. Rep.* **302**, 211 (1998).

[29] U. V. Riss and H. D. Meyer, *J. Phys. B* **26**, 4503 (1993); J. G. Muga, J. P. Palao, B. Navarro, and I. L. Egusquiza, *Phys. Rep.* **395**, 357 (2004).

[30] N. Moiseyev, *J. Phys. B* **31**, 1431 (1998); U. V. Riss and H. D. Meyer, *J. Phys. B* **31**, 2279 (1998).

[31] M. Musial, S. A. Kucharski, and R. J. Bartlett, *J. Chem. Phys.* **118**, 1128 (2003).

[32] R. J. Bartlett and M. Musial, *Rev. Mod. Phys.* **79**, 291 (2007).

[33] D. I. Lyakh, M. Musial, V. F. Lotrich, and R. J. Bartlett, *Chem. Rev.* **112**, 182 (2012).

[34] T. H. Dunning, Jr., *J. Chem. Phys.* **90**, 1007 (1989).

[35] M. W. Schmidt, K. K. Baldridge, J. A. Boatz, S. T. Elbert, M. S. Gordon, J. H. Jensen, S. Koseki, N. Matsunaga, K. A. Nguyen, S. Su, T. L. Windus, M. Dupuis, and J. A. Montgomery, 'GAMESS: General atomic and molecular electronic structure system,' *J. Comput. Chem.* **14**, 1347 (1993).